
Solar Axions

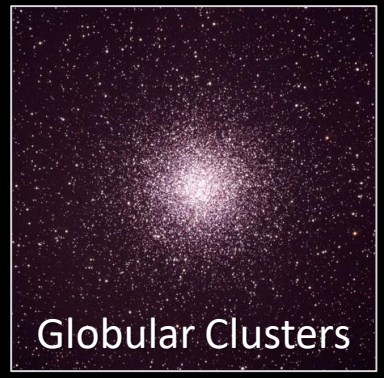
Globular Clusters


Supernova 1987A

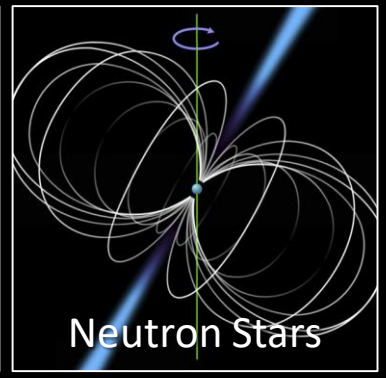
Neutron Stars

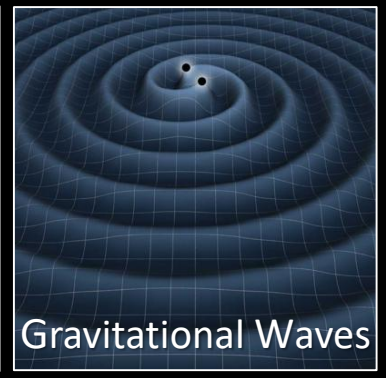
Gravitational Waves

Axions and the Stars

Old Ideas and New Developments

GGI, Florence, April 2023

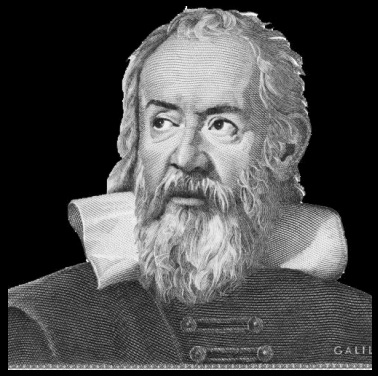

ORIGINS Excellence Cluster

COSMIC WISPERS CA21106

Max-Planck-Institut für Physik (Werner-Heisenberg-Institut)

SFB 1258 | Neutrinos Dark Matter Messengers

Georg G. Raffelt, Max-Planck-Institut für Physik, München

Axions and the Stars

Old Ideas and New Developments

GGI, Florence, April 2023

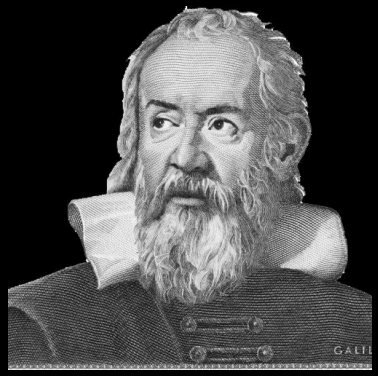

Lecture I: Axions and ordinary stars

- Detection opportunity from the Sun
- Photon-axion oscillations in astronomy
- Globular Clusters & White Dwarfs

Lecture II: Compact Stars

- SN 1987A and Neutron Stars
- Equation of State in Compact Stars
- Dark matter axions & radiowaves from pulsars
- Superradiance

High- and Low-Energy Frontiers in Particle Physics

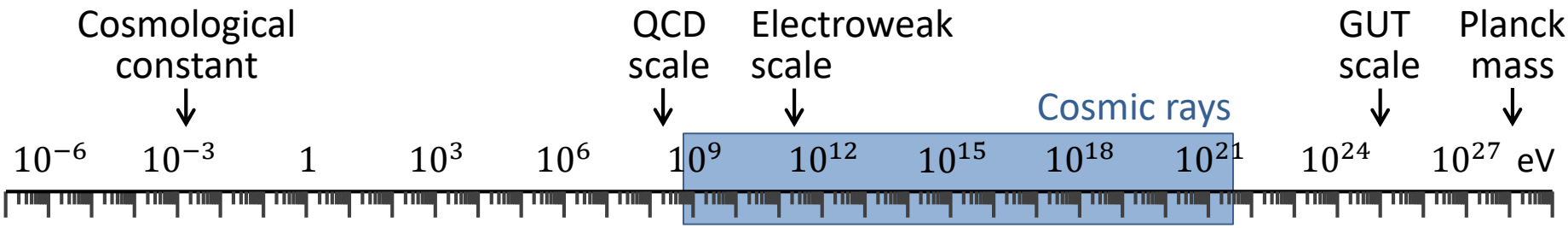

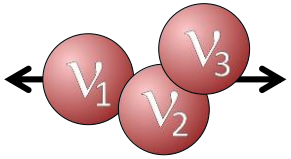

"Intensity Frontier"
(feeble interactions)

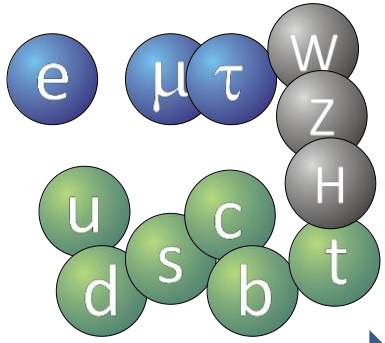

Low-E Frontier

High-Energy Frontier

High- and Low-Energy Frontiers in Particle Physics

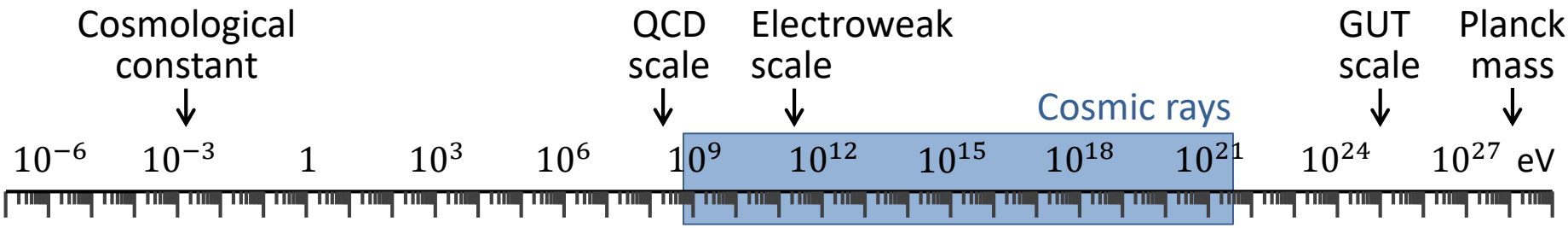

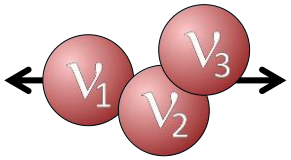

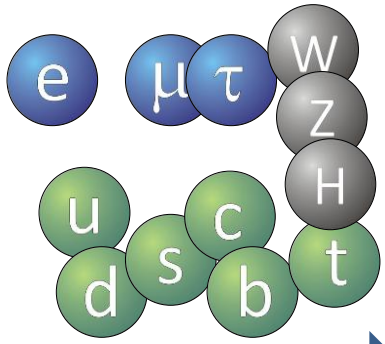

"Intensity Frontier"
(feeble interactions)

Low-E Frontier

High-Energy Frontier

Neutrinos (active & sterile)
Axions & friends
Dark photons, fuzzy dark matter,
muon-philic bosons, …

} Feebly-interacting particles (FIPs)
(e.g. CERN 2020 workshop report
arXiv:2102.12143)

Bestiarium of Low-Mass Bosons

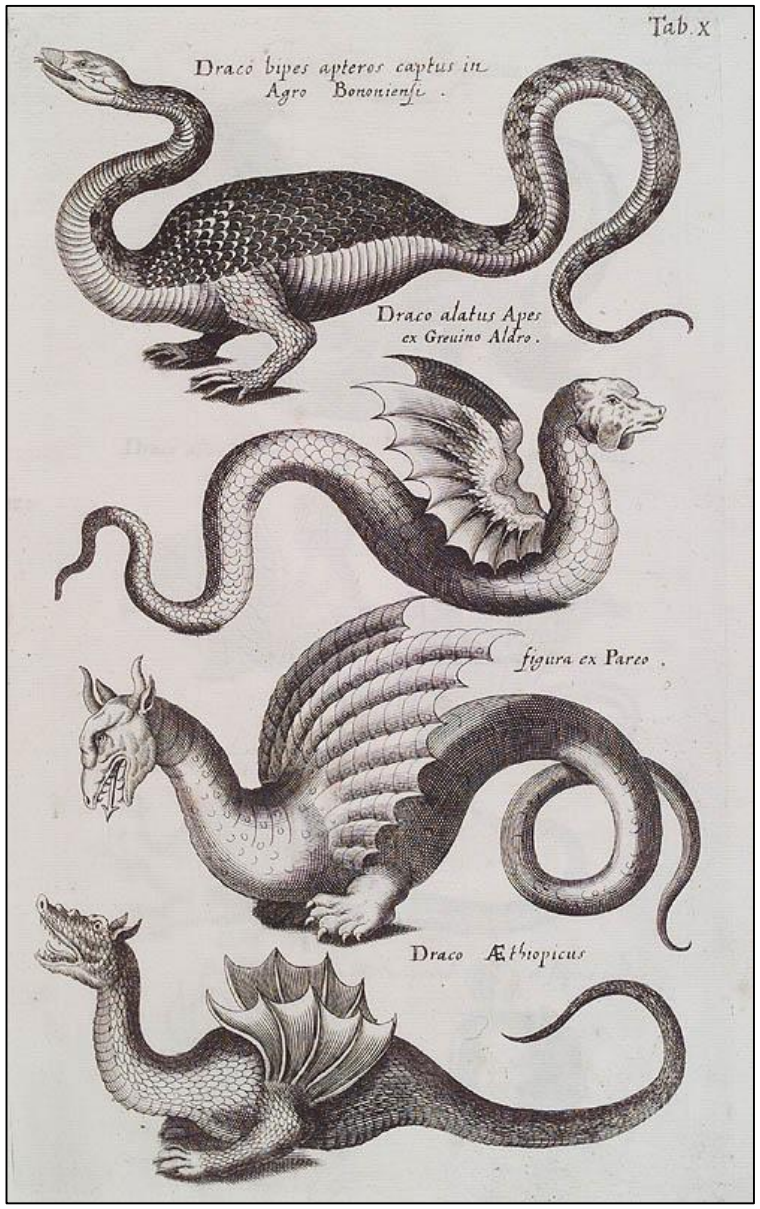

Weakly Interacting Sub-eV Particles (WISPs)

- **Axions** (1 parameter family $m_a f_a \sim m_\pi f_\pi$)
  Solves strong CP problem
  Could be dark matter
- **Axion-like particles (ALPs)**
  Generic two-photon vertex, could be dark matter
  (2 parameters m_a and $g_{a\gamma}$)
- **String axions**
  (almost massless pseudoscalars in string theory)
  One of them may solve CP problem
- **Hidden photons**
  Low-mass gauge bosons from $U'(1)$
  (kinetic mixing parameter χ and mass $m_{\gamma'}$)
- **Fifth force, fuzzy dark matter, ULAs, all sorts of FIPs, WISPs, ALPs, …**

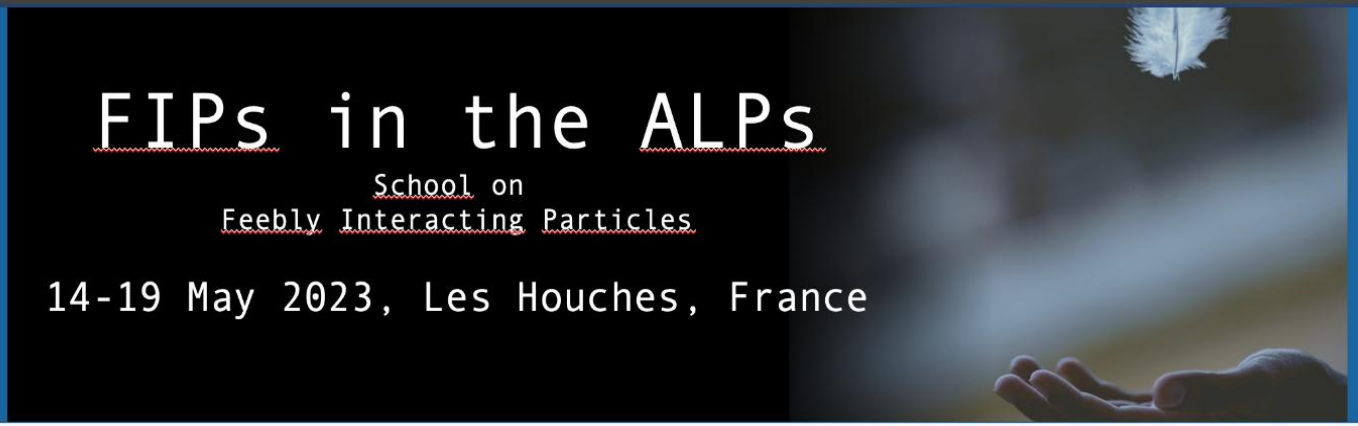

May 14 – 19, 2023
Europe/Zurich timezone

Enter your search term

Overview
Registration
Practical Information
- How to get to Les Houches
- Directions to Hostel/Meeting room
- Accommodation
- Access to Les Houches computing network

Participant List

Contacts
gaia.lanfranchi@lnf.infn.it
houches-secretariat@un...

FIPs in the ALPs is the first edition of a foreseen series of schools fully dedicated to the physics of feebly-interacting particles and aims to gathering together highly renowned experts from collider, beam dump, fixed target experiments, as well as from astroparticle, cosmology, axion/ALP, ultra-light particle searches, and dark matter direct and indirect detection communities along with a set of young and brilliant physicists to discuss progress in experimental searches and underlying theory models for FIP physics.

The school is organized by the FIP Physics Centre of the Physics Beyond Colliders study group at CERN: https://pbc.web.cern.ch/fpc-mandate

The aim of the school is to embedding a new generation of physicists into the activities of the study group.

The School is organized along three main directions:

1. **MeV-GeV Dark Matter** and its searches at accelerator, direct and indirect detection experiments;
2. **Heavy neutral leptons** and their connection to active neutrino physics;
3. **Ultra-light (< 1 eV) FIPs** in particle physics, astroparticle, and cosmology.

Advanced PhD students and PostDocs are strongly encouraged to apply.

The Organizers:

The FIP Physics Centre of the Physics Beyond Colliders at CERN.

https://pbc.web.cern.ch/fpc-mandate

Killing Two Birds With One Stone

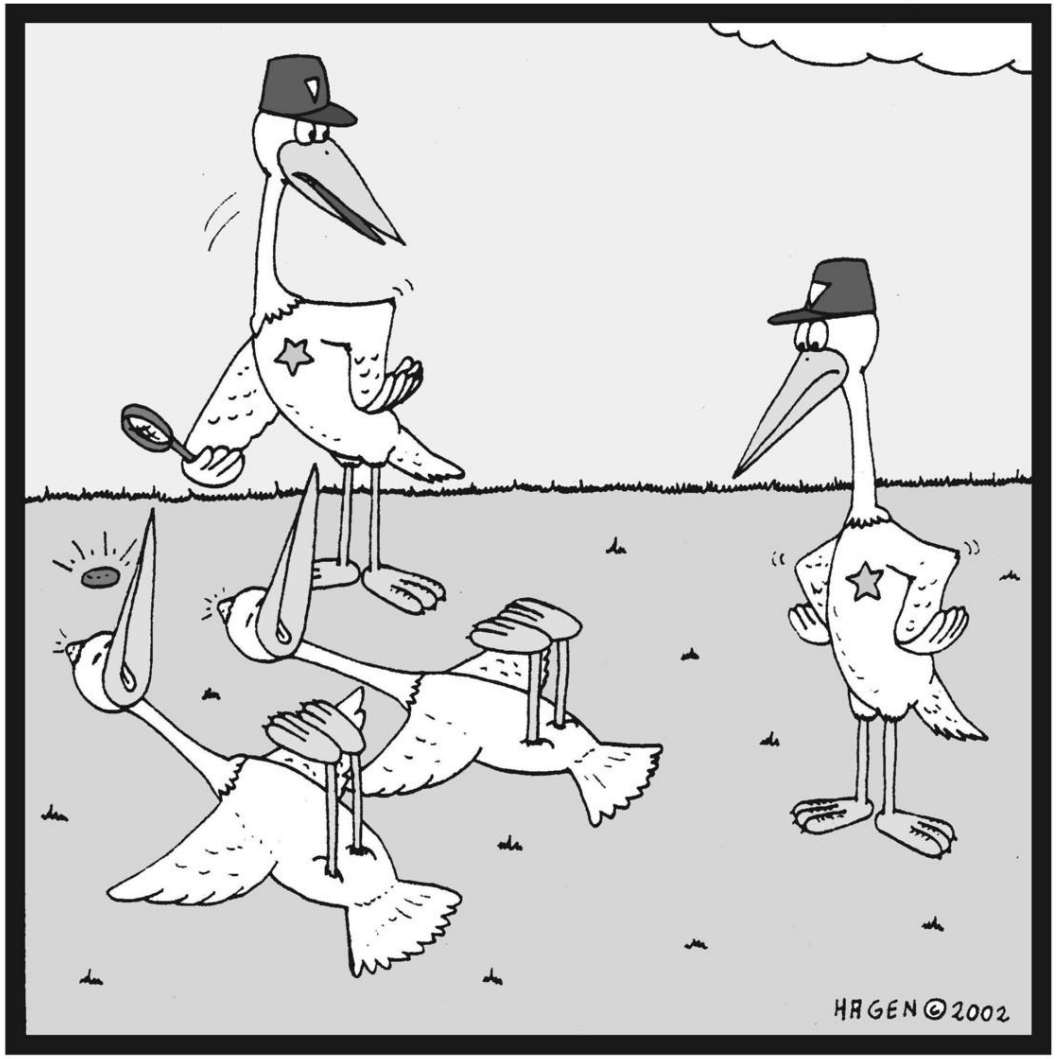

Unbelievable! It looks like they've both been killed by the same stone...

Peccei-Quinn mechanism
- Solves strong CP problem
- May provide dark matter in the form of axions

More agnostic view today,
following Galileo's Advice

Measure what
can be measured,
and make measurable
what cannot be.

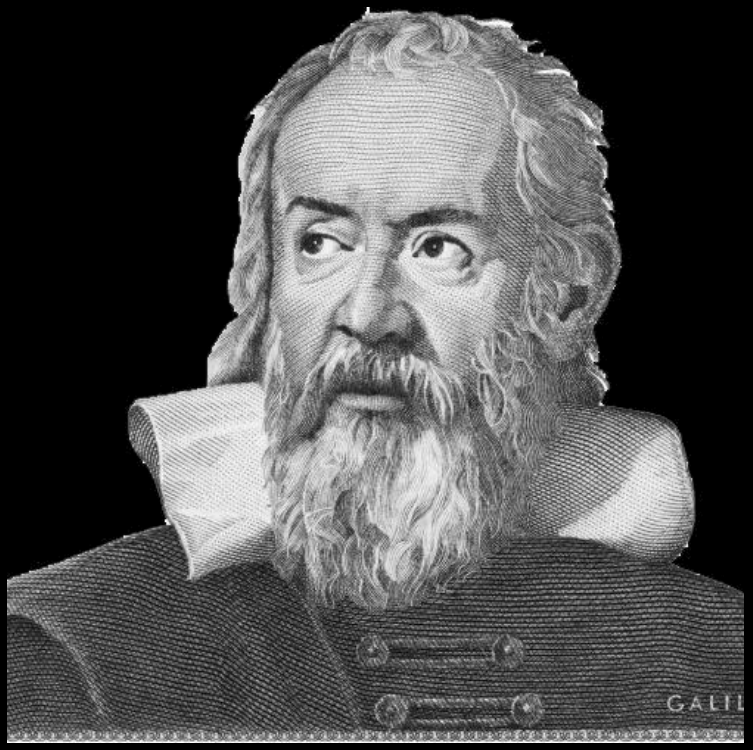

EVOLUTION OF STARS

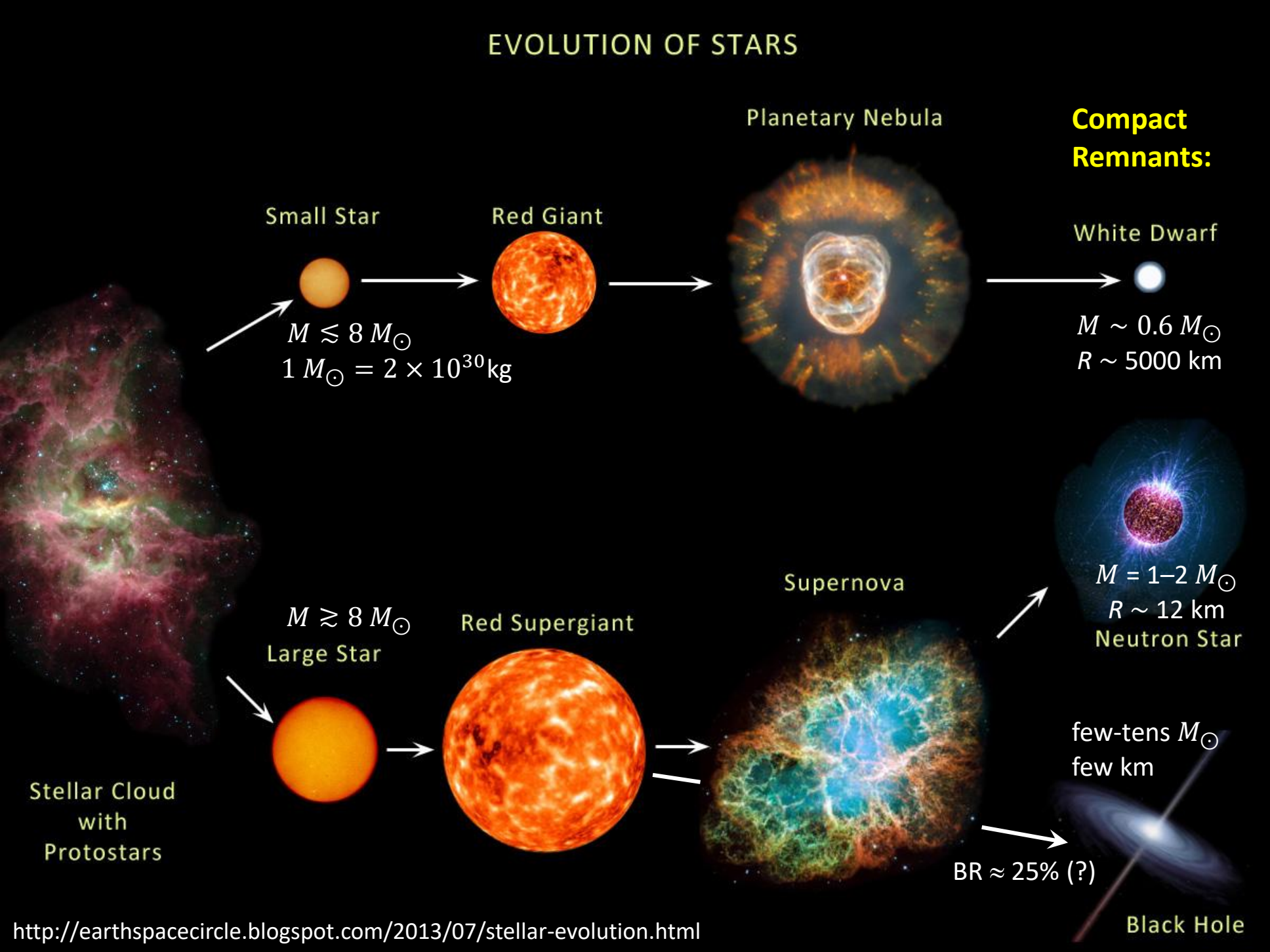

http://earthspacecircle.blogspot.com/2013/07/stellar-evolution.html

EVOLUTION OF STARS

Stellar Cloud with Protostars

Small Star

$M \lesssim 8\ M_\odot$

$1\ M_\odot = 2 \times 10^{30}$kg

Red Giant

Planetary Nebula

White Dwarf

$M \sim 0.6\ M_\odot$

$R \sim 5000$ km

Compact Remnants:

Surface T ~ eV (IR to UV)

Inner T ~ 1–100 keV

$M \gtrsim 8\ M_\odot$

Large Star

Red Supergiant

Supernova

Inner T ~ 30 MeV

Surface T ~ keV

Nuclear density

M = 1–2 $M_\odot$

$R \sim 12$ km

Neutron Star

few-tens $M_\odot$

few km

BR ≈ 25% (?)

Black Hole

http://earthspacecircle.blogspot.com/2013/07/stellar-evolution.html

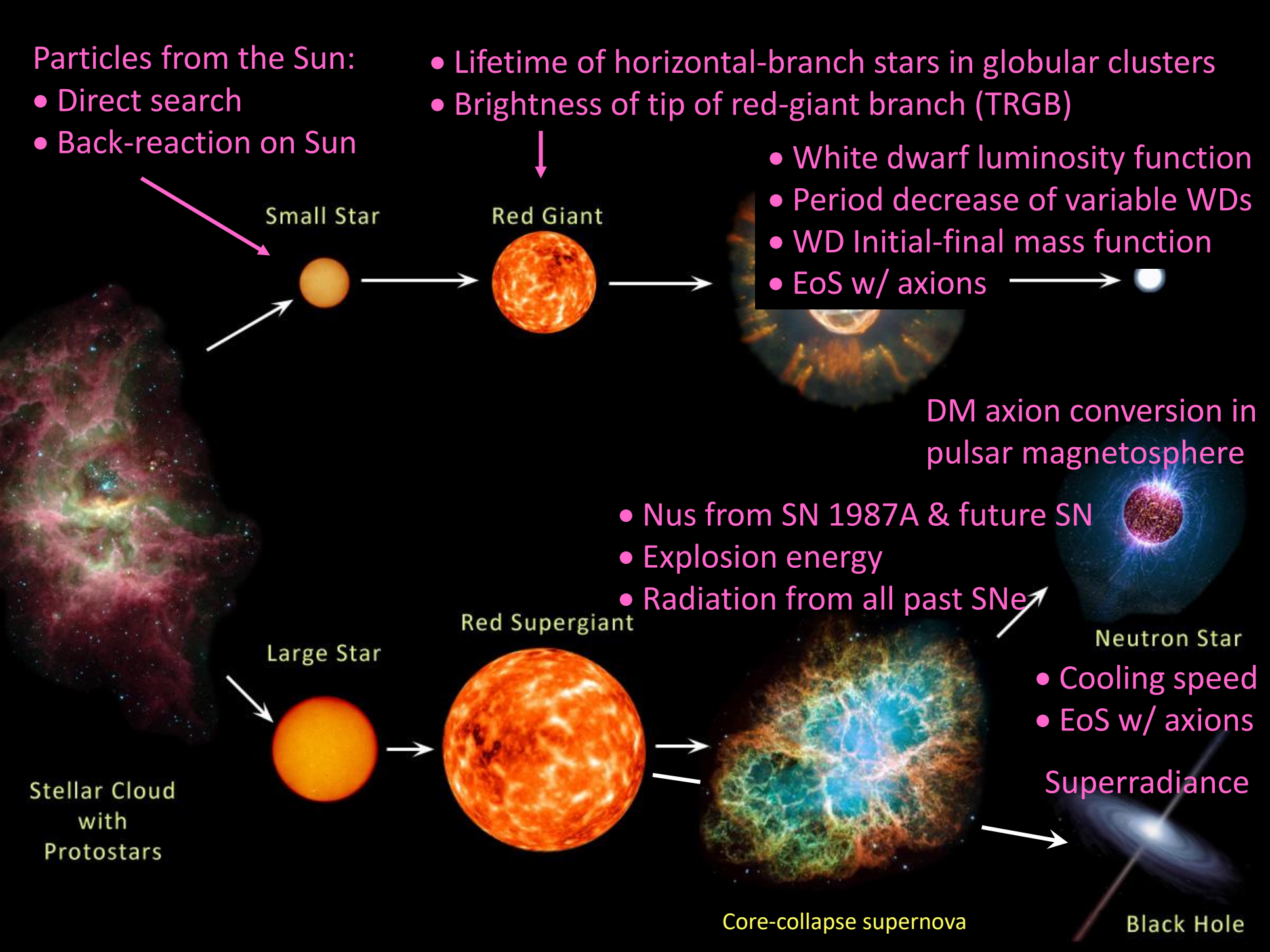
Particles from the Sun:
• Direct search
• Back-reaction on Sun
• Lifetime of horizontal-branch stars in globular clusters
• Brightness of tip of red-giant branch (TRGB)
• White dwarf luminosity function
• Period decrease of variable WDs
• WD Initial-final mass function
• EoS w/ axions
Small Star
Red Giant
DM axion conversion in pulsar magnetosphere
• Nus from SN 1987A & future SN
• Explosion energy
• Radiation from all past SNe
Red Supergiant
Large Star
Neutron Star
• Cooling speed
• EoS w/ axions
Superradiance
Stellar Cloud with Protostars
Core-collapse supernova
Black Hole

Some Early Papers on Stellar Particle Physics

Neutrinos

- Bernstein, Ruderman & Feinberg:
  Electromagnetic properties of the neutrino, Phys. Rev. 132 (1963) 1227
- Gribov & Pontecorvo:
  Neutrino astronomy and lepton charge, PLB 28 (1969) 493
- Cowsik:
  Limits on the radiative decay of neutrinos, PRL 39 (1978) 511
- Falk & Schramm:
  Limits from supernovae on neutrino radiative lifetimes, PLB 79 (1978) 511

Axions & light Higgs (ca 1978)

- Vysotsky, Zeldovich, Khlopov & Chechetkin:
  Some astrophysical limitations on the axion mass,
  Pisma Zh. Eksp. Teor. Fiz. 27 (1978) 533 [JETP Lett. 27 (1978) 502]
- Dicus, Kolb, Teplitz & Wagoner:
  Astrophysical bounds on the masses of axions and Higgs particles, PRD 18 (1978) 1829
- K. O. Mikaelian: Astrophysical implications of new light Higgs bosons, PRD 18 (1978) 3605
- K. Sato: Astrophysical constraints on the axion mass and the number of quark flavors,
  Prog. Theor. Phys. 60 (1978) 1942

Particles from the Sun

2002 Solar Neutrinos (R.Davis, M.Koshiba)

2015 Solar Nu Oscillations (A.McDonald)

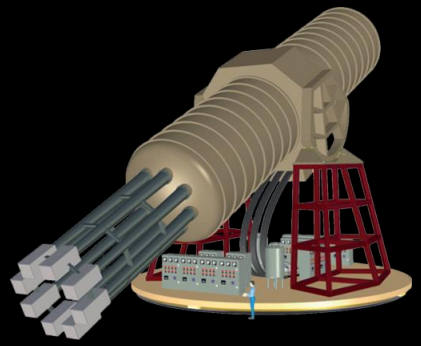

Search for solar axions
with CAST and future IAXO

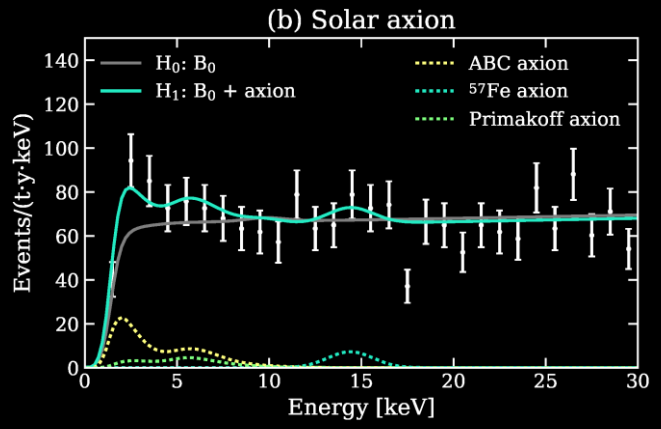

Excess events in
XENON1T DM search.
Solar axions?
arXiv:2006.09721
XENONnT: no signal
arXiv:2207.11330

Hydrogen Burning in Stars

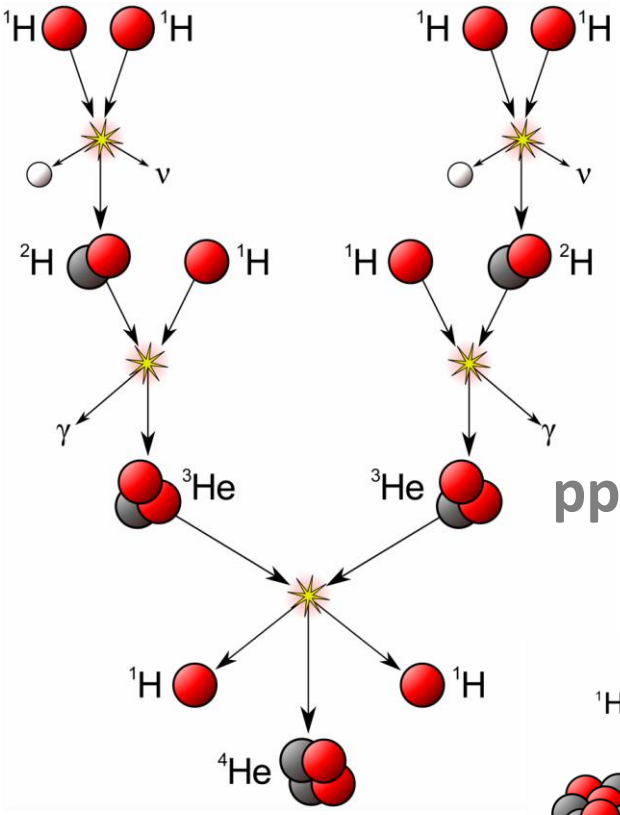

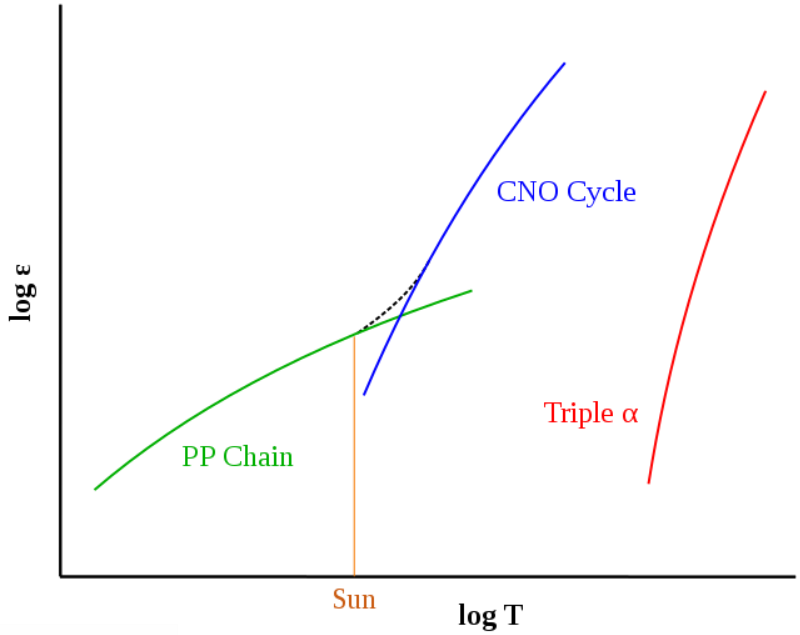

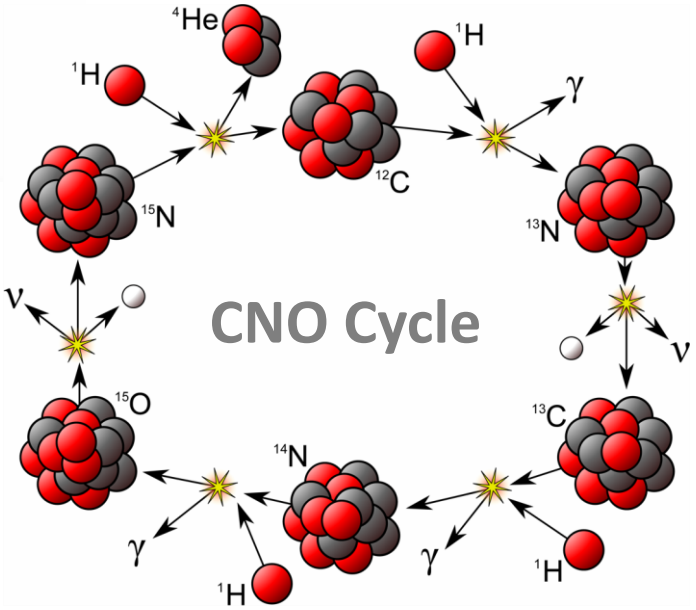

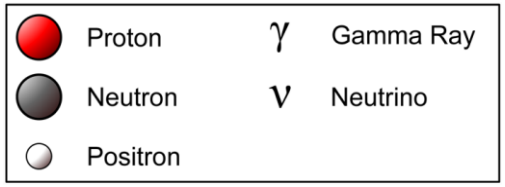

Picture credit Wikipedia

Solar Neutrinos from Nuclear Reactions

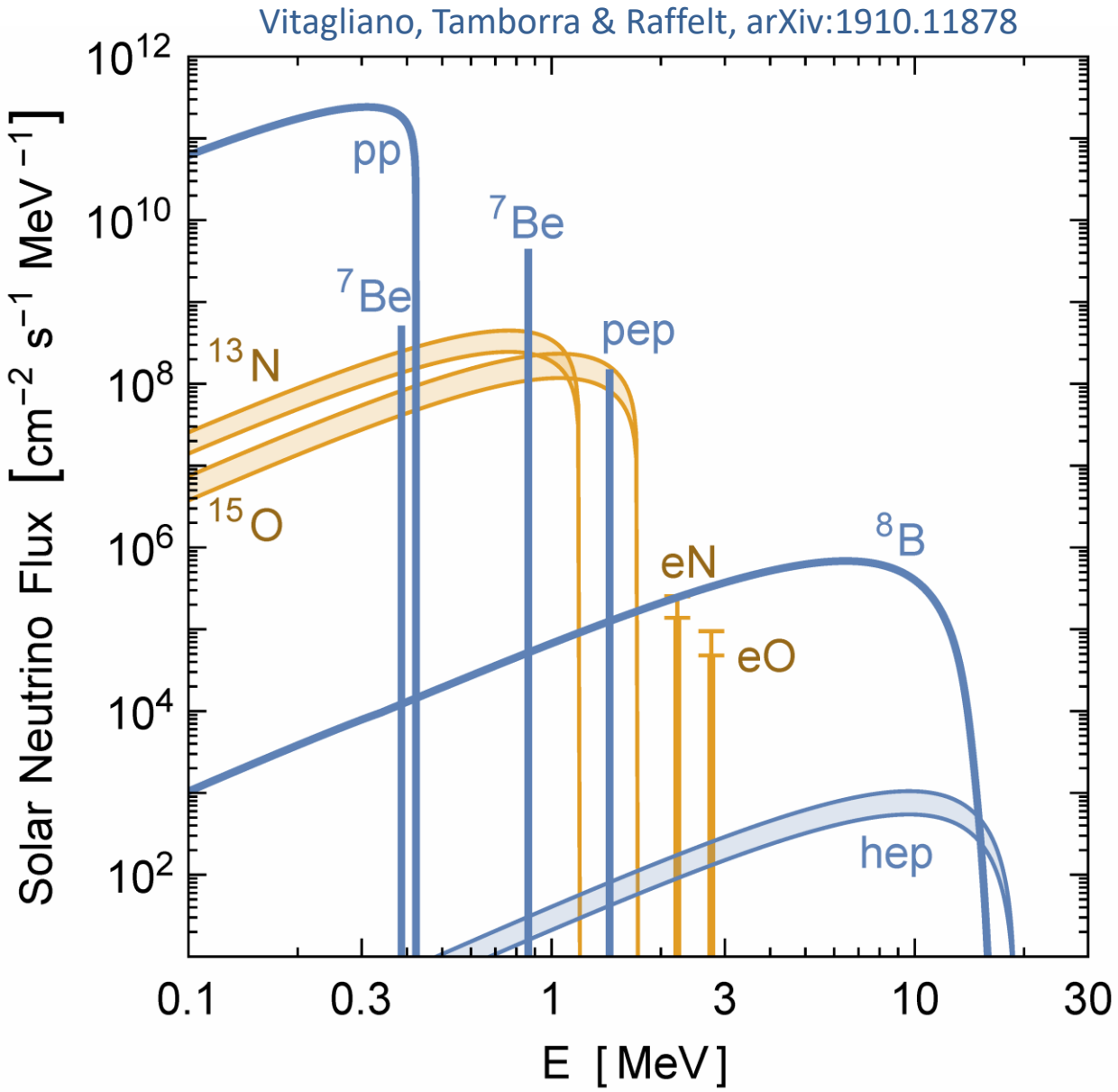

All components of pp chains (blue) have been measured

Very recently direct experimental evidence for CNO fluxes (orange) in Borexino
arXiv:2006.15115 (06/2020)
Nature 587 (2020) 577
and arXiv:2205.15975

Favors higher flux, and thus "high" CNO abundance

Grand Unified Neutrino Spectrum (GUNS) at Earth

Vitagliano, Tamborra & Raffelt, arXiv:1910.11878

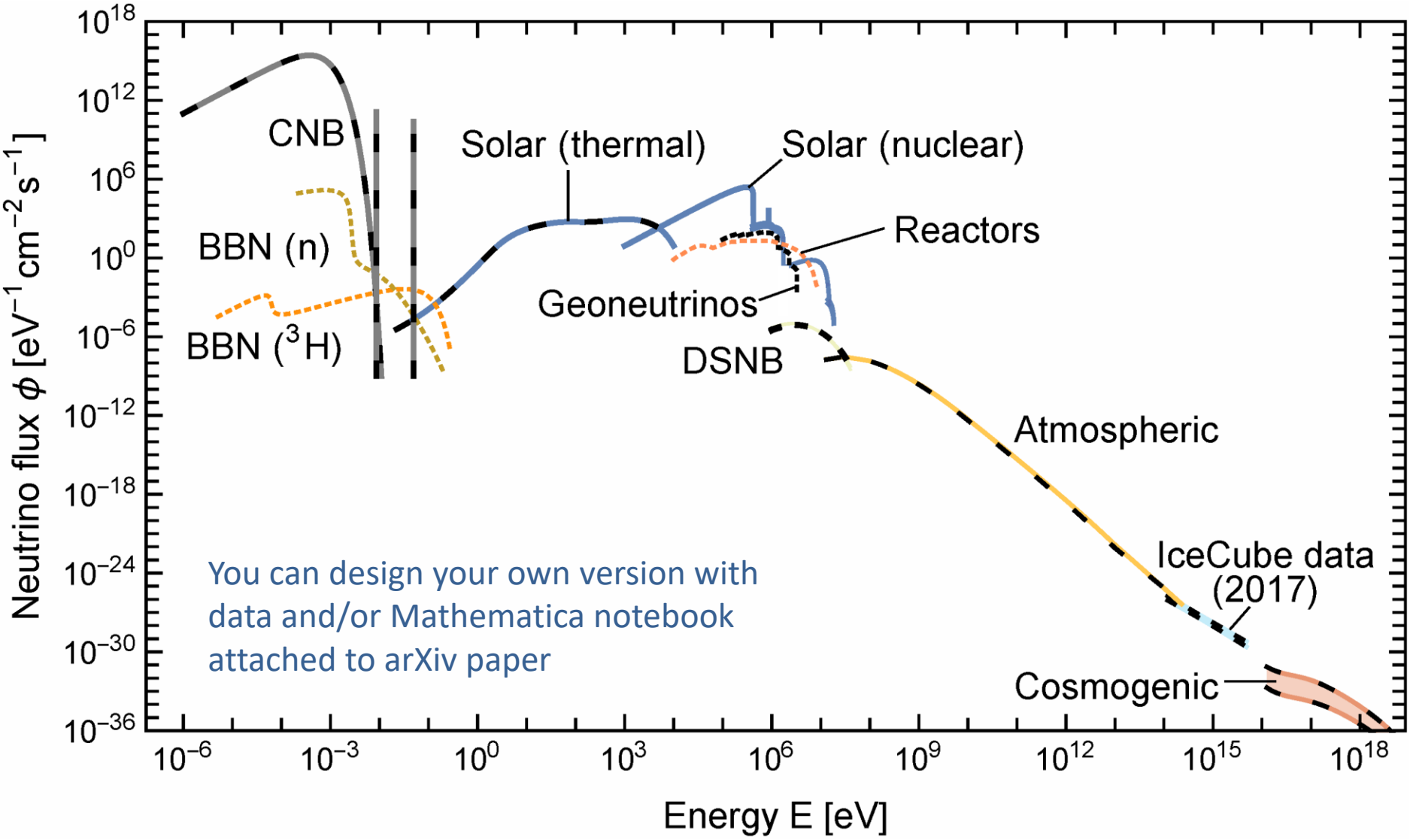

Thermal Neutrinos: Production Processes

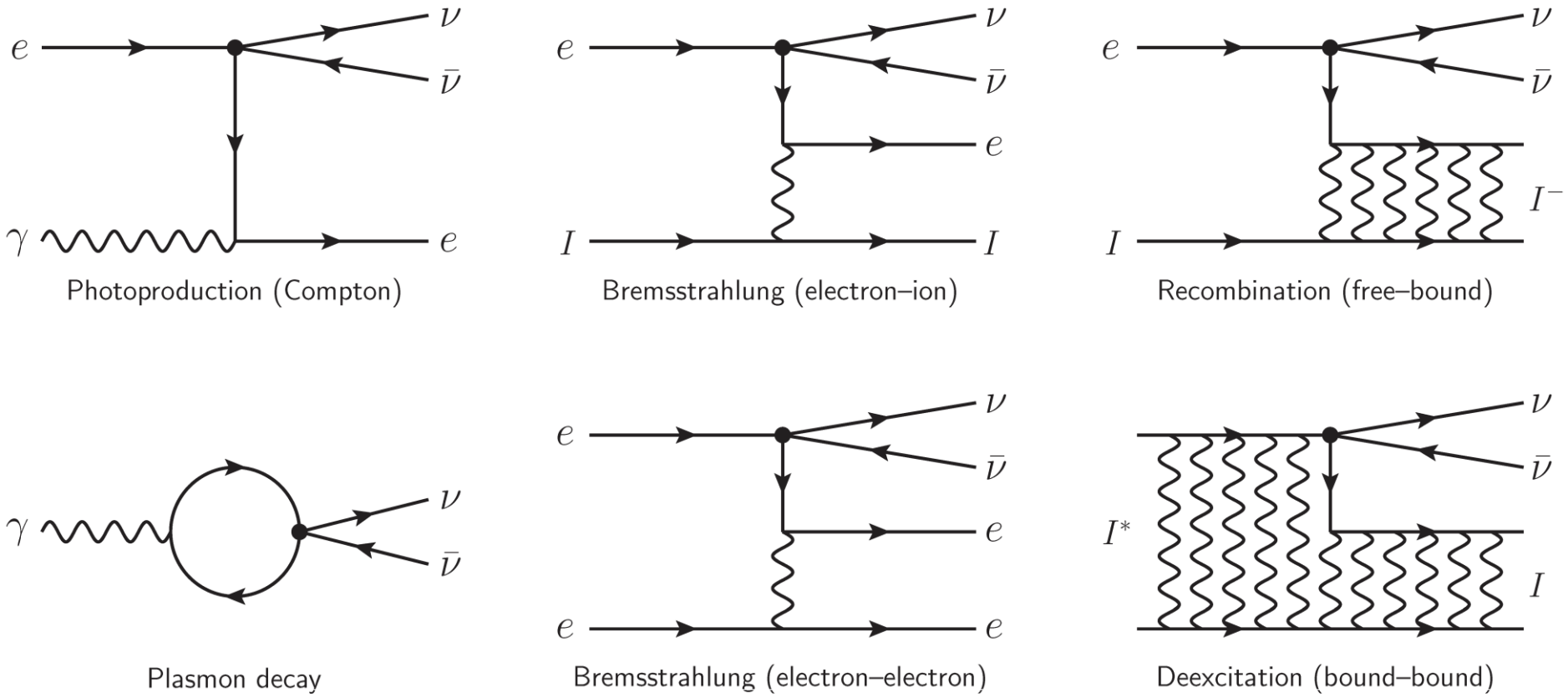

Figure 1. Processes for thermal neutrino pair production in the Sun.

Vitagliano, Redondo & Raffelt, arXiv:1708.02248

Thermal Axions: Production Processes

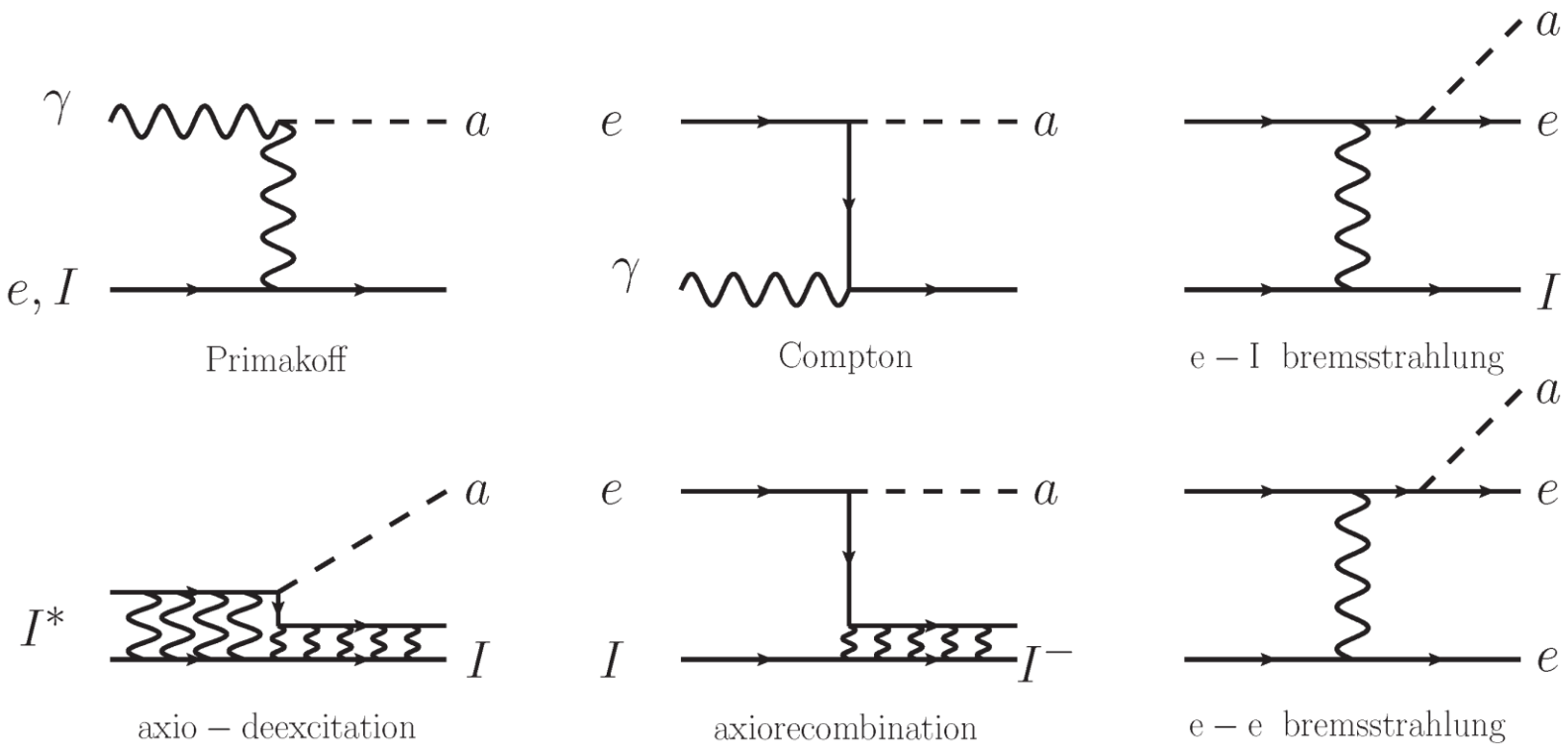

Figure 1. ABC reactions responsible for the solar axion flux in non-hadronic axion models.

Redondo, arXiv:1310.0823

Temperature in the Sun

Virial Theorem $\langle E_{\rm kin}\rangle = -\frac{1}{2}\langle E_{\rm grav}\rangle$

Approximate Sun as a homogeneous sphere with

Mass $M_{\rm sun} = 1.99 \times 10^{33}\,{\rm g}$

Radius $R_{\rm sun} = 6.96 \times 10^{10}\,{\rm cm}$

Gravitational potential energy of a proton near center of the sphere

$$\langle E_{\rm grav}\rangle = -\frac{3}{2}\frac{G_N M_{\rm sun} m_p}{R_{\rm sun}} = -3.2\ {\rm keV}$$

Thermal velocity distribution

$$\langle E_{\rm kin}\rangle = \frac{3}{2}k_{\rm B}T = -\frac{1}{2}\langle E_{\rm grav}\rangle$$

Estimated temperature

$T = 1.1\ {\rm keV}$

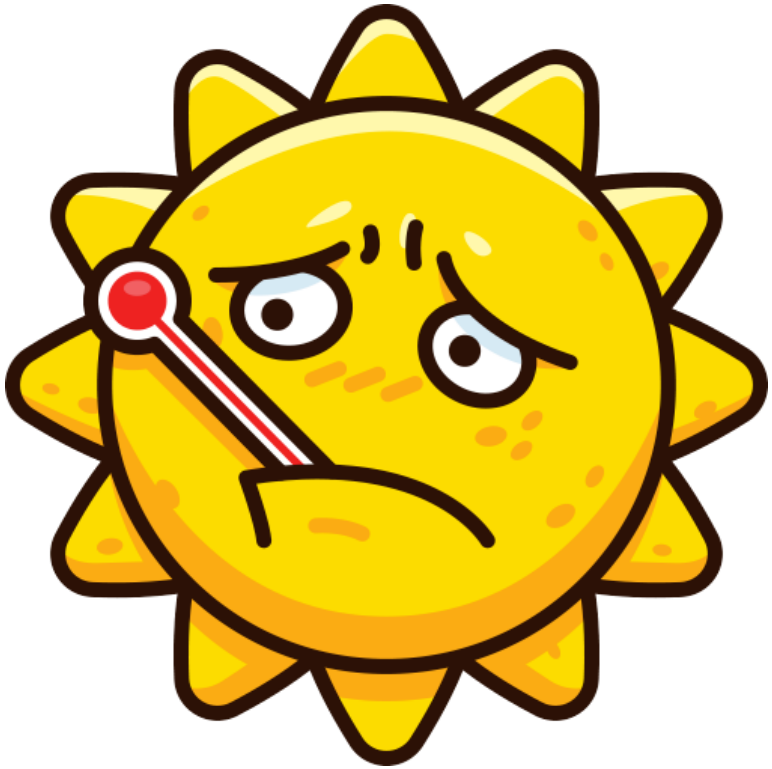

Central temperature from standard solar models

$T_{\rm c} = 1.56 \times 10^{7}\,{\rm K} = 1.34\ {\rm keV}$

Virial Theorem – Dark Matter in Galaxy Clusters

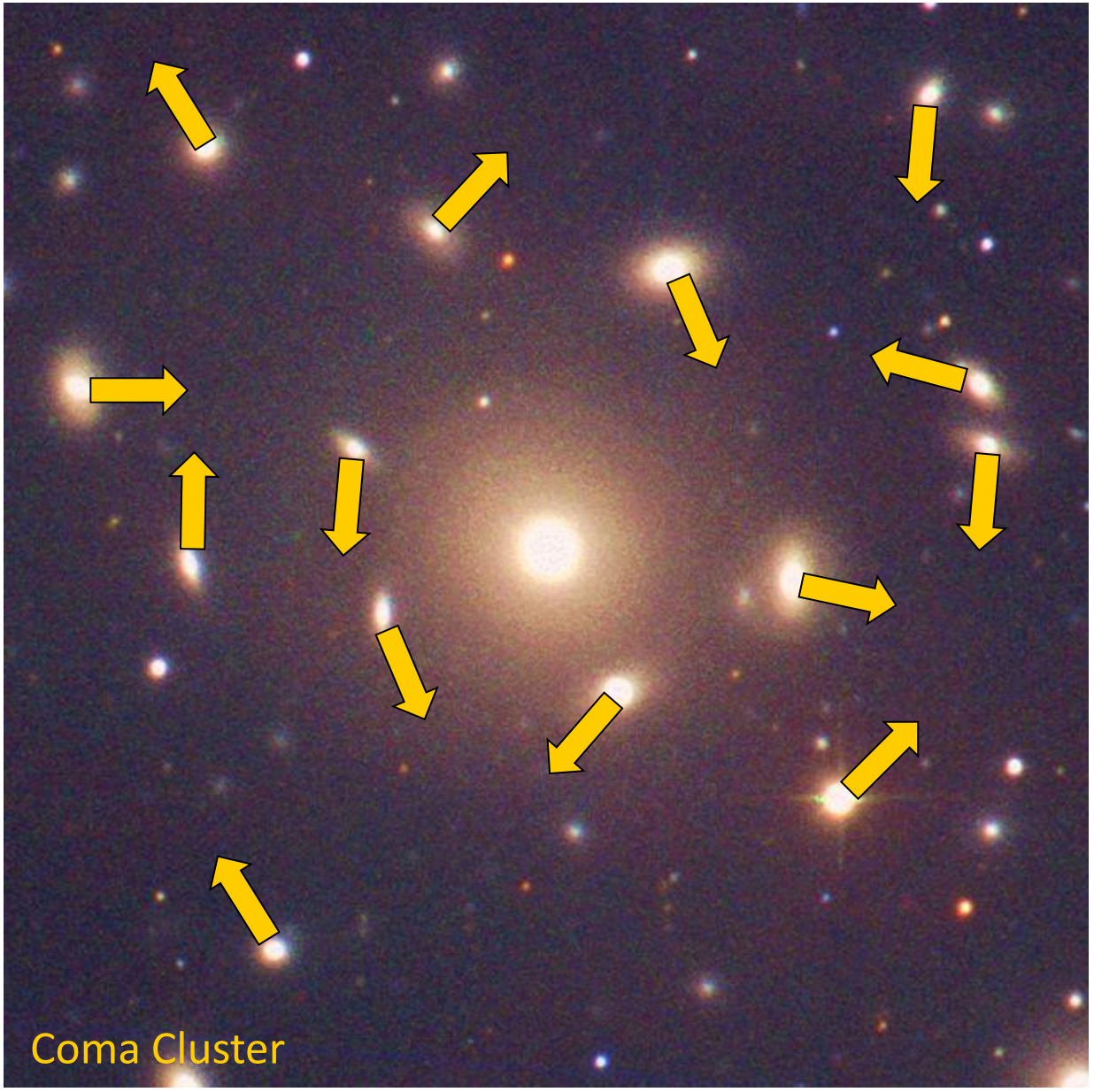

A gravitationally bound system of many particles obeys the virial theorem

$$2\langle E_{\mathrm{kin}}\rangle = -\langle E_{\mathrm{grav}}\rangle$$

$$2\left\langle \frac{mv^2}{2}\right\rangle = \left\langle \frac{G_N M_r m}{r}\right\rangle$$

$$\langle v^2\rangle \approx G_N M_r \langle r^{-1}\rangle$$

Velocity dispersion from Doppler shifts and geometric size

Total Mass

Standard Solar Model: Internal Structure

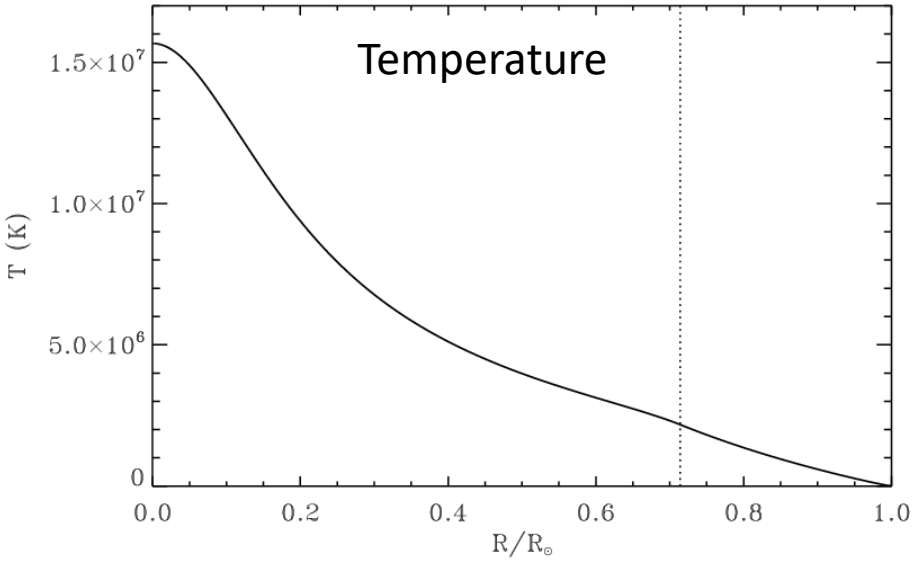

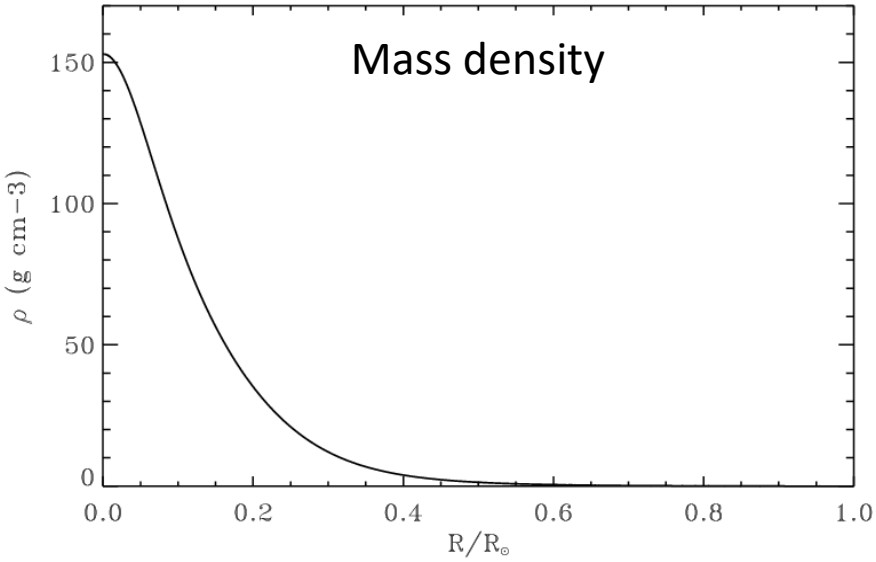

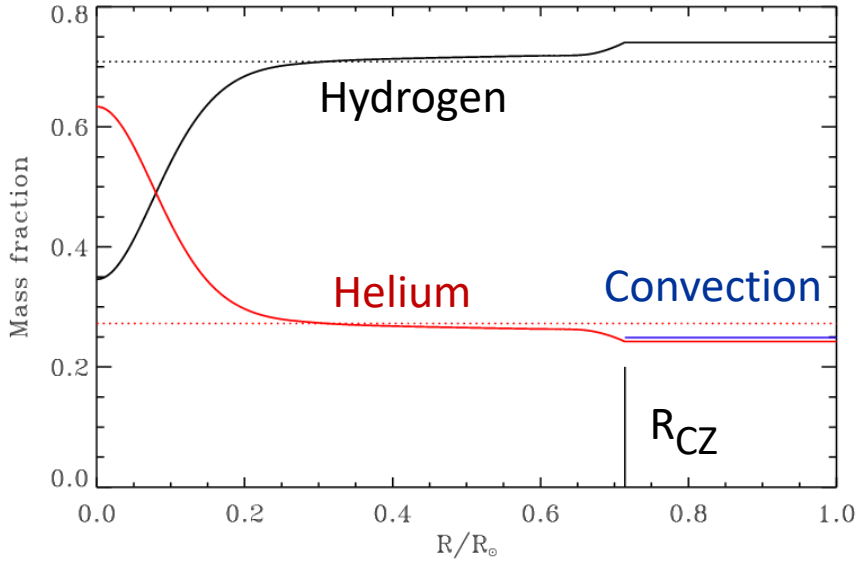

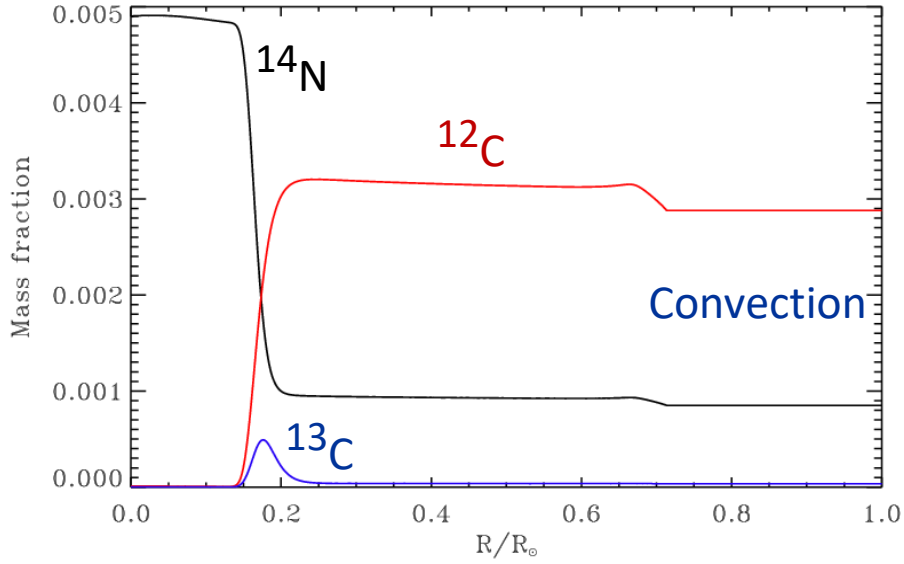

Axion-Photon Coupling

Gluon coupling (generic), defines normalization of axion scale f_a

$$\mathcal{L}_{aG} = \frac{\alpha_s}{8\pi}\frac{a}{f_a} G\tilde{G}$$

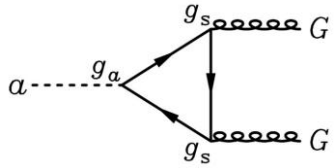

Mass (generic) depends on up/down quark masses

$$m_a = \frac{\sqrt{m_u m_d}}{m_u + m_d}\frac{m_\pi f_\pi}{f_a} = \frac{5.70\ \mu\text{eV}}{f_a/10^{12}\ \text{GeV}}$$

Axion-photon coupling (model dependent)

Generic from a-π-η mixing

$$\mathcal{L}_{a\gamma} = -\frac{g_{a\gamma}}{4} F\tilde{F} a = g_{a\gamma}\,\mathbf{E}\cdot\mathbf{B}\,a = \frac{\alpha}{2\pi}\left(\frac{E}{N} - 1.92\right)\frac{a}{f_a}\mathbf{E}\cdot\mathbf{B}$$

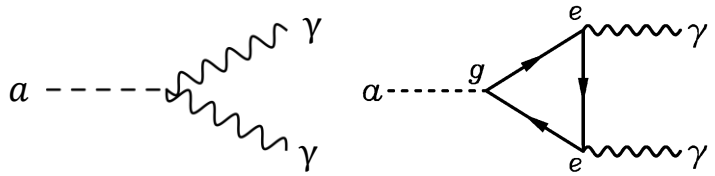

Model-dependent,
E/N = 0 (KSVZ), 8/3 (DFSZ), many others

$$g_{a\gamma} = \left(\frac{E}{N} - 1.92\right)\frac{0.203\ m_a}{\text{GeV}^2} = \left(\frac{E}{N} - 1.92\right) 2.03\times 10^{-16}\ \text{GeV}^{-1}\,\frac{m_a}{1\mu\text{eV}}$$

The QCD axion, precisely, Grilli di Cortona+, 1511.02867

PHYSICAL REVIEW D VOLUME 18, NUMBER 6 15 SEPTEMBER 1978

Astrophysical bounds on the masses of axions and Higgs particles

Rocky Kolb's PhD work

Duane A. Dicus and Edward W. Kolb*
Center for Particle Theory, The University of Texas, Austin, Texas 78712
Vigdor L. Teplitz†
Department of Physics, Virginia Polytechnic Institute and State University, Blacksburg, Virginia 24061
Robert V. Wagoner
Institute of Theoretical Physics, Department of Physics, Stanford University, Stanford, California 94305

(Received 27 April 1978)

Lower bounds on the mass of a light scalar (Higgs) or pseudoscalar (axion) particle are found in three ways: (1) by requiring that their effect on primordial nucleosynthesis not yield a deuterium abundance outside present experimental limits, (2) by requiring that the photons from their decay thermalize and not distort the microwave background, and (3) by requiring that their emission from helium-burning stars (red giants) not disrupt stellar evolution. The best bound is from (3); it requires the axion or Higgs-particle mass to be greater than about 0.2 MeV.

The first process considered is the Primakoff process,[16] $\gamma + Z \to \phi + Z$, shown in Fig. 2. The cross section for this process near threshold is

$$|v|\sigma = 64\pi\alpha Z^2 \frac{\omega\Gamma(\phi\to 2\gamma)}{m_\phi{}^2} \frac{(\omega^2 - m_\phi{}^2)^{1/2}(\omega - m_\phi)}{(m_\phi{}^2 - 2\omega m_\phi)^2}, \quad (7)$$

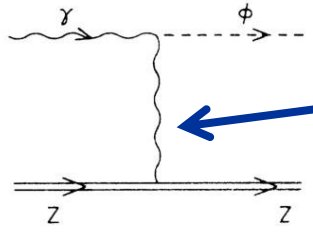

FIG. 2. $\gamma + Z \to \phi + Z$ via the Primakoff process.

First discussion of Primakoff effect for WW axions ($m_a \gg T$)

For "invisible axions" ($m_a \ll T$)
Plasma screening effects crucial
in G.Raffelt's PhD work & PRD 33,897:1986
Still used today

Solar Neutrino Limit on Solar Energy Losses

Self-consistent models of the present-day Sun provide a simple power-law connection between a new energy loss L_a (e.g. axions) and the solar neutrino flux from B^8

Schlattl, Weiss & Raffelt, hep-ph/9807476

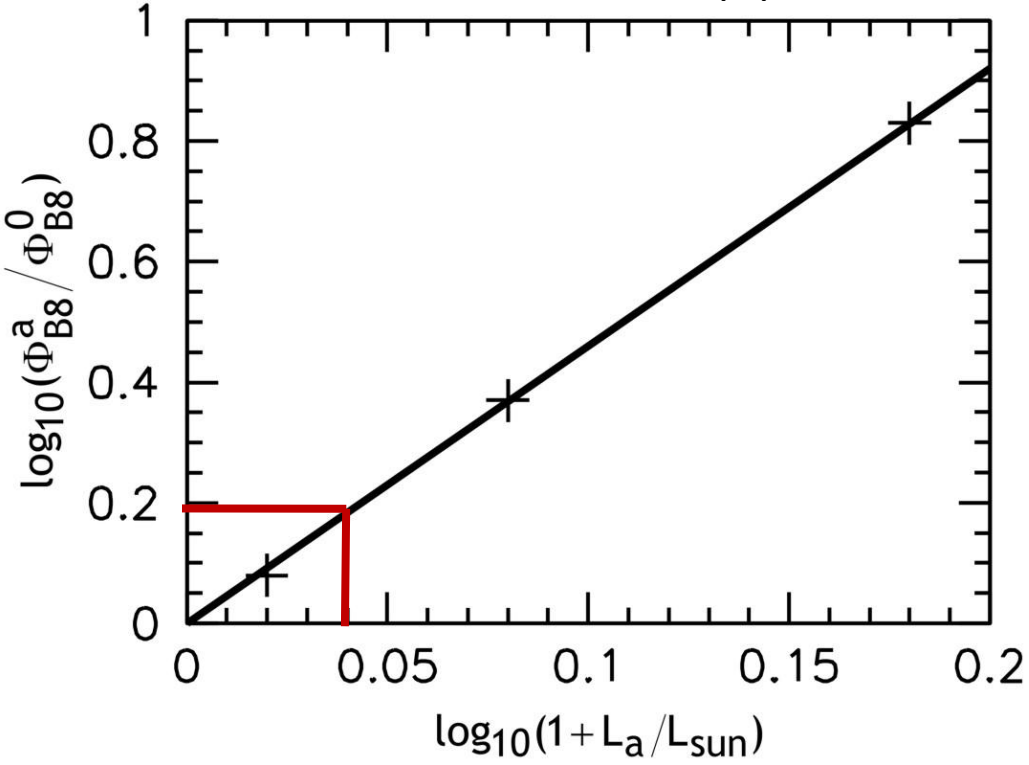

Gondolo & Raffelt, arXiv:0807.2926

$$T_{c,a} = T_{c,0}\left(\frac{L_\odot + L_a}{L_\odot}\right)^{0.22}$$

$$\Phi_{\rm B8} \propto T_c^{18}$$

$$\Phi_{{\rm B8},a} = \Phi_{{\rm B8},a}\left(\frac{L_\odot + L_a}{L_\odot}\right)^{4.6}$$

Solar models with SNO all-flavor measurements imply roughly

$$L_a \lesssim 0.1\, L_\odot$$

$$L_a = \left(\frac{g_{a\gamma}}{10^{-10}\,{\rm GeV}^{-1}}\right)^2 1.85\times 10^{-3} L_\odot \;\Rightarrow\; g_{a\gamma} \lesssim 7\times 10^{-10}\,{\rm GeV}^{-1}$$

Solar Observables Modified by Axion Losses

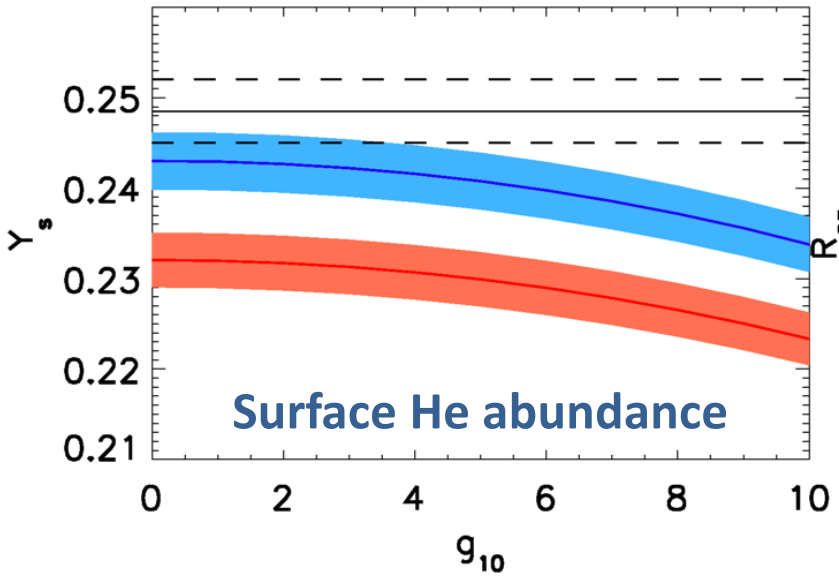

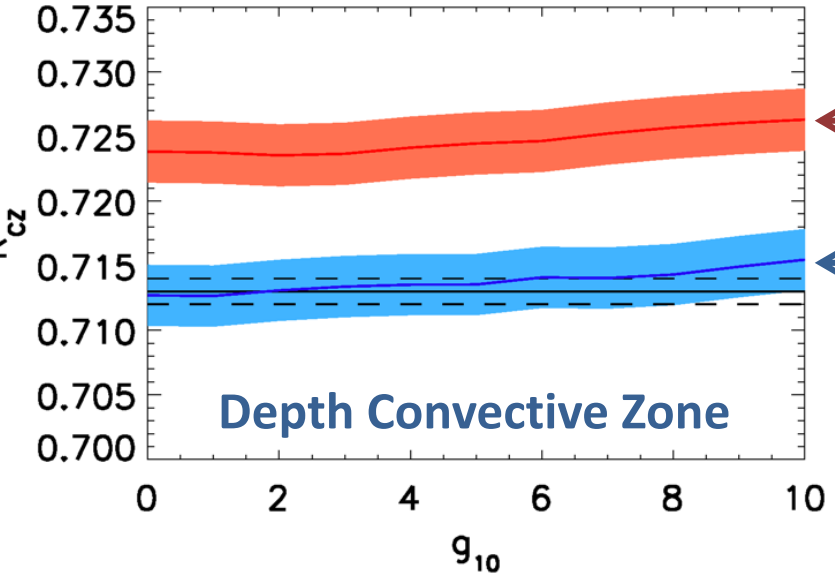

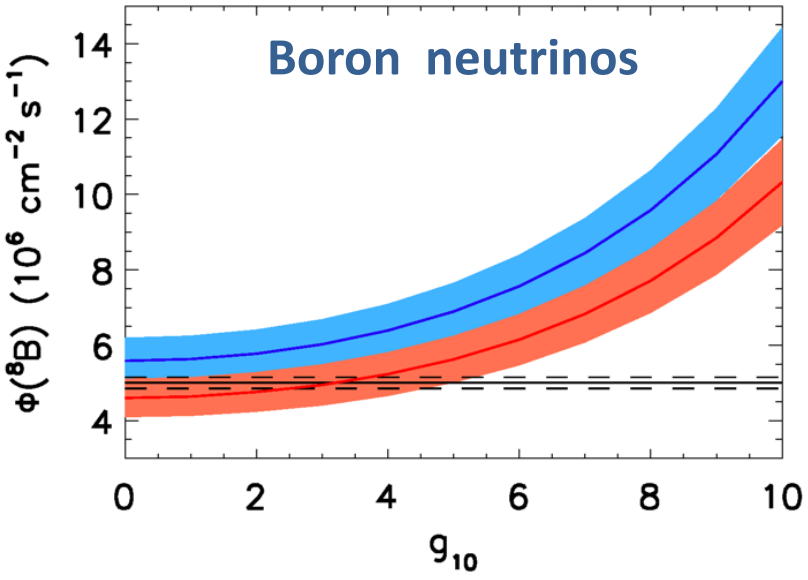

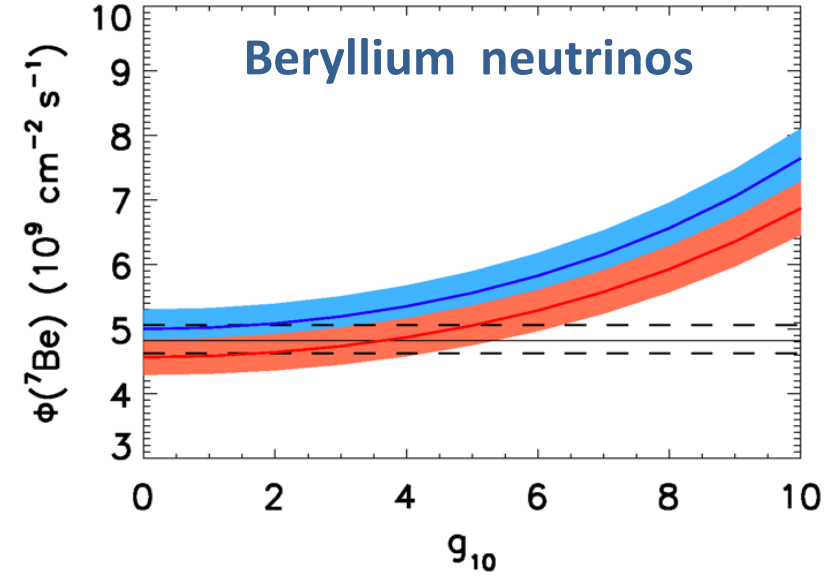

Vinyoles, Serenelli, Villante, Basu, Redondo & Isern, arXiv:1501.01639

Global Fit from Solar Observables

Allow all input parameters to float, including chemical composition, and marginalize except for axion losses

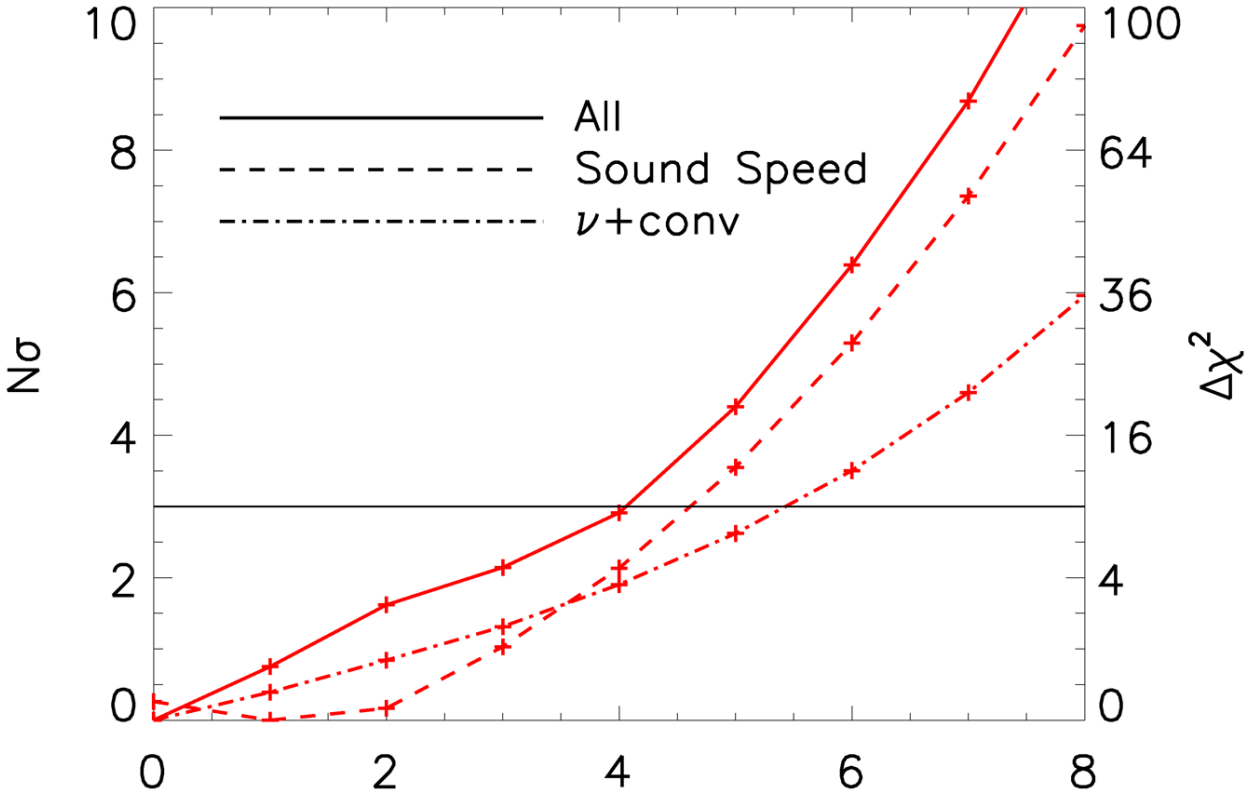

VOLUME 51, NUMBER 16 PHYSICAL REVIEW LETTERS 17 OCTOBER 1983

Experimental Tests of the "Invisible" Axion

P. Sikivie
Physics Department, University of Florida, Gainesville, Florida 32611
(Received 13 July 1983)

Experiments are proposed which address the question of the existence of the "invisible" axion for the whole allowed range of the axion decay constant. These experiments exploit the coupling of the axion to the electromagnetic field, axion emission by the sun, and/or the cosmological abundance and presumed clustering of axions in the halo of our galaxy.

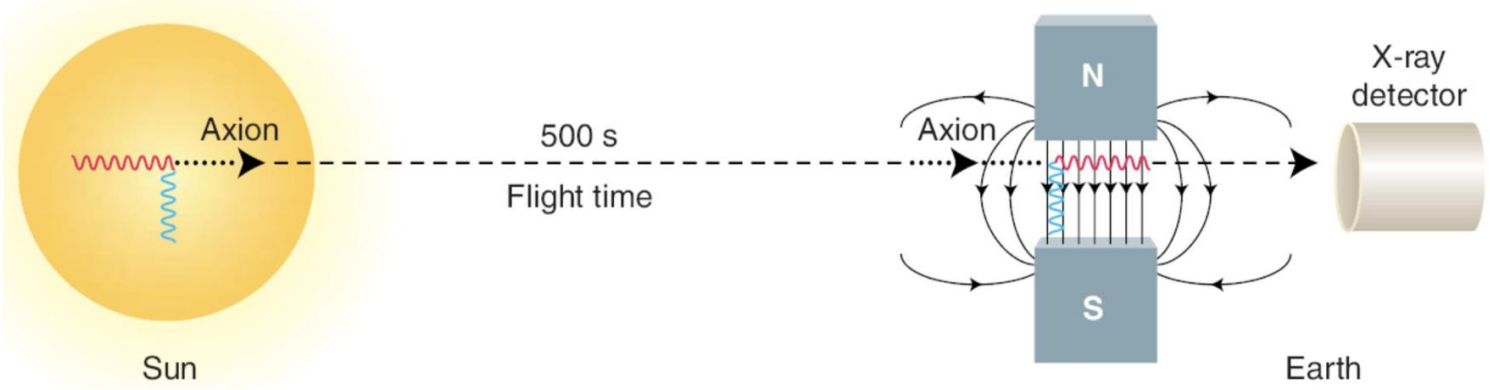

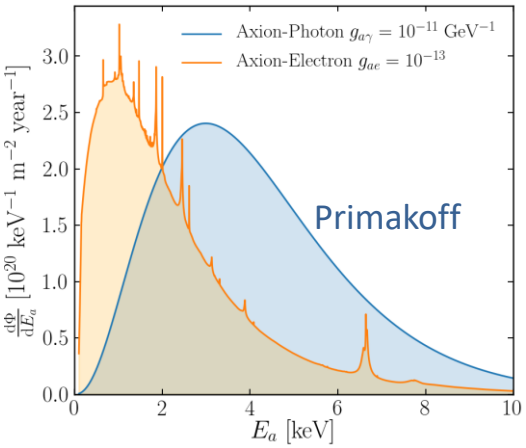

- Large coherence length overcomes small coupling
- Axion-photon conversion in B-field similar to neutrino flavor oscillation, PRD 37 (1988) 1237
- Can be enhanced with gas filling van Bibber+ PRD 39 (1989) 2089

https://cajohare.github.io/IAXOmass/

Let's point a magnet at the sun…

© Sebastian Baum

…and look for X-Rays!

Rochester-Brookhaven-FermiLab

Lazarus+ PRL 69 (1992) 2333

Few hours of data, fixed magnet

$G_{a\gamma\gamma} < 0.77 \times 10^{-8}\ \mathrm{GeV}^{-1}$

Tokyo Helioscope (Sumico)

Fully stearable, 2.3 m long, 4 Tesla

Moriyama+ [hep-ex/9805026]

$G_{a\gamma\gamma} < 0.60 \times 10^{-9}\ \mathrm{GeV}^{-1}$

See also Ohta+ [1201.4622]

CAST (1998–2021)

Stearable, 9.26 m long, 9 Tesla

Anastassopoulos+ [1705.02290]

$G_{a\gamma\gamma} < 0.66 \times 10^{-10}\ \mathrm{GeV}^{-1}$

CAST Movie on YouTube

https://youtu.be/XY2lFDXz8aQ

Where is the Sun?

Visual Sun,
near horizon lifted by
atmospheric refraction by
approx. one solar diameter

Axion Sun
at true position

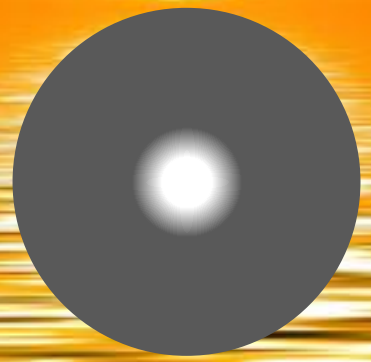

Axion-Photon-Transitions as Particle Oscillations

Raffelt & Stodolsky, PRD 37 (1988) 1237

Photon refractive and birefringence effects
(Faraday rotation, Cotton-Mouton-effect)

Stationary Klein-Gordon equation for coupled a-γ-system

$$\left[\omega^2 + \nabla^2 + 2\omega^2 \begin{pmatrix} n_\perp - 1 & n_F & 0 \\ n_F & n_\parallel & \frac{g_{a\gamma}B}{2\omega} \\ 0 & \frac{g_{a\gamma}B}{2\omega} & -\frac{m_a^2}{2\omega^2} \end{pmatrix}\right] \begin{pmatrix} A_\perp \\ A_\parallel \\ a \end{pmatrix} = 0$$

Axion-photon transitions

- Axions roughly like another photon polarization state
- In a homogeneous or slowly varying B-field, a photon beam develops a coherent axion component

Axion-Photon Conversion in CAST

$$P(a \to \gamma) = \left(\frac{g_{a\gamma} B L}{2} \frac{\sin(qL/2)}{qL/2} \right)^2 = \left(\frac{g_{a\gamma} B}{2} \right)^2 \times \begin{cases} L^2 & \text{for } qL \ll 1 \\ 1/2q^2 & \text{for } qL \gg 1 \end{cases}$$

Momentum transfer $q = (m_a^2 - m_\gamma^2)/2\omega$

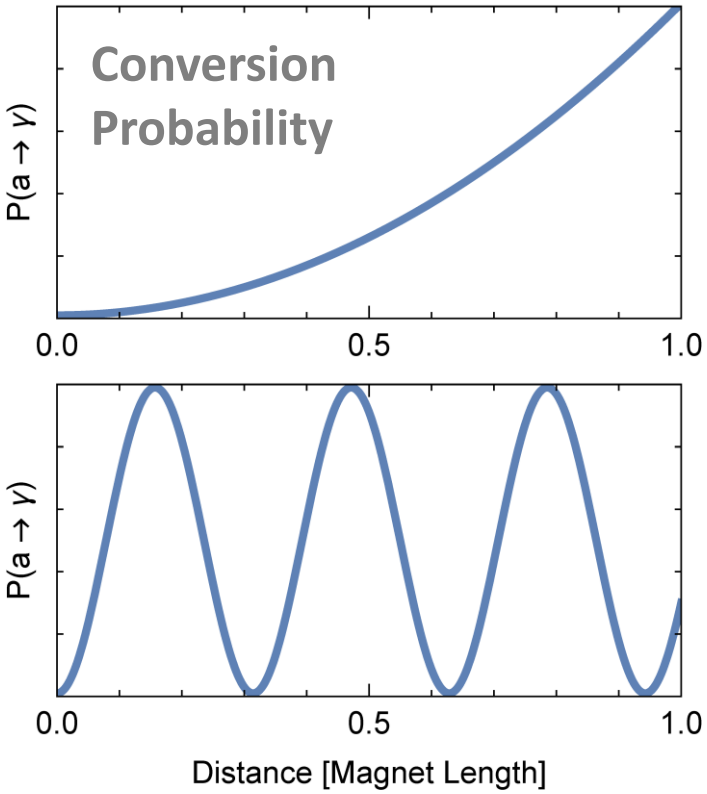

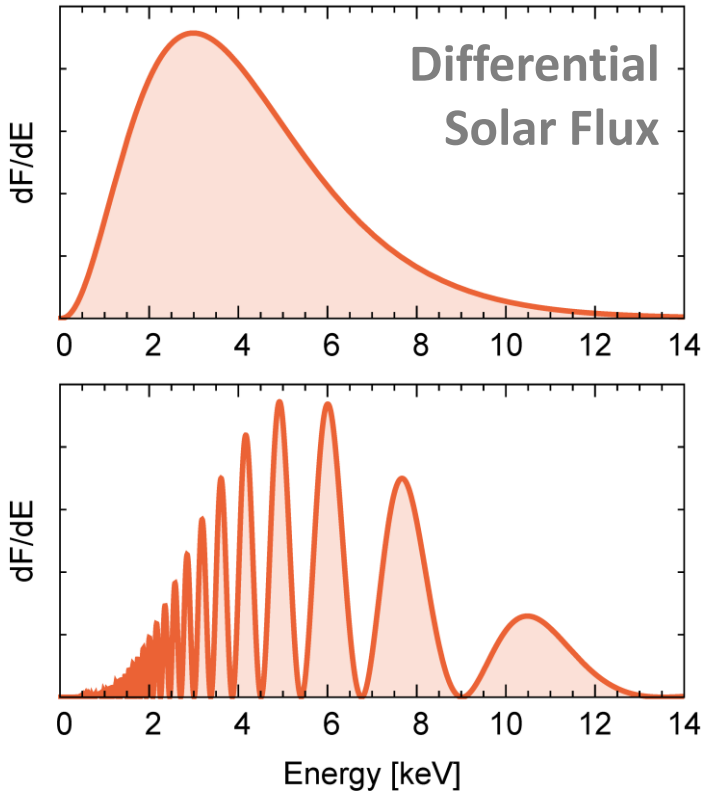

Small mass ("coherent")

Large mass ("incoherent")

Can "weigh" axions
arXiv:1811.09290

Parameter Space for Axion-Like Particles (ALPs)

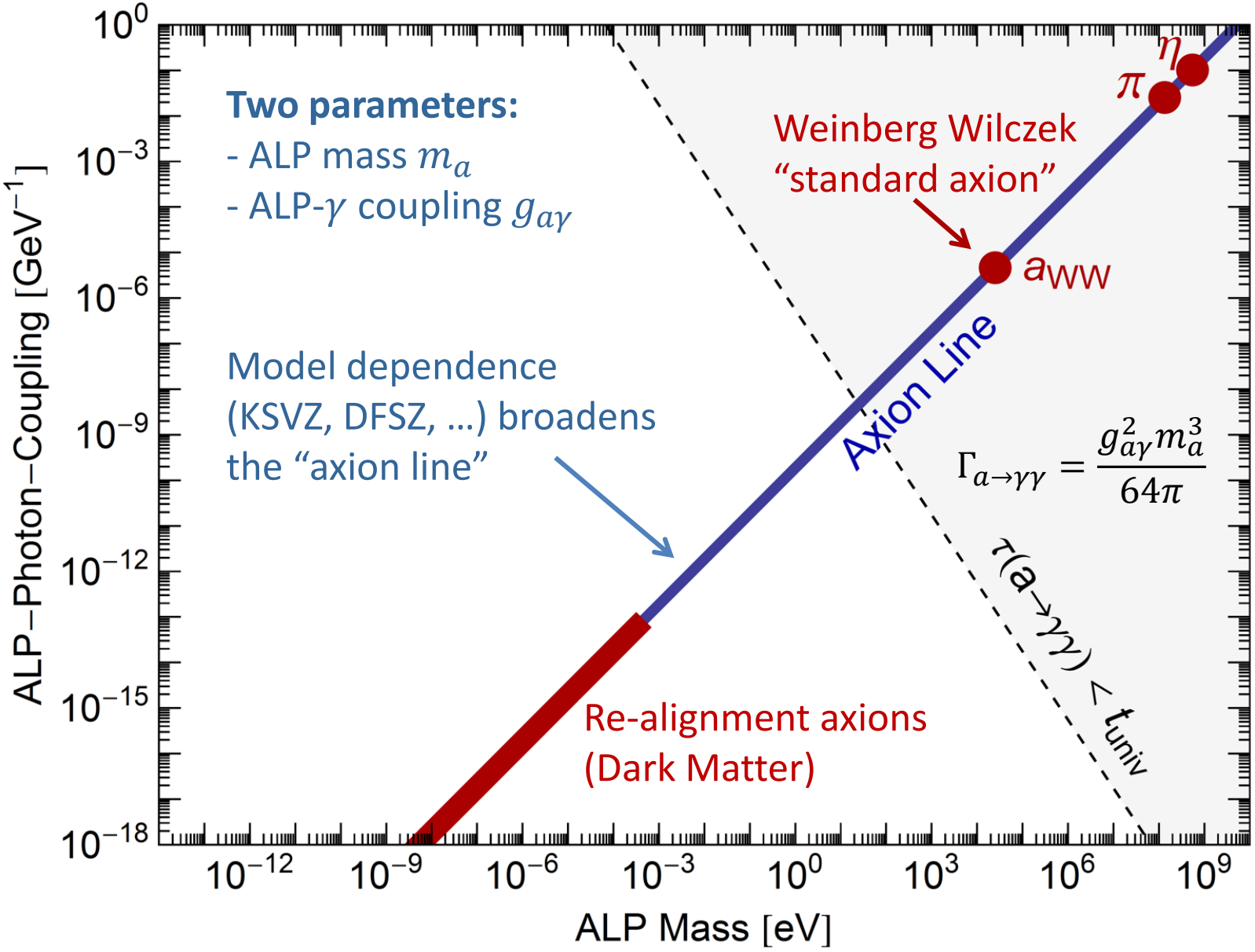

Parameter Space for Axion-Like Particles (ALPs)

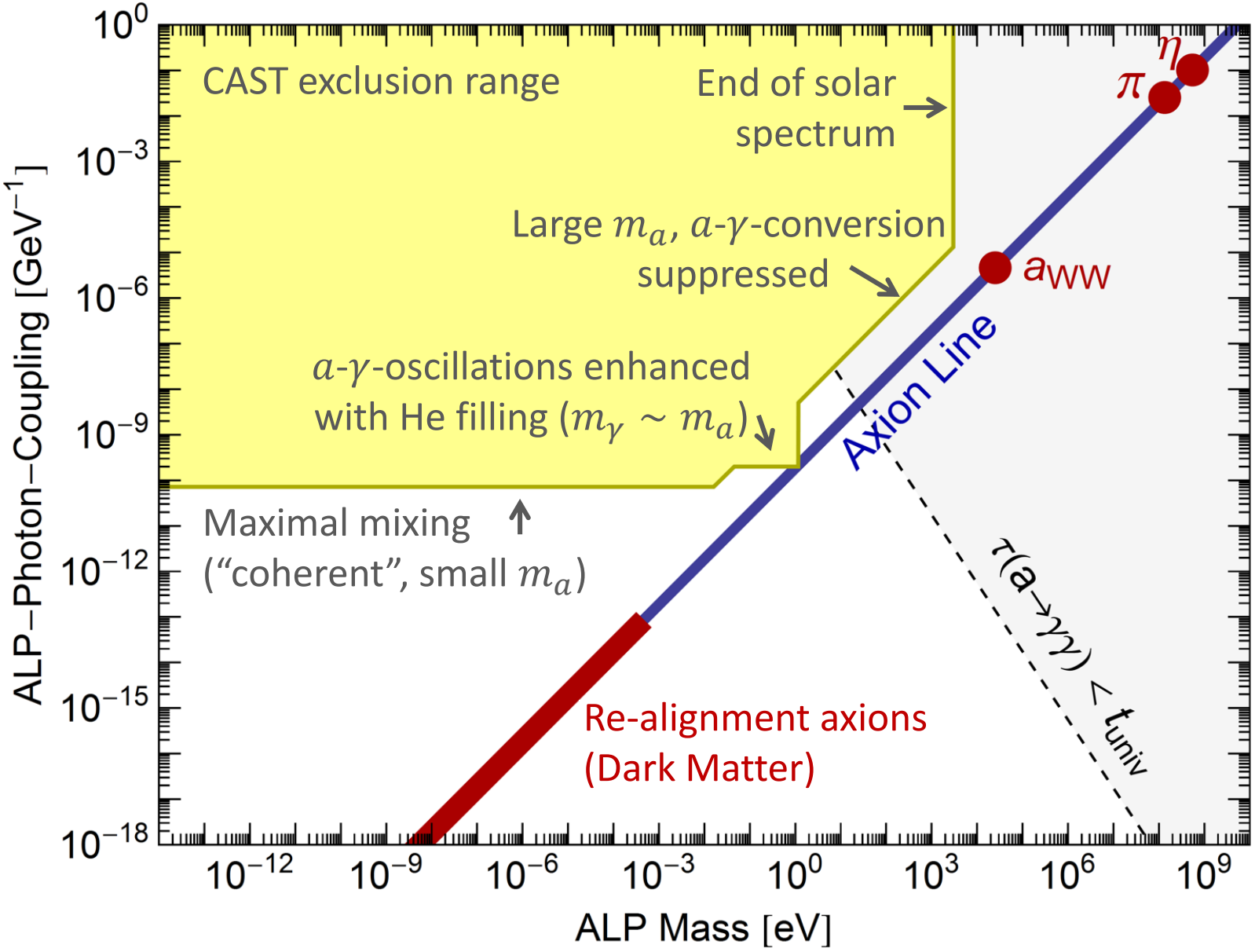

Extending to higher mass values with gas filling

Axion-photon transition probability

$$P_{a\to\gamma} = \left(\frac{g_{a\gamma}B}{q}\right)^2 \sin^2\left(\frac{qL}{2}\right)$$

Axion-photon momentum transfer

$$q = \left|\frac{m_a^2 - m_\gamma^2}{2E}\right|$$

Transition is suppressed for $qL \gtrsim 1$

Gas filling: Give photons a refractive mass to restore full transition strength

$$m_\gamma^2 = \frac{4\pi\alpha}{m_e}\, n_e$$

$$m_\gamma = 28.9\ \text{eV}\left(\frac{Z}{A}\,\rho_{\text{gas}}\right)^{1/2}$$

He-4 vapour pressure at 1.8 K is

$$\rho \approx 0.2 \times 10^{-3}\ \text{g cm}^{-3}$$

$$m_\gamma = 0.4\ \text{eV}$$

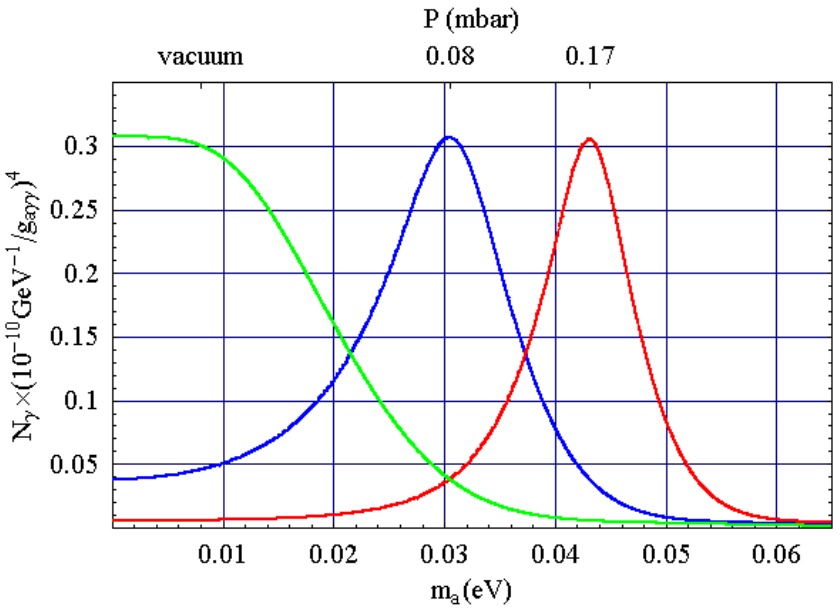

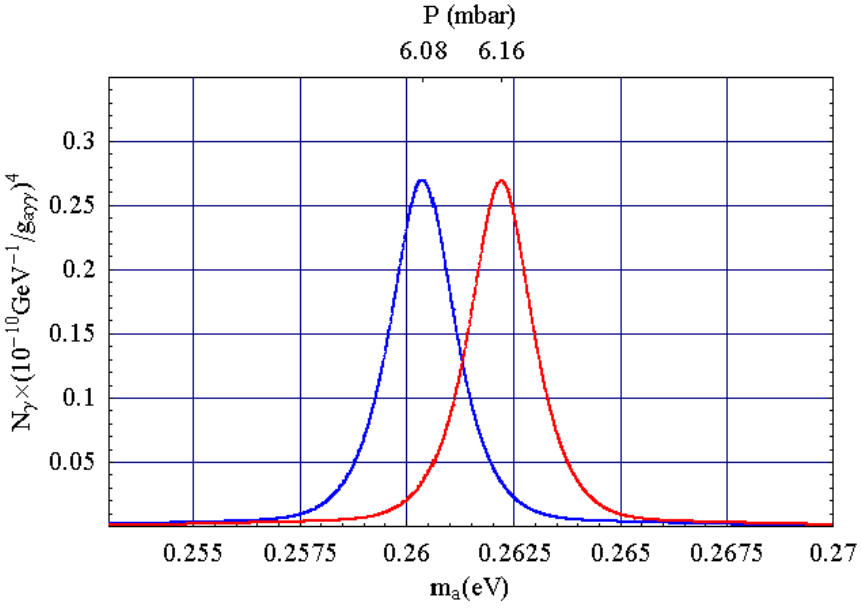

Helioscope Limits

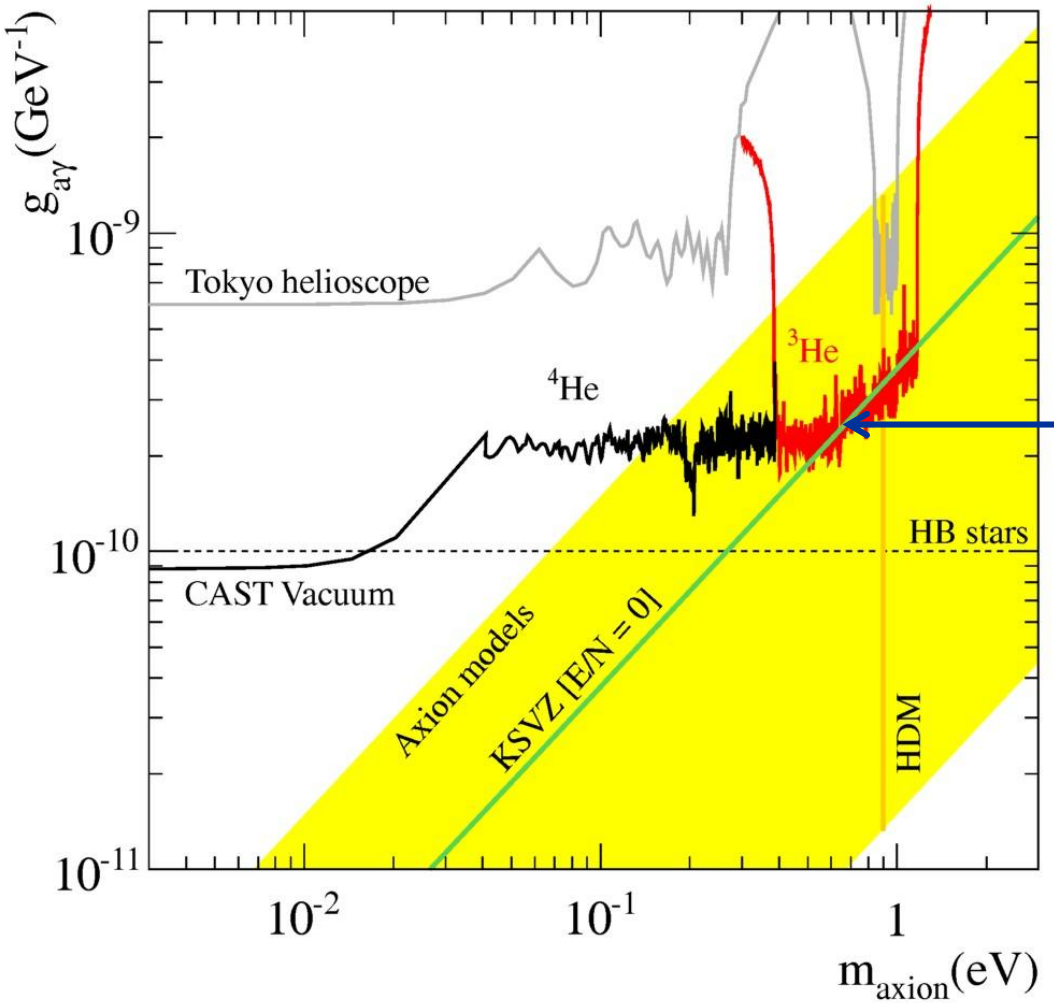

First experimental crossing of the KSVZ line

CAST-I results: PRL 94:121301 (2005) and JCAP 0704 (2007) 010
CAST-II results (He-4 filling): JCAP 0902 (2009) 008
CAST-II results (He-3 filling): PRL 107: 261302 (2011) and PRL 112, 091302 (2014)

Advanced Helioscope

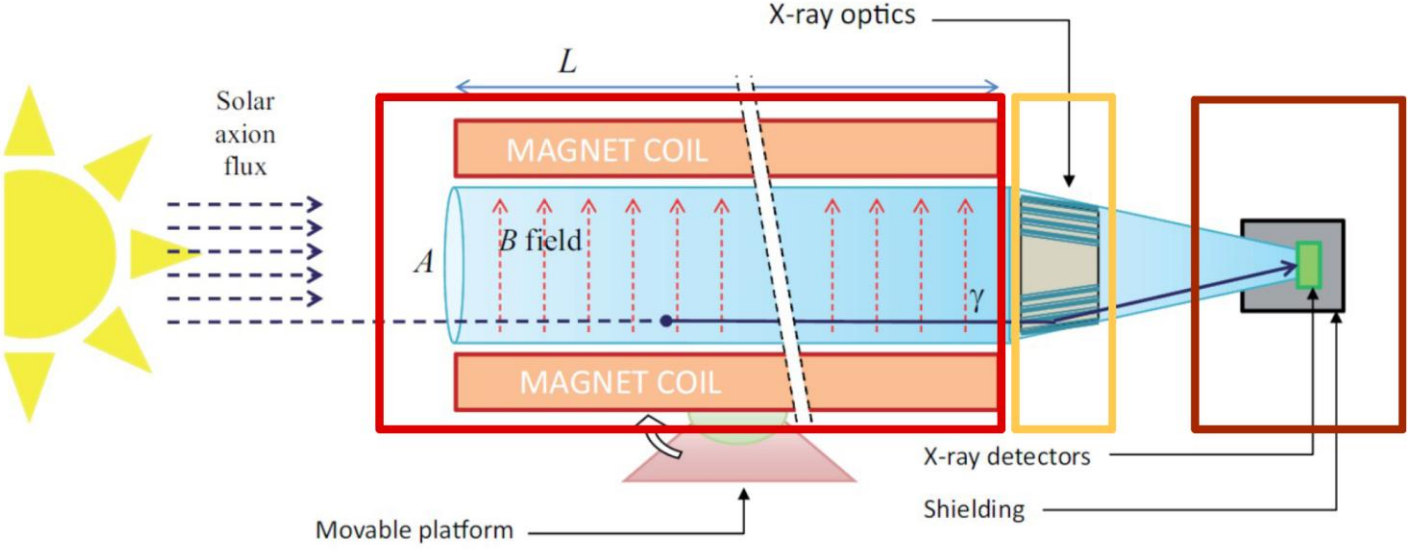

Sensitivity to axion-photon coupling

$$g_{a\gamma}^4 \propto \boxed{B^2 L^2 A} \cdot \boxed{\varepsilon_o \alpha^{-1/2}} \cdot \boxed{\varepsilon_d b^{-1/2}} \cdot \boxed{\varepsilon_t t^{-1/2}}$$

Magnet | Optics | Detector | Time

CAST, BabyIAXO, IAXO

- 20 years experience from CAST
- IAXO will have a 300 times better magnet Figure of merit (FoM)
- BabyIAXO an intermediate state technology demonstrator
- BabyIAXO will be built at DESY (Hamburg)

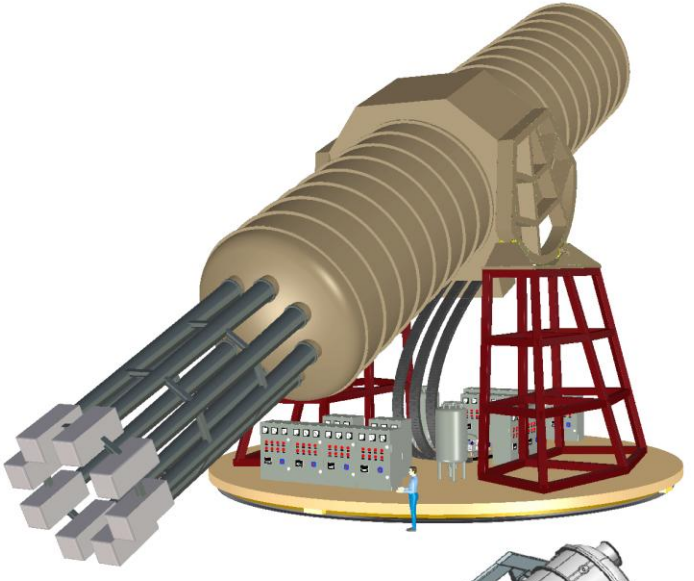

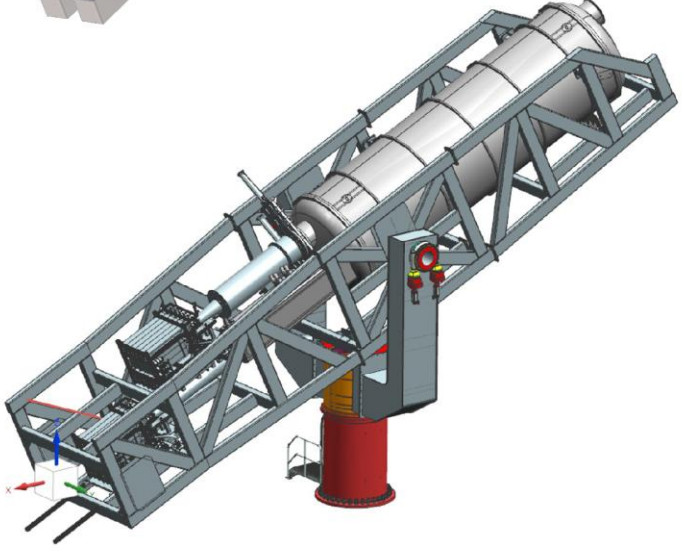

(Baby) IAXO Sensitivity Forecast

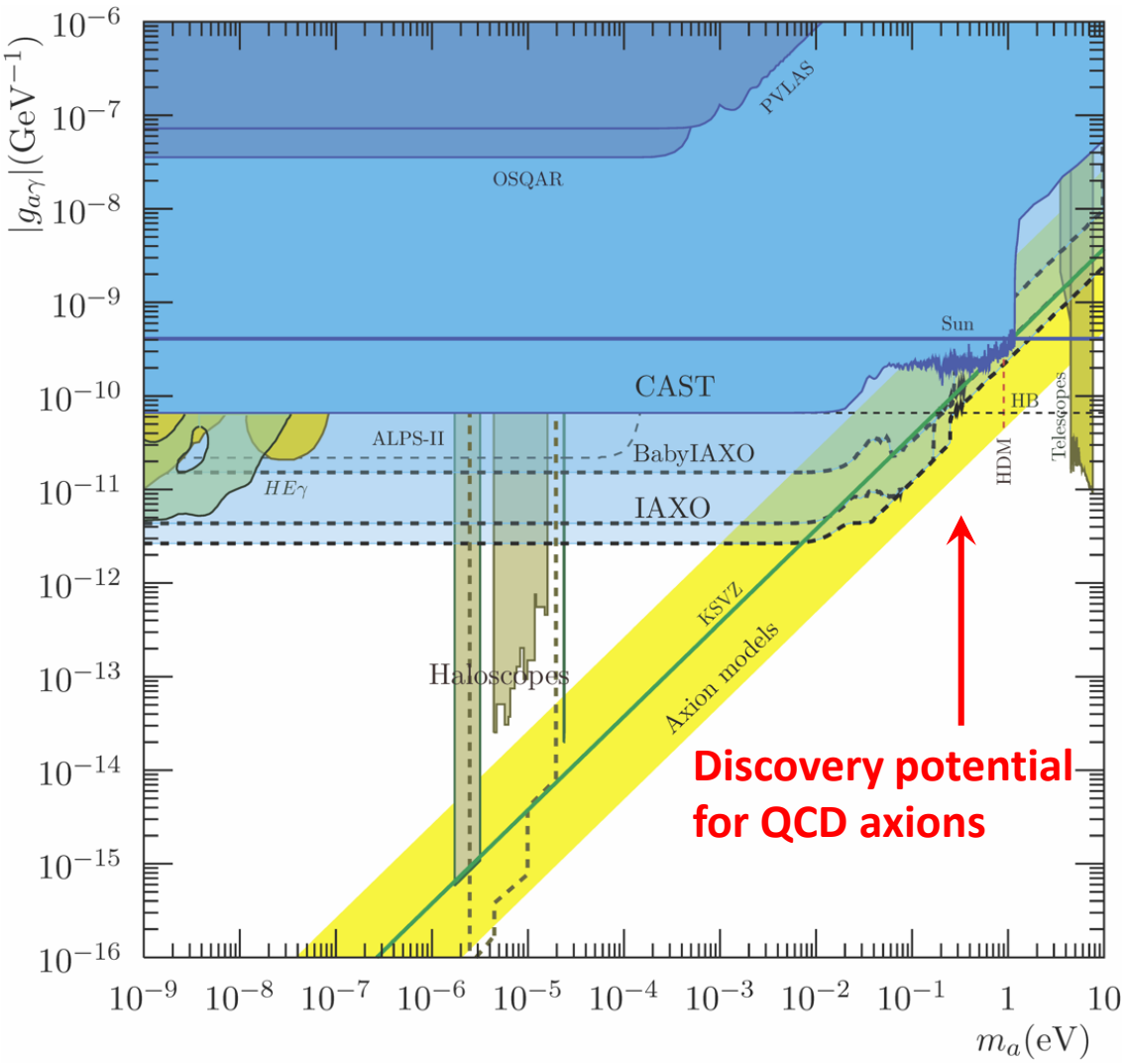

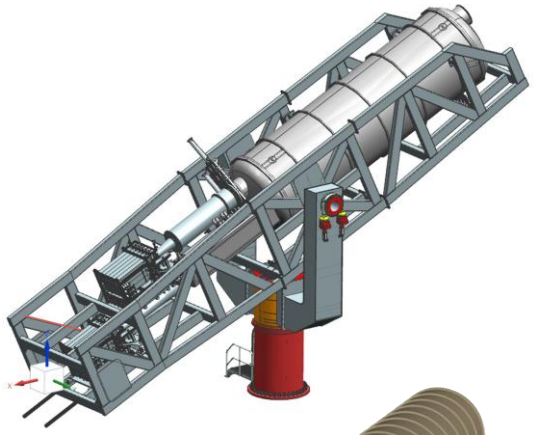

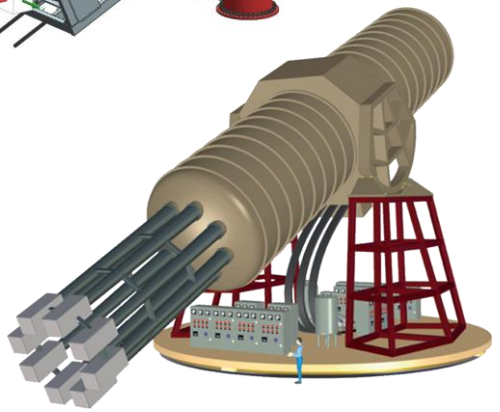

Physics potential of the International Axion Observatory (IAXO)
JCAP 1906 (2019) 047, arXiv:1904.09155

Grand Unified ALP Scape

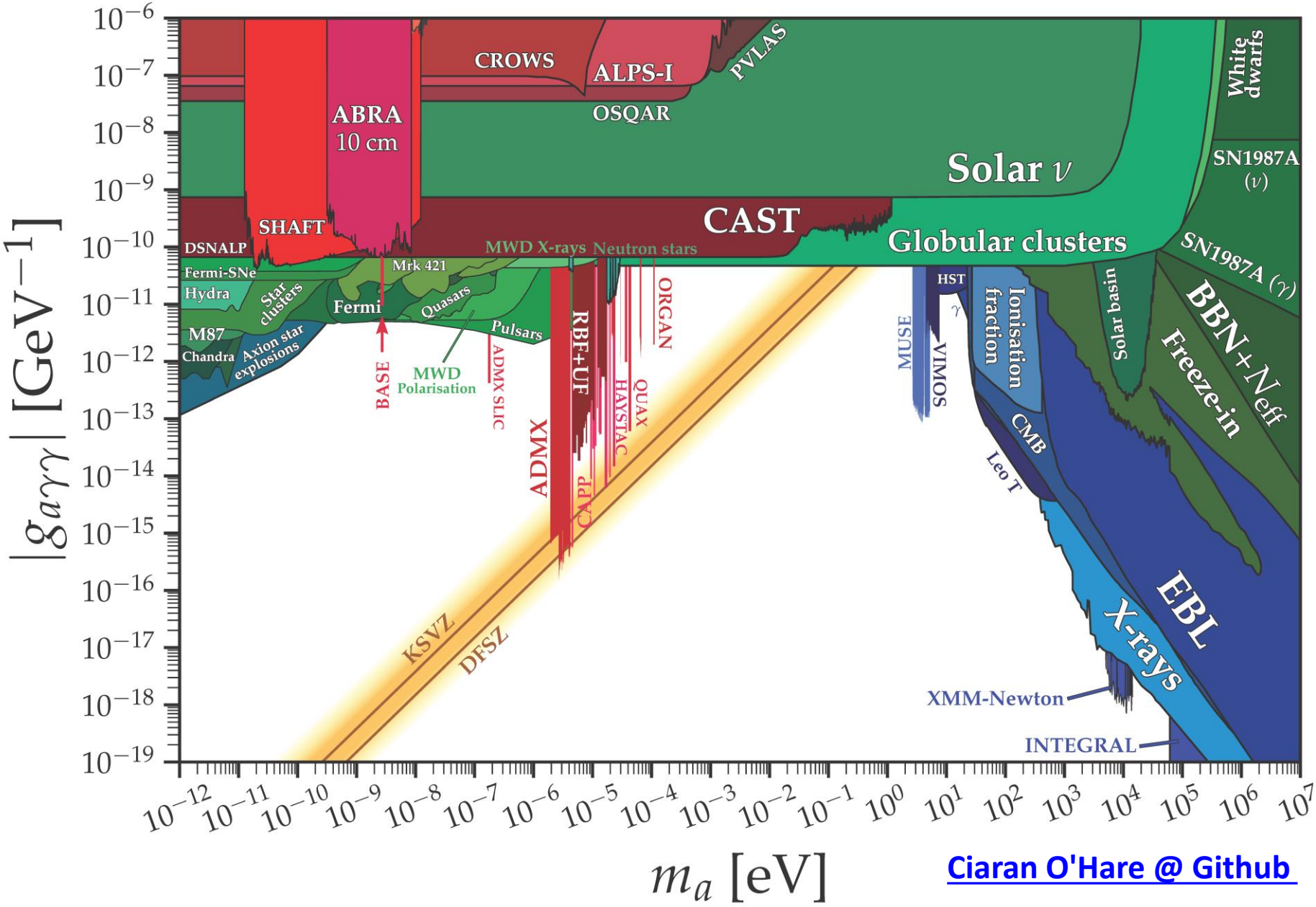

Ciaran O'Hare @ Github

Axion Emission – Backreaction on Stars

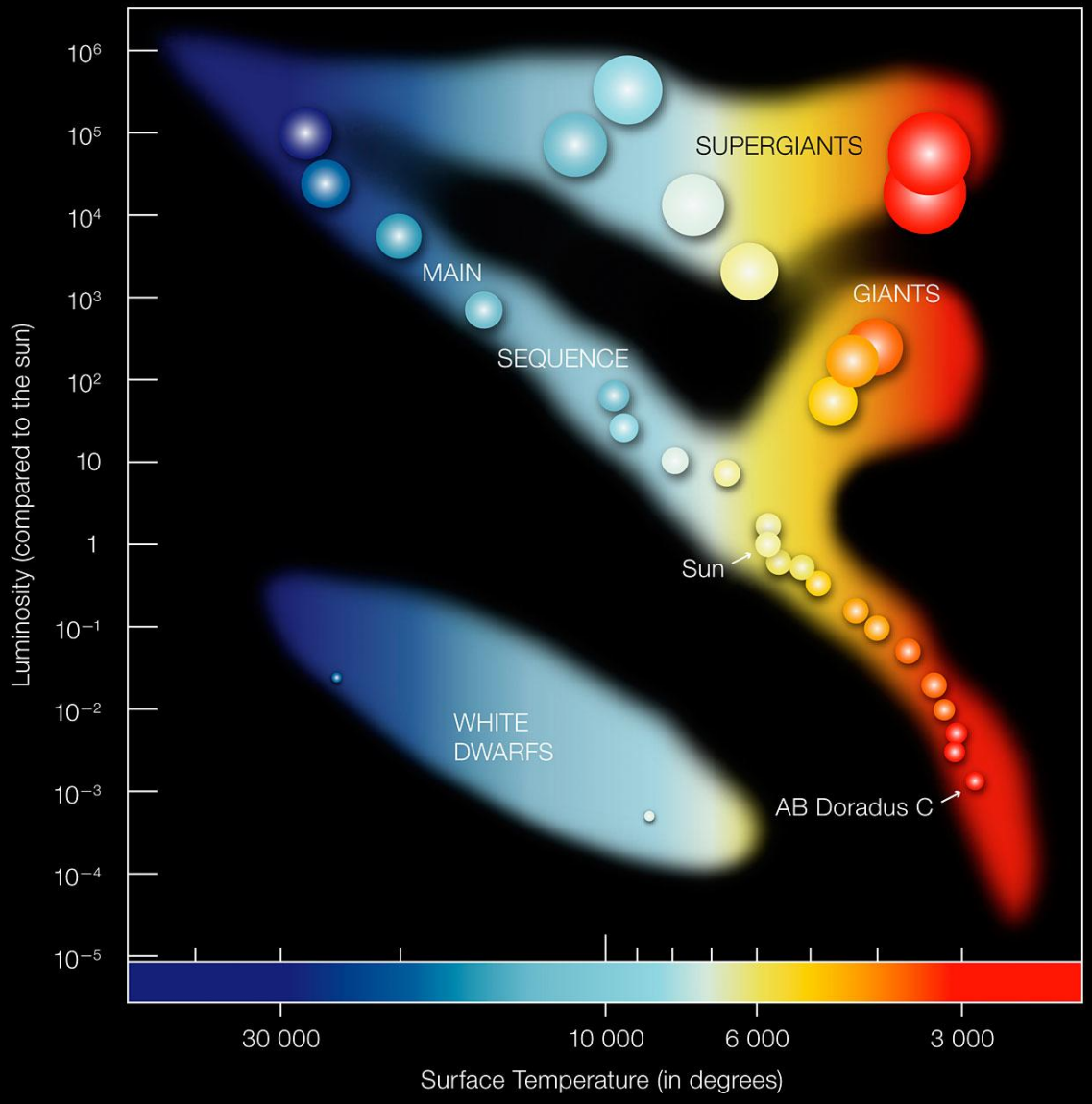

Hertzsprung Russell Diagram

https://www.eso.org/public/images/eso0728c/

Equations of Stellar Structure

Assume spherical symmetry and static structure (neglect kinetic energy)
Excludes: Rotation, convection, magnetic fields, supernova-dynamics, …

Hydrostatic equilibrium

$$\frac{dP}{dr} = -\frac{G_N M_r \rho}{r^2}$$

Energy conservation

$$\frac{dL_r}{dr} = 4\pi r^2 \epsilon \rho$$

Energy transfer

$$L_r = \frac{4\pi r^2}{3\kappa\rho}\frac{d\left(aT^4\right)}{dr}$$

Literature

- Clayton: Principles of stellar evolution and nucleosynthesis (Univ. Chicago Press 1968)
- Kippenhahn & Weigert: Stellar structure and evolution (Springer 1990)

r	Radius from center
P	Pressure
G_N	Newton's constant
ρ	Mass density
M_r	Integrated mass up to r
L_r	Luminosity (energy flux)
ϵ	Local rate of energy generation $[\mathrm{erg\,g^{-1}s^{-1}}]$ $\epsilon = \epsilon_{\mathrm{nuc}} + \epsilon_{\mathrm{grav}} - \epsilon_{\nu}$
κ	Opacity $\kappa^{-1} = \kappa_{\gamma}^{-1} + \kappa_{\mathrm{c}}^{-1}$
κ_{γ}	Radiative opacity $\kappa_{\gamma}\rho = \langle\lambda_{\gamma}\rangle_{\mathrm{Rosseland}}^{-1}$
κ_{c}	Electron conduction

Convection in Main-Sequence Stars

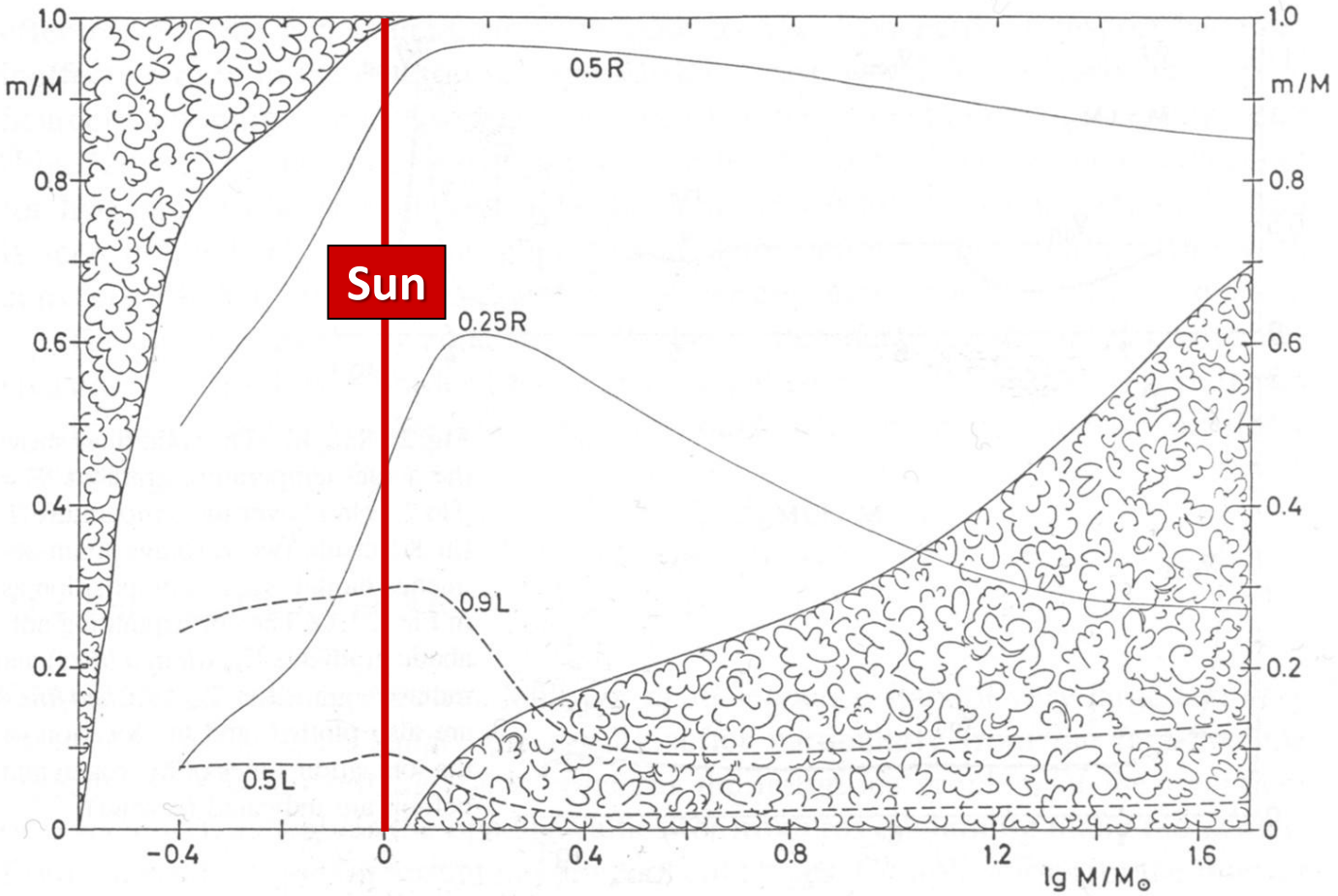

Fig. 22.7. The mass values m from centre to surface are plotted against the stellar mass M for the same zero-age main-sequence models as in Fig. 22.1. "Cloudy" areas indicate the extension of convective zones inside the models. Two solid lines give the m values at which r is 1/4 and 1/2 of the total radius R. The dashed lines show the mass elements inside which 50% and 90% of the total luminosity L are produced

Kippenhahn & Weigert, Stellar Structure and Evolution

Self-Regulated Nuclear Burning

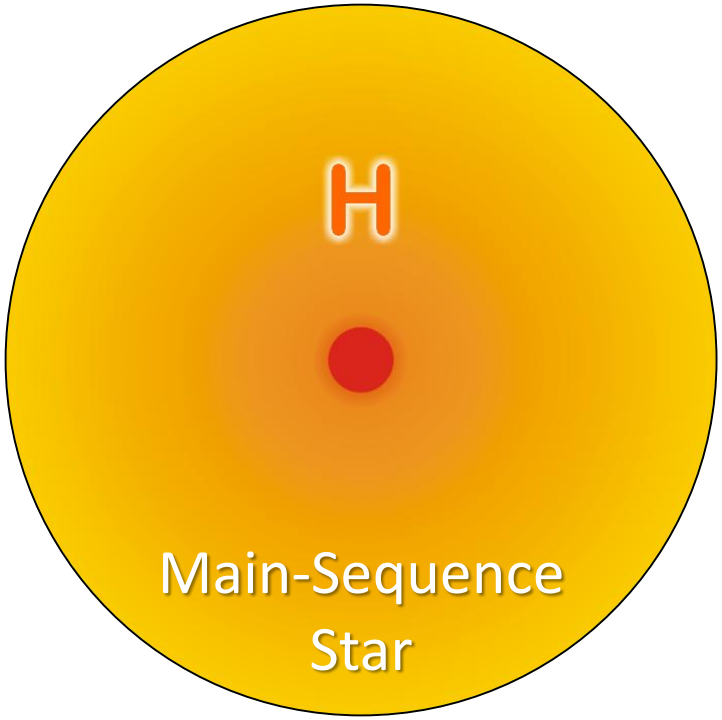

Virial Theorem: $\langle E_{\rm kin} \rangle = -\frac{1}{2} \langle E_{\rm grav} \rangle$

Small Contraction
→ Heating
→ Increased nuclear burning
→ Increased pressure
→ Expansion

Additional energy loss ("cooling")
→ Loss of pressure
→ Contraction
→ Heating
→ Increased nuclear burning

Hydrogen burning at nearly fixed T
→ Gravitational potential nearly fixed:
$G_{\rm N} M/R \sim$ constant
→ $R \propto M$ (More massive stars bigger)

Nuclear Binding Energy

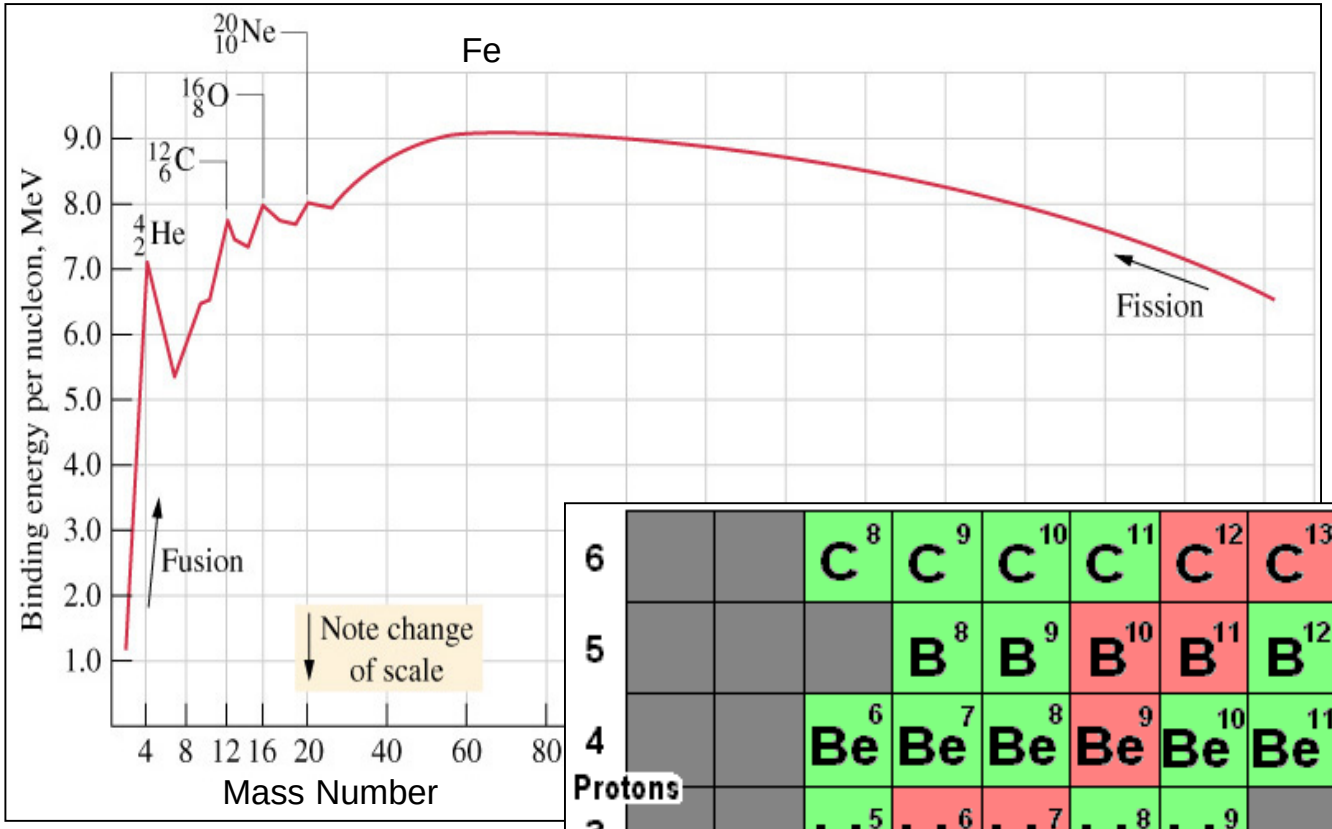

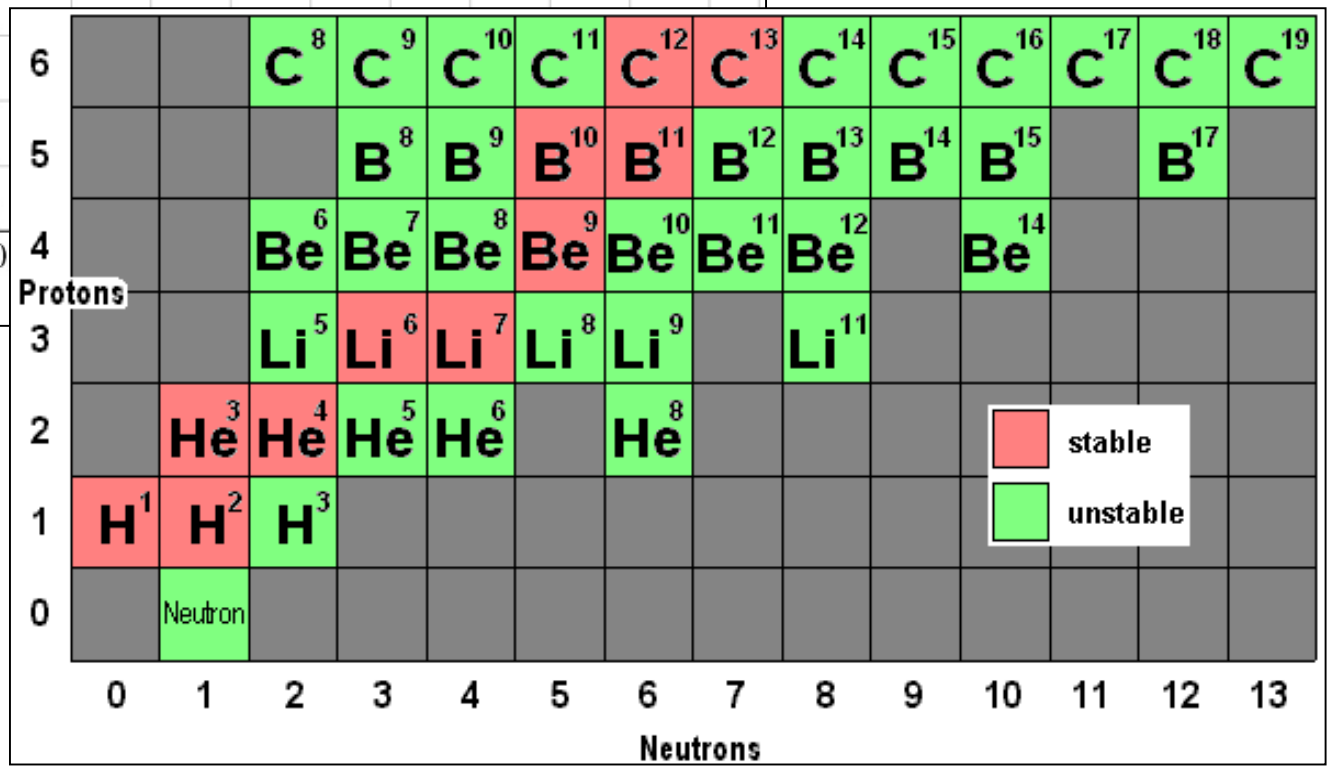

Thermonuclear Reactions and Gamow Peak

Coulomb repulsion prevents nuclear reactions, except for Gamow tunneling

Tunneling probability

$$p \propto E^{-1/2} e^{-2\pi\eta}$$

where the Sommerfeld parameter is

$$\eta = \left(\frac{m}{2E}\right)^{1/2} Z_1 Z_2 e^2$$

Parameterize cross section with astrophysical S-factor

$$S(E) = \sigma(E)\, E\, e^{2\pi\eta(E)}$$

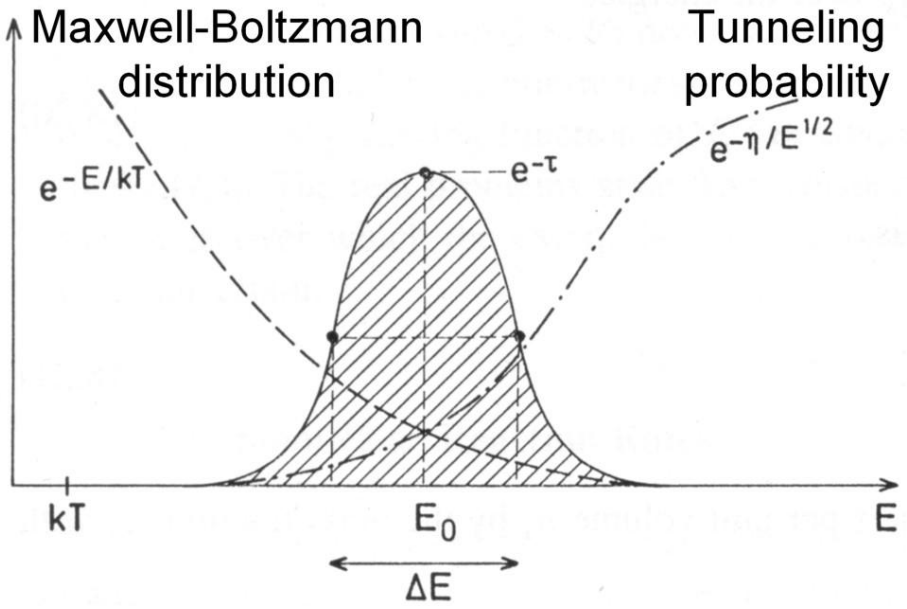

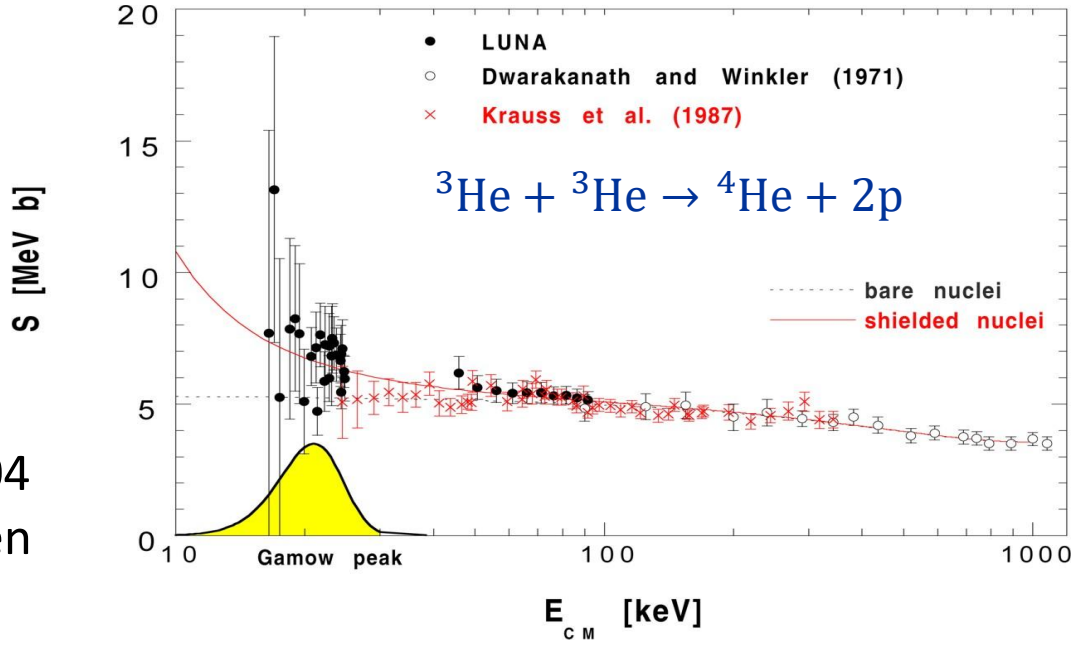

LUNA Collaboration, nucl-ex/9902004
many more measurements since then

Main Nuclear Burning Stages

Hydrogen burning $4\mathrm{p} + 2\mathrm{e}^- \rightarrow {}^4\mathrm{He} + 2\nu_e$

- Proceeds by pp chains and CNO cycle
- No higher elements are formed because no stable isotope with mass number 8
- Neutrinos from $\mathrm{p} \rightarrow \mathrm{n}$ conversion
- Typical temperatures: 10^7 K (~1 keV)

Helium burning

$$ {}^4\mathrm{He} + {}^4\mathrm{He} + {}^4\mathrm{He} \leftrightarrow {}^8\mathrm{Be} + {}^4\mathrm{He} \rightarrow {}^{12}\mathrm{C} $$

"Triple alpha reaction" because ^{8}Be unstable, builds up with concentration ~ 10^{-9}

$$ {}^{12}\mathrm{C} + {}^4\mathrm{He} \rightarrow {}^{16}\mathrm{O} $$
$$ {}^{16}\mathrm{O} + {}^4\mathrm{He} \rightarrow {}^{20}\mathrm{Ne} $$

Typical temperatures: 10^8 K (~10 keV)

Carbon burning

Many reactions, for example

$$ {}^{12}\mathrm{C} + {}^{12}\mathrm{C} \rightarrow {}^{23}\mathrm{Na} + \mathrm{p} \text{ or } {}^{20}\mathrm{Ne} + {}^4\mathrm{He} \text{ etc} $$

Typical temperatures: 10^9 K (~100 keV)

- Each type of burning occurs at a very different T but a broad range of densities
- Never co-exist in the same location

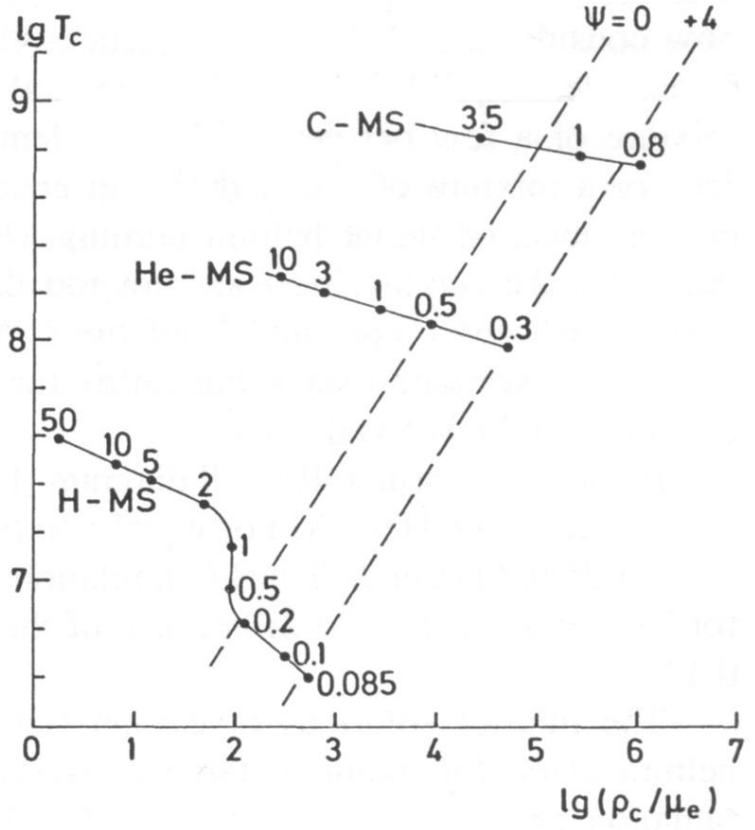

Hydrogen Exhaustion

Main-sequence star

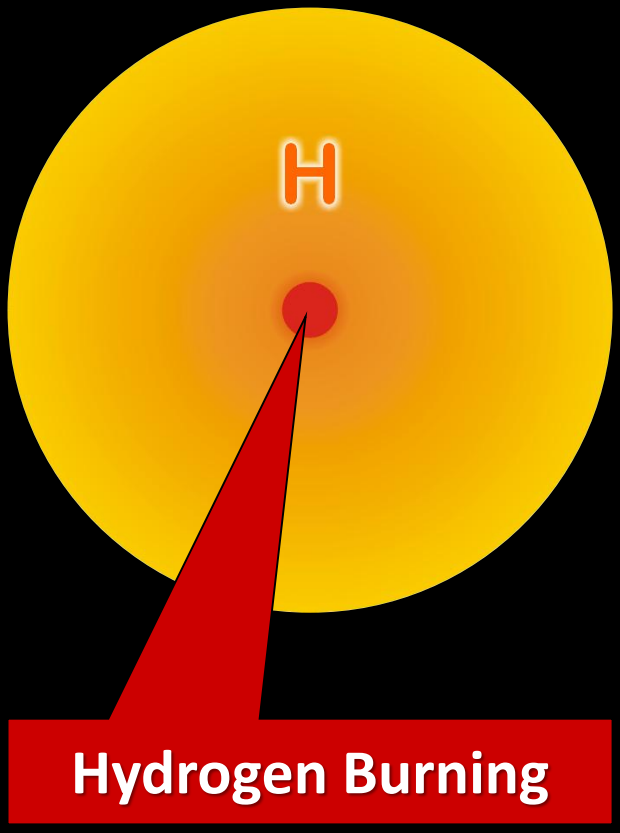

Helium-burning star

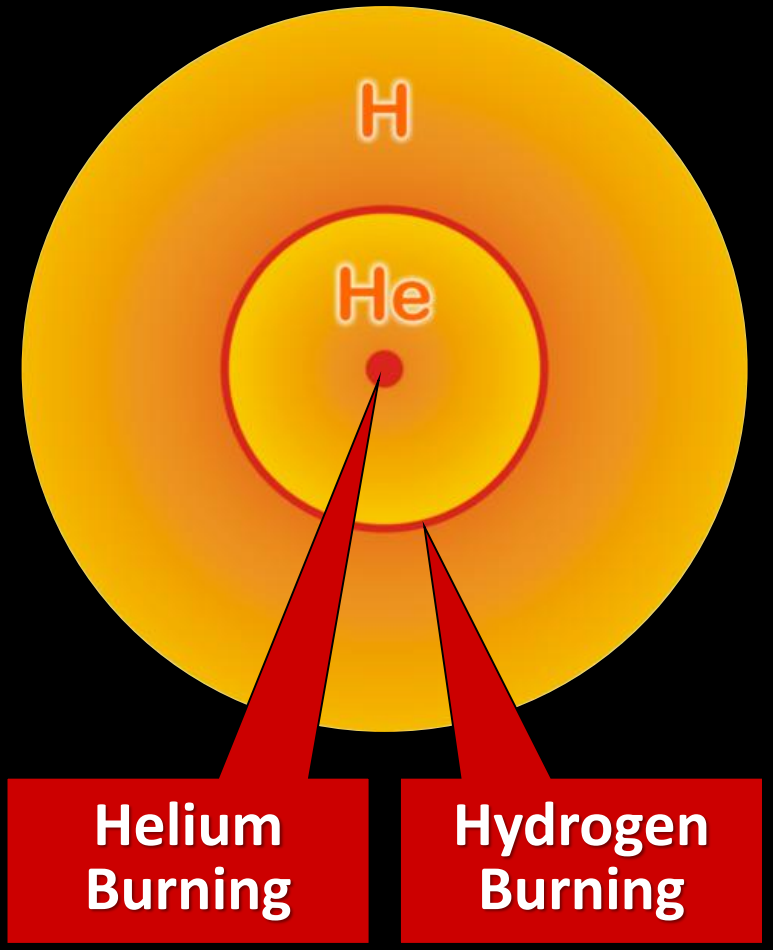

Burning Phases of a 15 Solar-Mass Star

L_γ [10^4 L_{sun}]

Burning Phase		Dominant Process	T_c [keV]	ρ_c [g/cm^3]	L_γ	L_ν/L_γ	Duration [years]
	Hydrogen	H → He	3	5.9	2.1	–	1.2×10^7
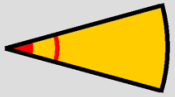	Helium	He → C, O	14	1.3×10^3	6.0	1.7×10^{-5}	1.3×10^6
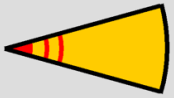	Carbon	C → Ne, Mg	53	1.7×10^5	8.6	1.0	6.3×10^3
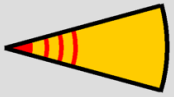	Neon	Ne → O, Mg	110	1.6×10^7	9.6	1.8×10^3	7.0
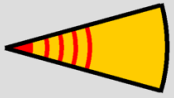	Oxygen	O → Si	160	9.7×10^7	9.6	2.1×10^4	1.7
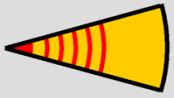	Silicon	Si → Fe, Ni	270	2.3×10^8	9.6	9.2×10^5	6 days

Degenerate Stars ("White Dwarfs")

Assume temperature very small
→ No thermal pressure
→ Electron degeneracy is pressure source

Pressure ~ Momentum density × Velocity

- Electron density $n_e = p_\mathrm{F}^3/(3\pi^3)$
- Momentum p_F (Fermi momentum)
- Velocity $v \propto p_\mathrm{F}/m_e$
- Pressure $P \propto p_\mathrm{F}^5 \propto \rho^{5/3} \propto M^{5/3}R^{-5}$
- Density $\rho \propto MR^{-3}$

Hydrostatic equilibrium

$$\frac{dP}{dr} = -\frac{G_\mathrm{N} M_r \rho}{r^2}$$

With $dP/dr \sim -P/R$ we have

$P \propto G_\mathrm{N} M \rho R^{-1} \propto G_\mathrm{N} M^2 R^{-4}$

Inverse mass radius relationship

$R \propto M^{-1/3}$

$$R = 10{,}500\ \mathrm{km} \left(\frac{0.6\ M_\odot}{M}\right)^{1/3} (2Y_e)^{5/3}$$

(Y_e electrons per nucleon)

For sufficiently large stellar mass M, electrons become relativistic

- Velocity = speed of light
- Pressure

$P \propto p_\mathrm{F}^4 \propto \rho^{4/3} \propto M^{4/3}R^{-4}$

No stable configuration

Chandrasekhar mass limit

$$M_\mathrm{Ch} = 1.457\ M_\odot\ (2Y_e)^2$$

Chandrasekhar Mass for Particle Physicists

Degeneracy pressure balances gravity

- N nucleons, nucleon mass m_N
- $M_{\rm star} = N\, m_N$
- Semirelativistic particles (mass m): $E_{\rm F} \simeq p_{\rm F} \simeq m$
- Degeneracy energy: $E_{\rm deg} \simeq Nm$
- Number density: $n \simeq p_{\rm F}^3 \simeq m^3$

$$E_{\rm deg} \simeq -E_{\rm grav} \simeq \frac{GM_{\rm star}^2}{R_{\rm star}} \simeq \frac{N^2 m_N^2}{m_{\rm Planck}^2 R_{\rm star}}$$

$$R_{\rm star} \simeq \frac{m_{\rm Planck}}{m_N m}$$

$$M_{\rm star} \simeq m_N n \simeq \frac{m_{\rm Planck}^3}{m_N^2} = 3.75 \times 10^{33}\,{\rm g} \simeq M_\odot$$

- **Neutron Star (NS):**
  Degenerate particle: Nucleon, $m = m_N$
  $$R_{\rm NS} \simeq \frac{m_{\rm Planck}}{m_N^2} = 2.8\ {\rm km}$$
- **White Dwarf (WD):**
  Degenerate particle: Electron, $m = m_e \simeq m_N/2000$
  $$R_{\rm WD} \simeq \frac{m_{\rm Planck}}{m_e m_N} = \frac{m_N}{m_e} R_{\rm NS} = 5000\ {\rm km}$$

Galactic Globular Cluster M55

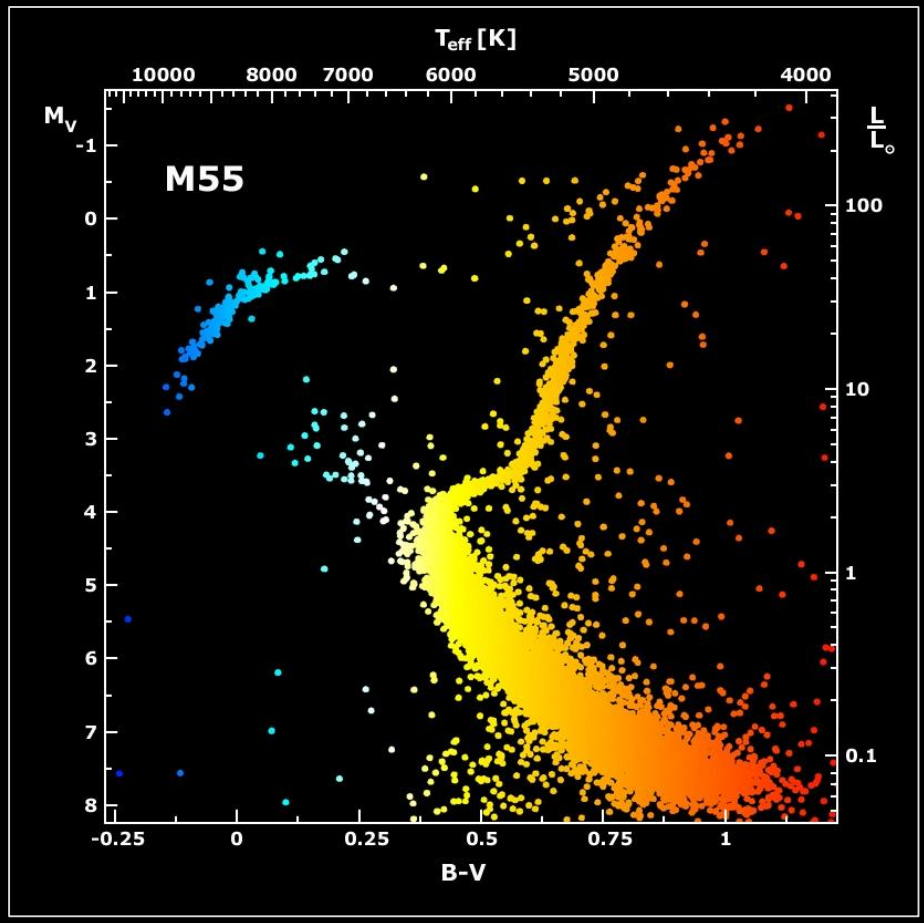

Globular Clusters of the Milky Way

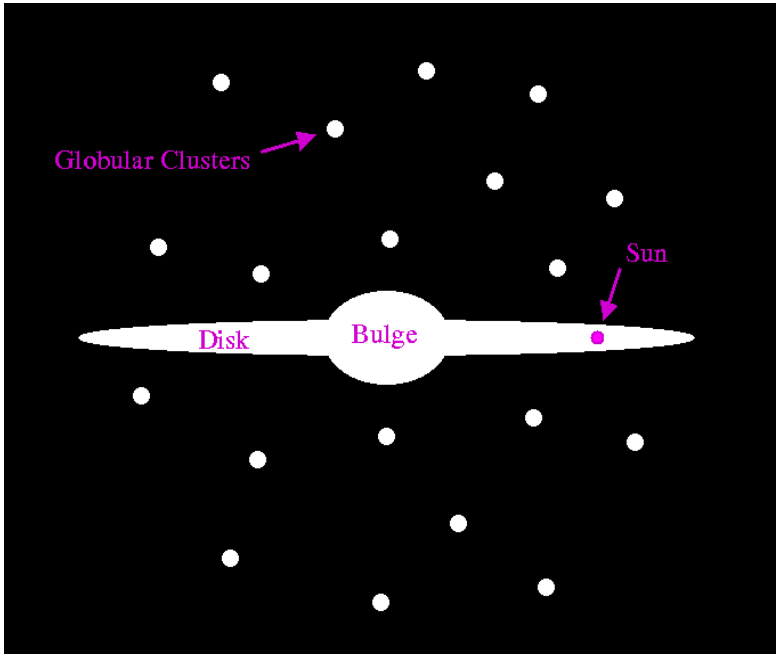

Globular clusters on top of the
FIRAS 2.2 micron map of the Galaxy

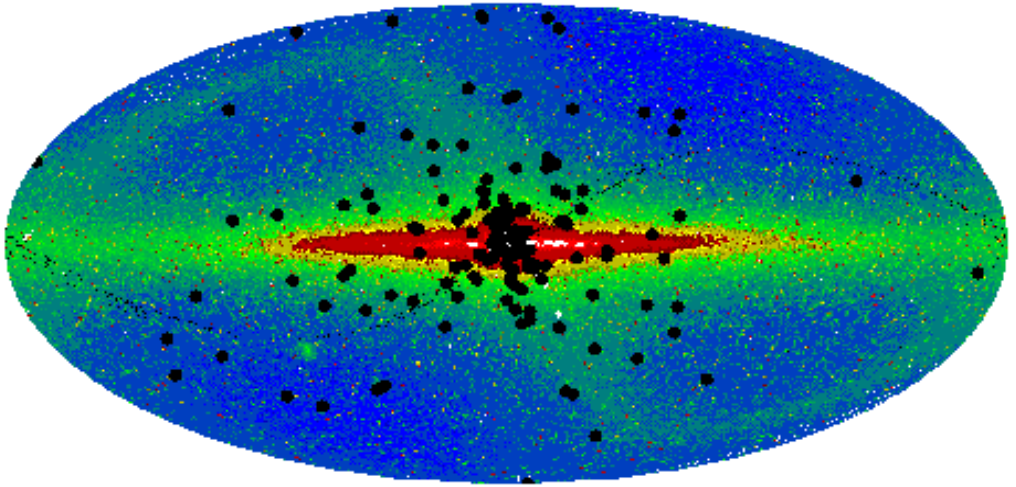

http://www.dartmouth.edu/~chaboyer/mwgc.html

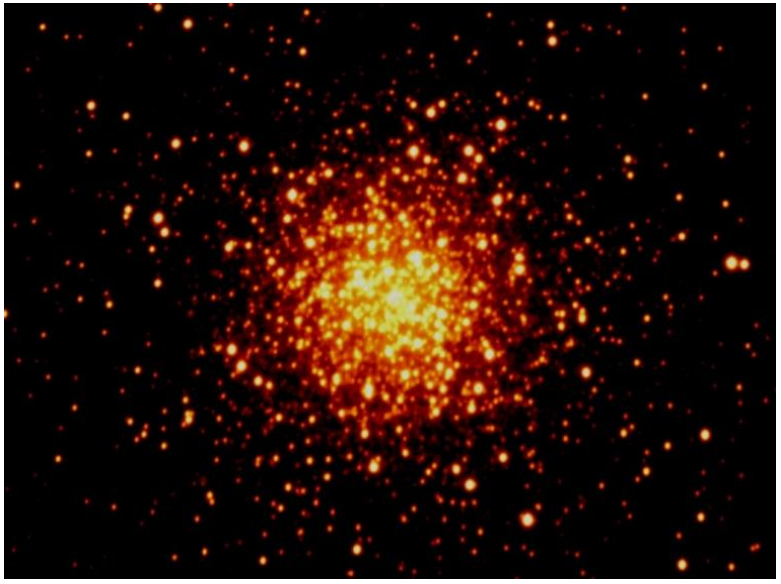

The galactic
globular cluster M3

Color-Magnitude Diagram for Globular Clusters

- Stars with M so large that they have burnt out in a Hubble time
- No new star formation in globular clusters

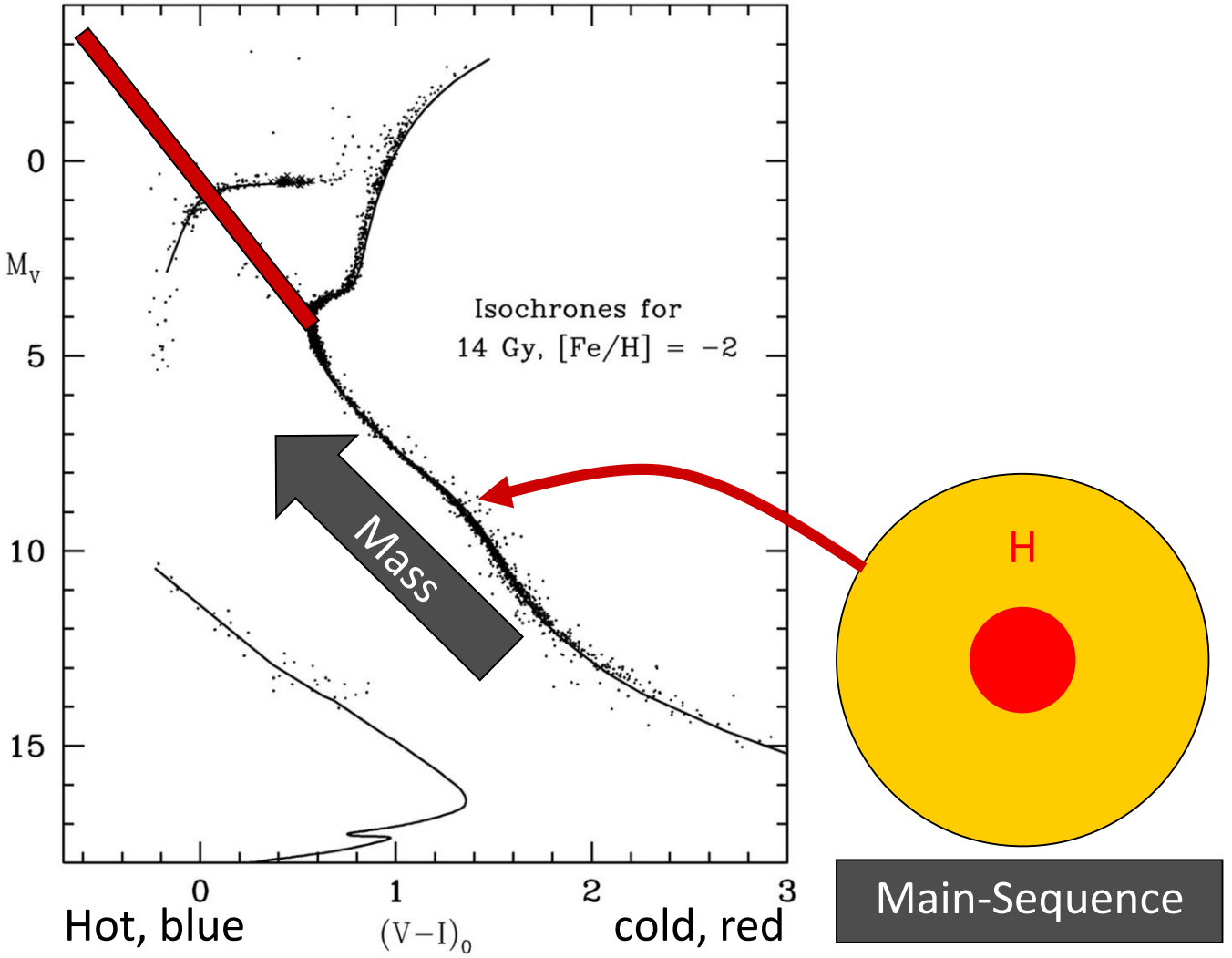

Color-magnitude diagram synthesized from several low-metallicity globular clusters and compared with theoretical isochrones (W.Harris, 2000)

Color-Magnitude Diagram for Globular Clusters

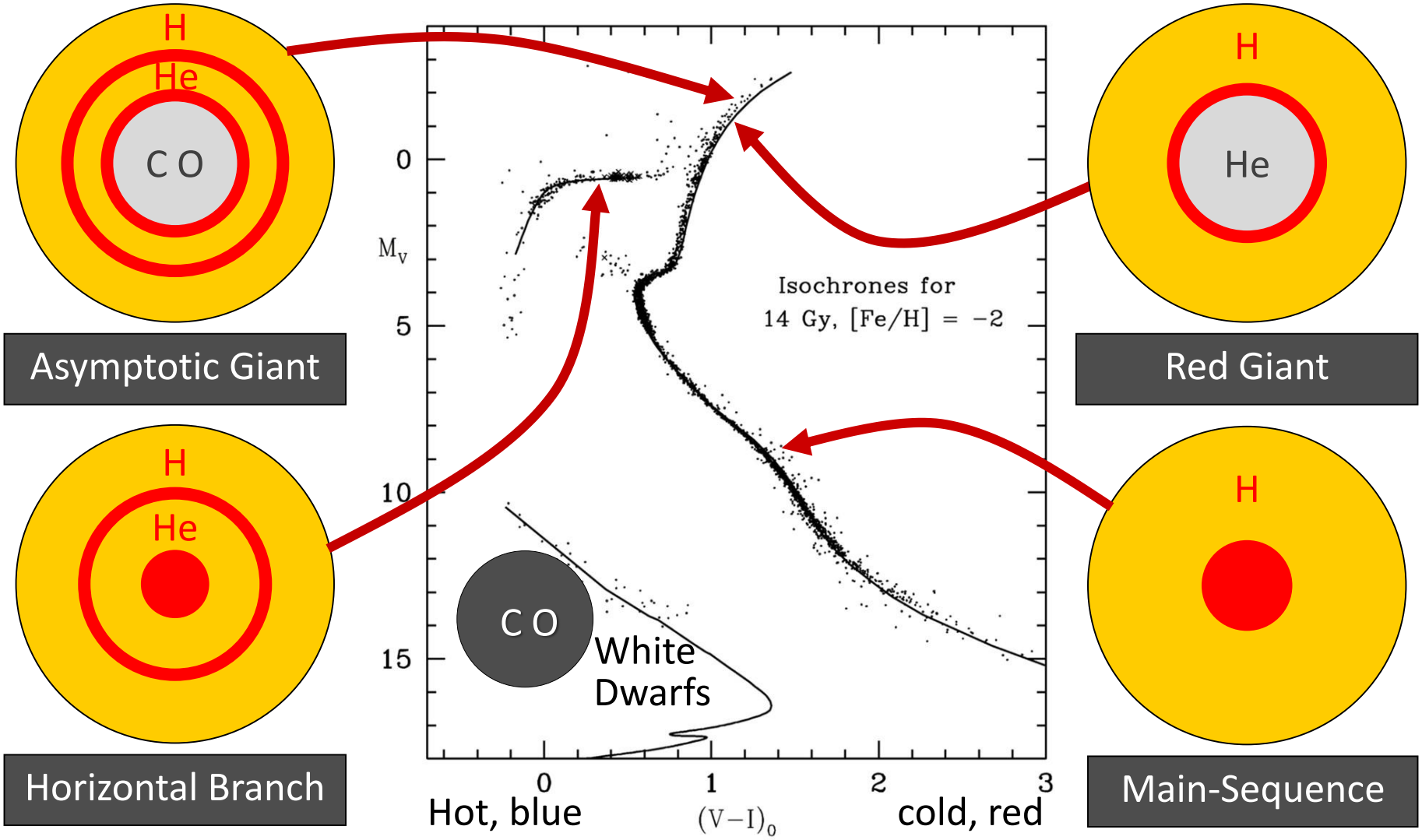

Color-magnitude diagram synthesized from several low-metallicity globular clusters and compared with theoretical isochrones (W.Harris, 2000)

Color-Magnitude Diagram for Globular Clusters

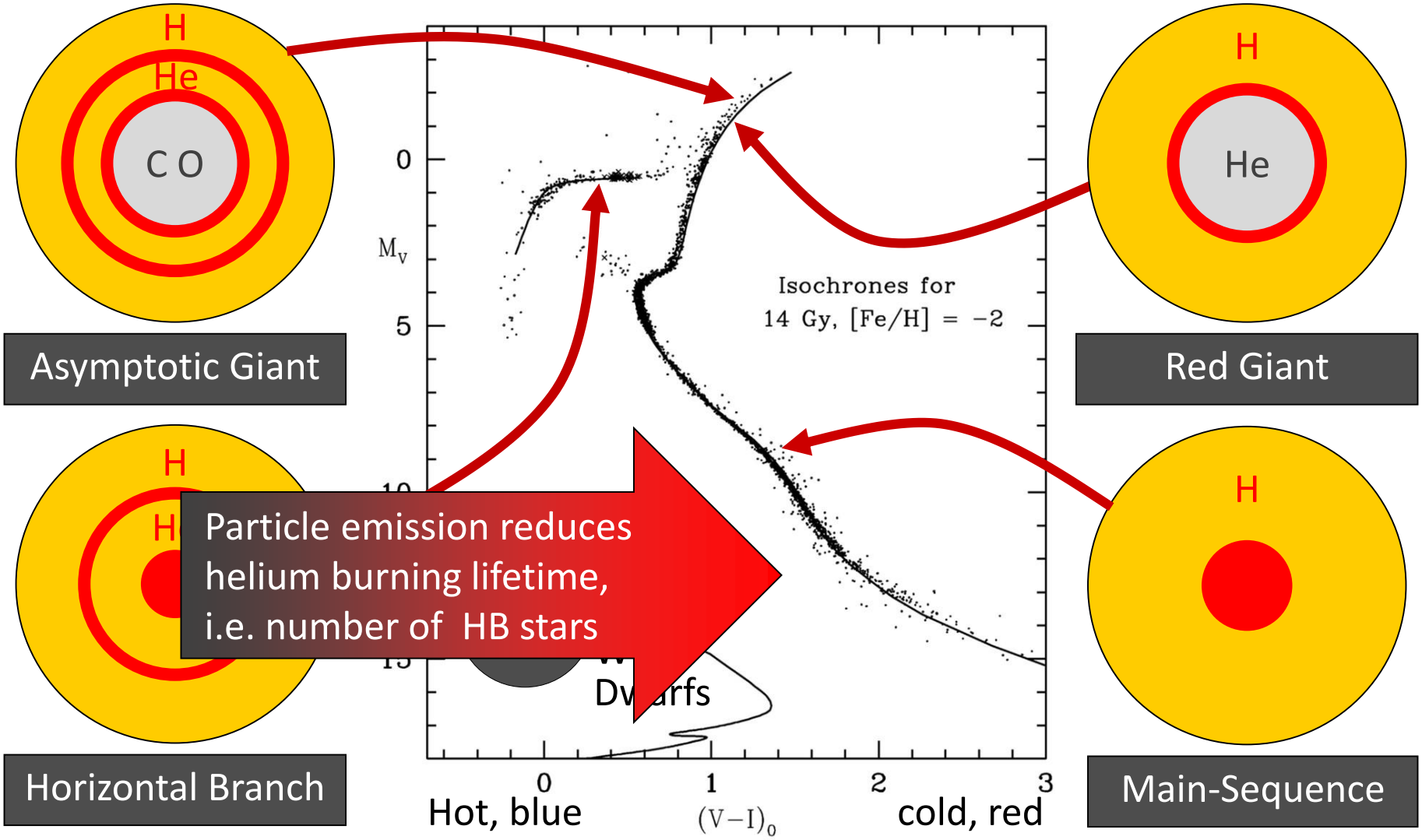

Color-magnitude diagram synthesized from several low-metallicity globular clusters and compared with theoretical isochrones (W.Harris, 2000)

Thermal Axions: Production Processes

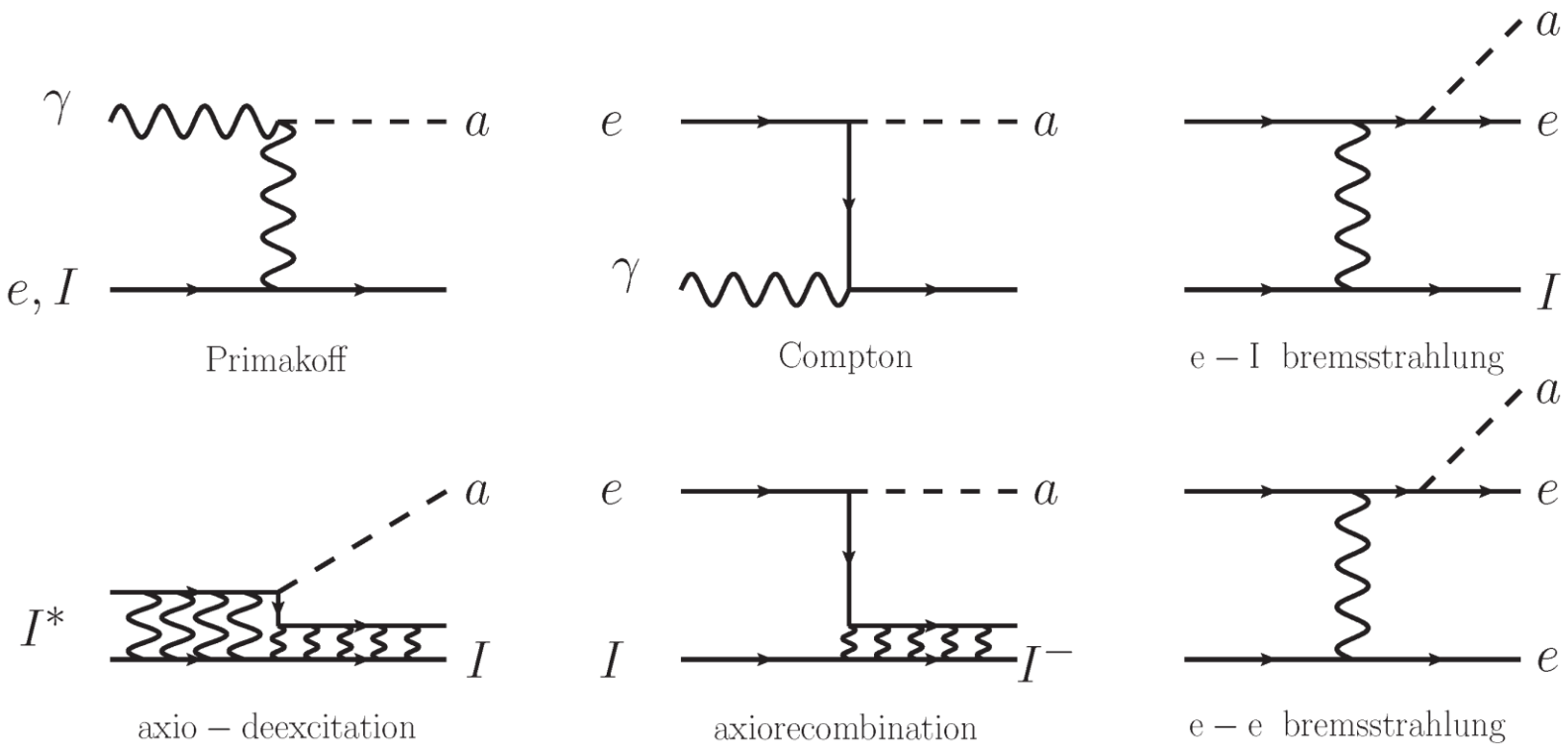

Figure 1. ABC reactions responsible for the solar axion flux in non-hadronic axion models.

Redondo, arXiv:1310.0823

Color-Magnitude Diagram for Globular Clusters

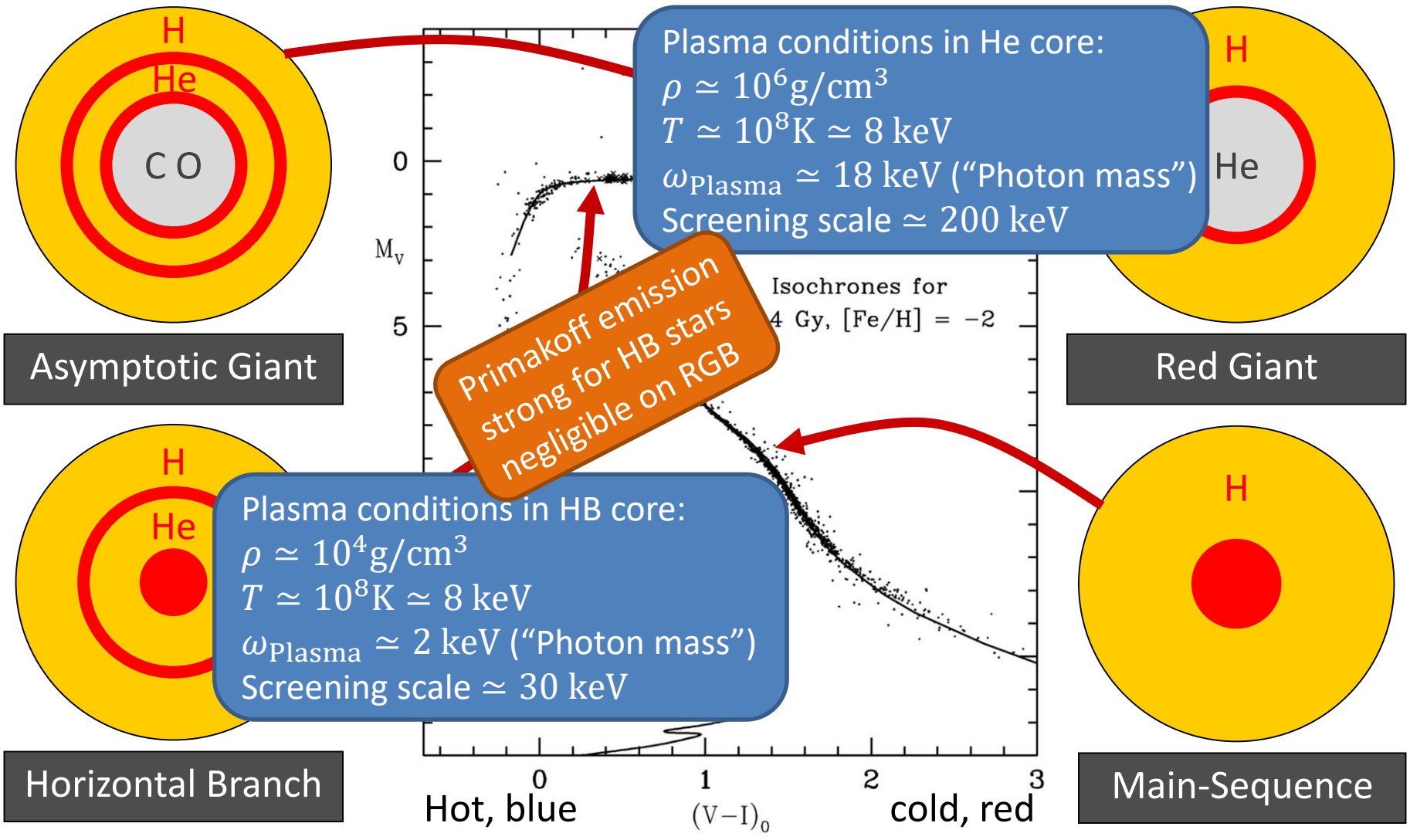

Color-magnitude diagram synthesized from several low-metallicity globular clusters and compared with theoretical isochrones (W.Harris, 2000)

Color-Magnitude Diagram for Globular Clusters

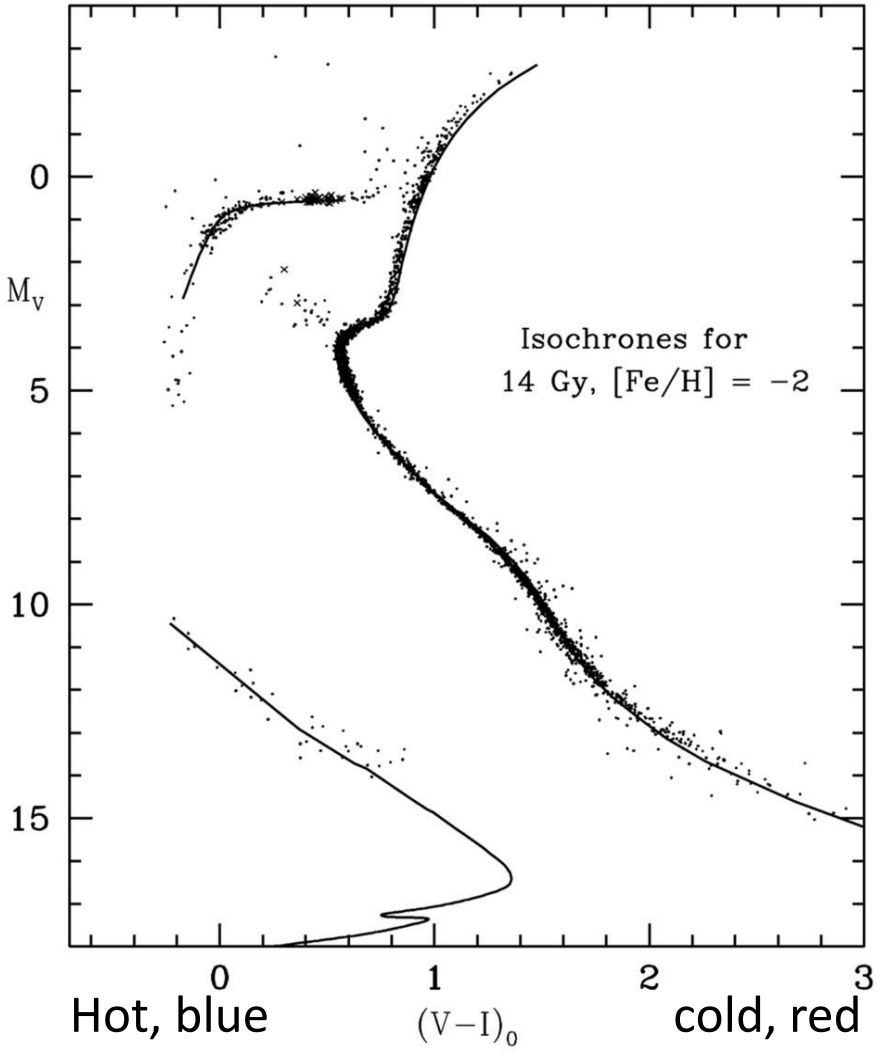

Color-magnitude diagram synthesized from several low-metallicity globular clusters and compared with theoretical isochrones (W.Harris, 2000)

Color-Magnitude Diagram for Globular Clusters

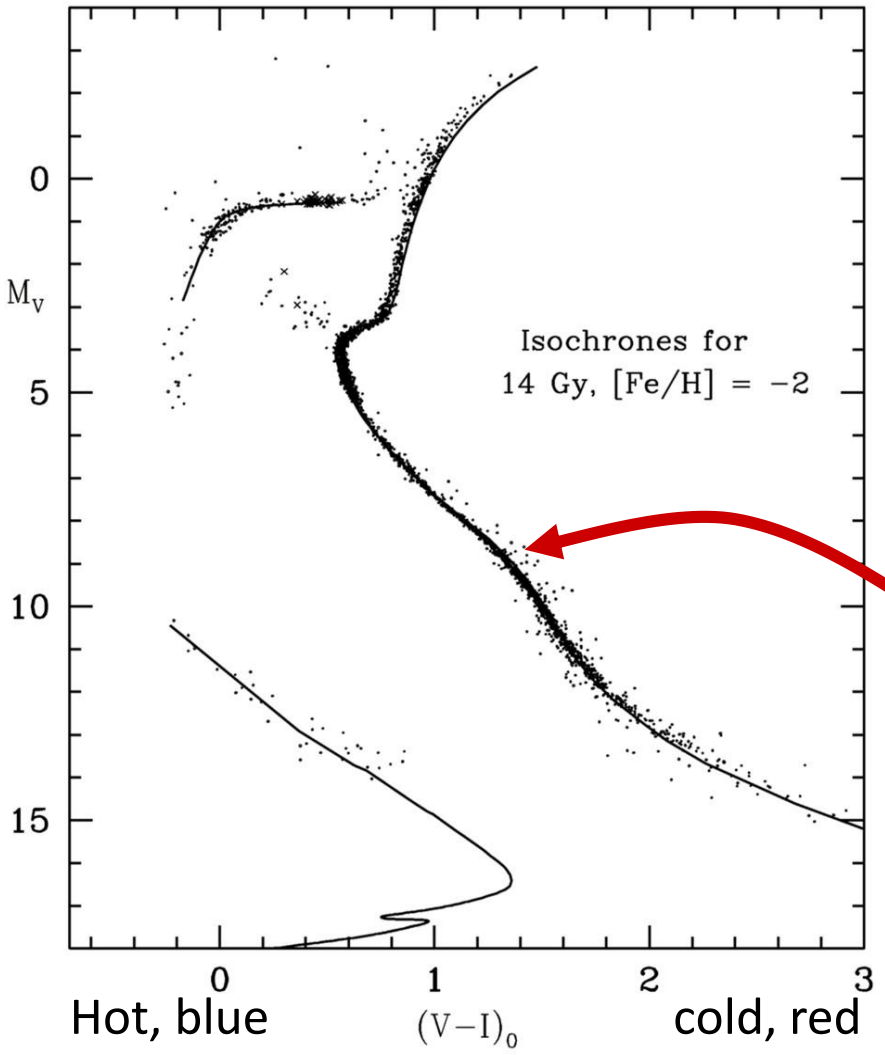

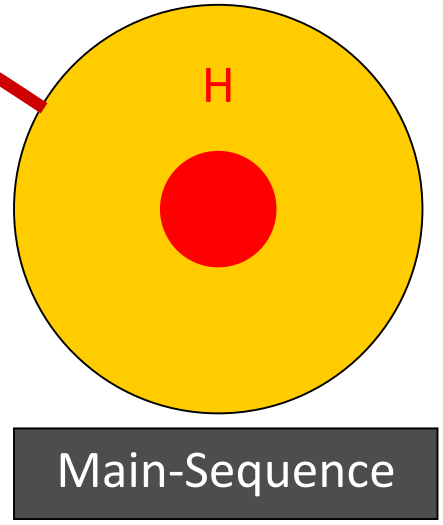

Color-magnitude diagram synthesized from several low-metallicity globular clusters and compared with theoretical isochrones (W.Harris, 2000)

Color-Magnitude Diagram for Globular Clusters

- Stars with M so large that they have burnt out in a Hubble time
- No new star formation in globular clusters

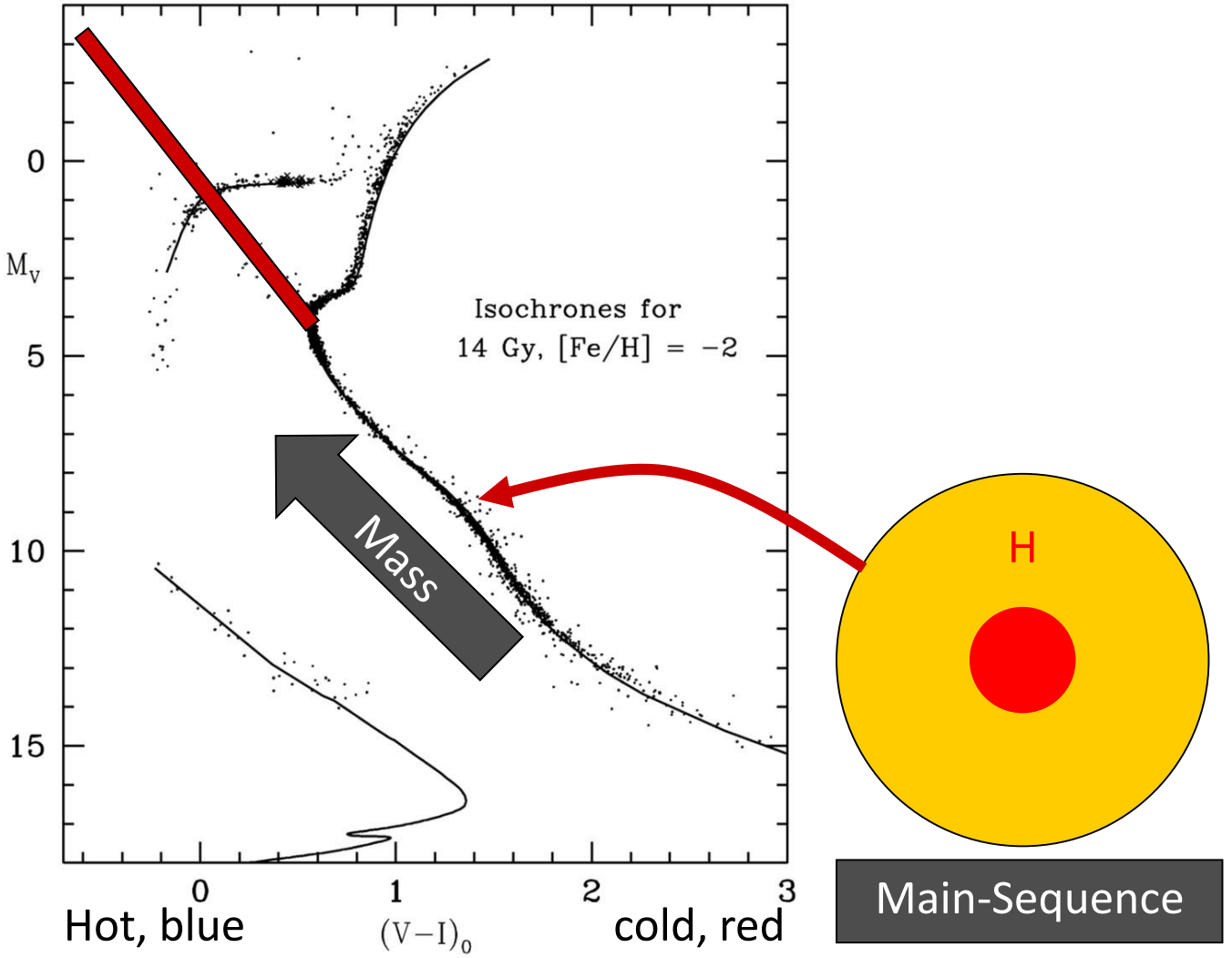

Color-magnitude diagram synthesized from several low-metallicity globular clusters and compared with theoretical isochrones (W.Harris, 2000)

Color-Magnitude Diagram for Globular Clusters

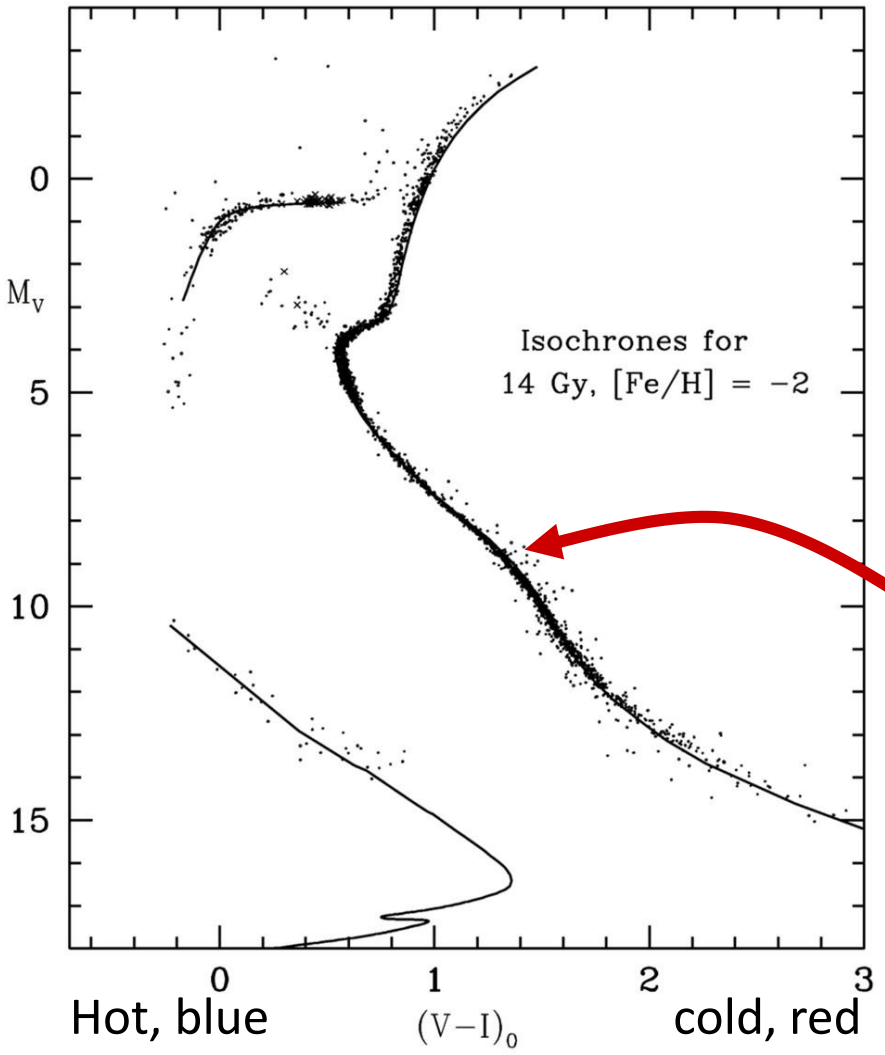

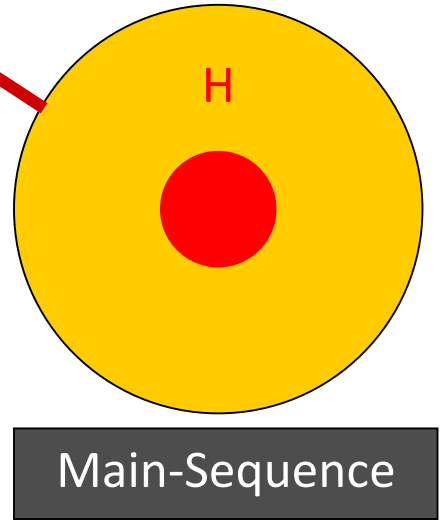

Color-magnitude diagram synthesized from several low-metallicity globular clusters and compared with theoretical isochrones (W.Harris, 2000)

Color-Magnitude Diagram for Globular Clusters

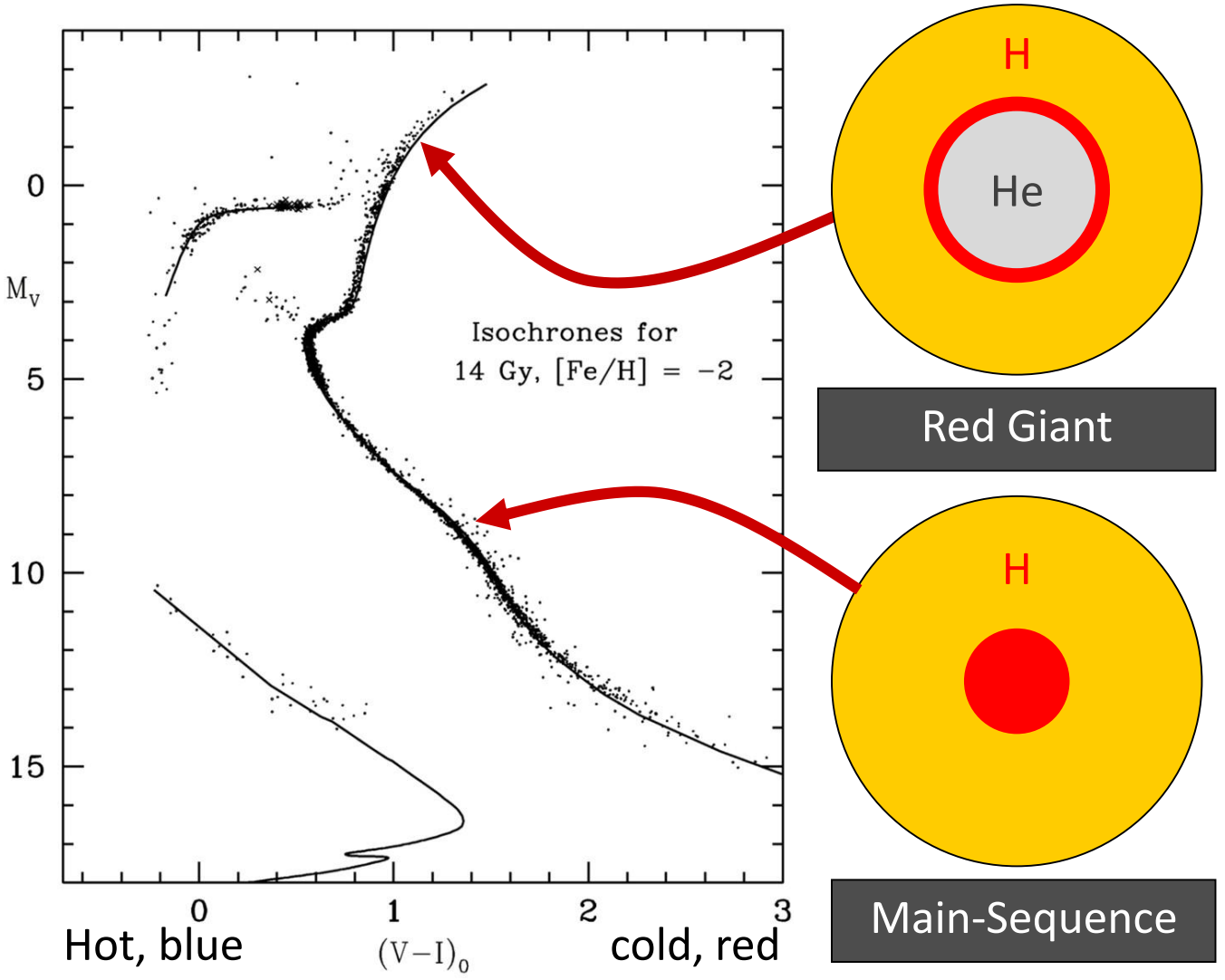

Color-magnitude diagram synthesized from several low-metallicity globular clusters and compared with theoretical isochrones (W.Harris, 2000)

Color-Magnitude Diagram for Globular Clusters

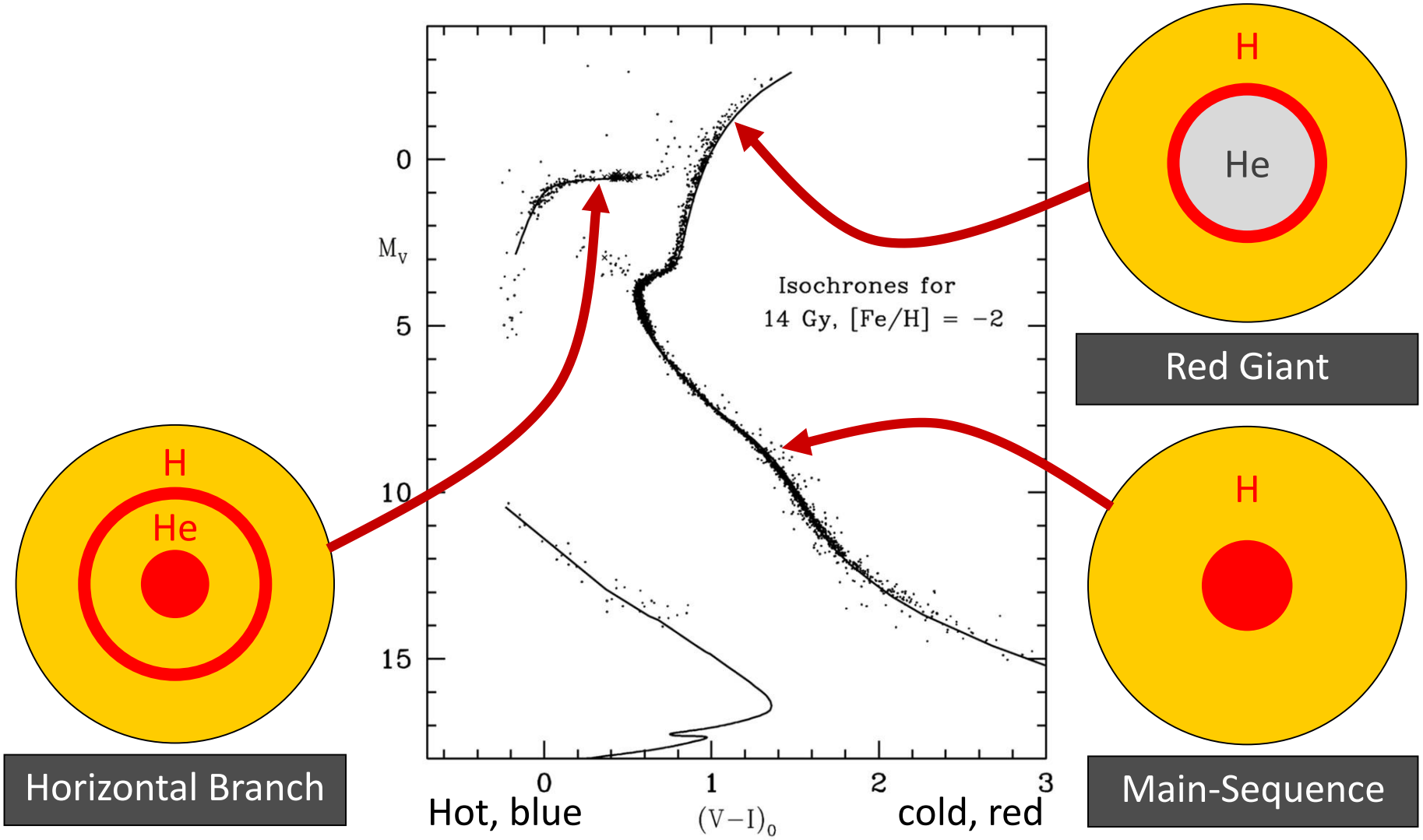

Color-magnitude diagram synthesized from several low-metallicity globular clusters and compared with theoretical isochrones (W.Harris, 2000)

Color-Magnitude Diagram for Globular Clusters

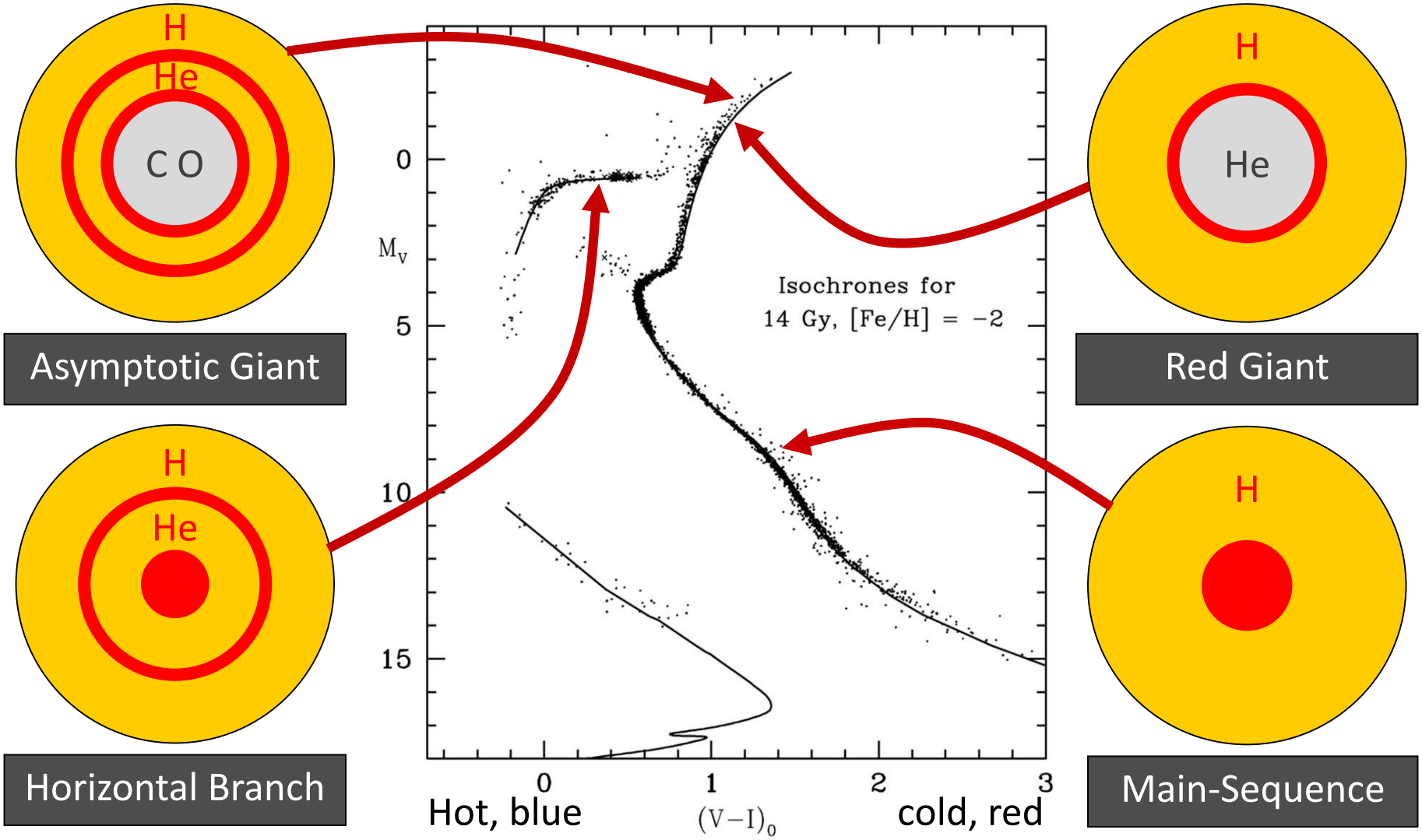

Color-magnitude diagram synthesized from several low-metallicity globular clusters and compared with theoretical isochrones (W.Harris, 2000)

Color-Magnitude Diagram for Globular Clusters

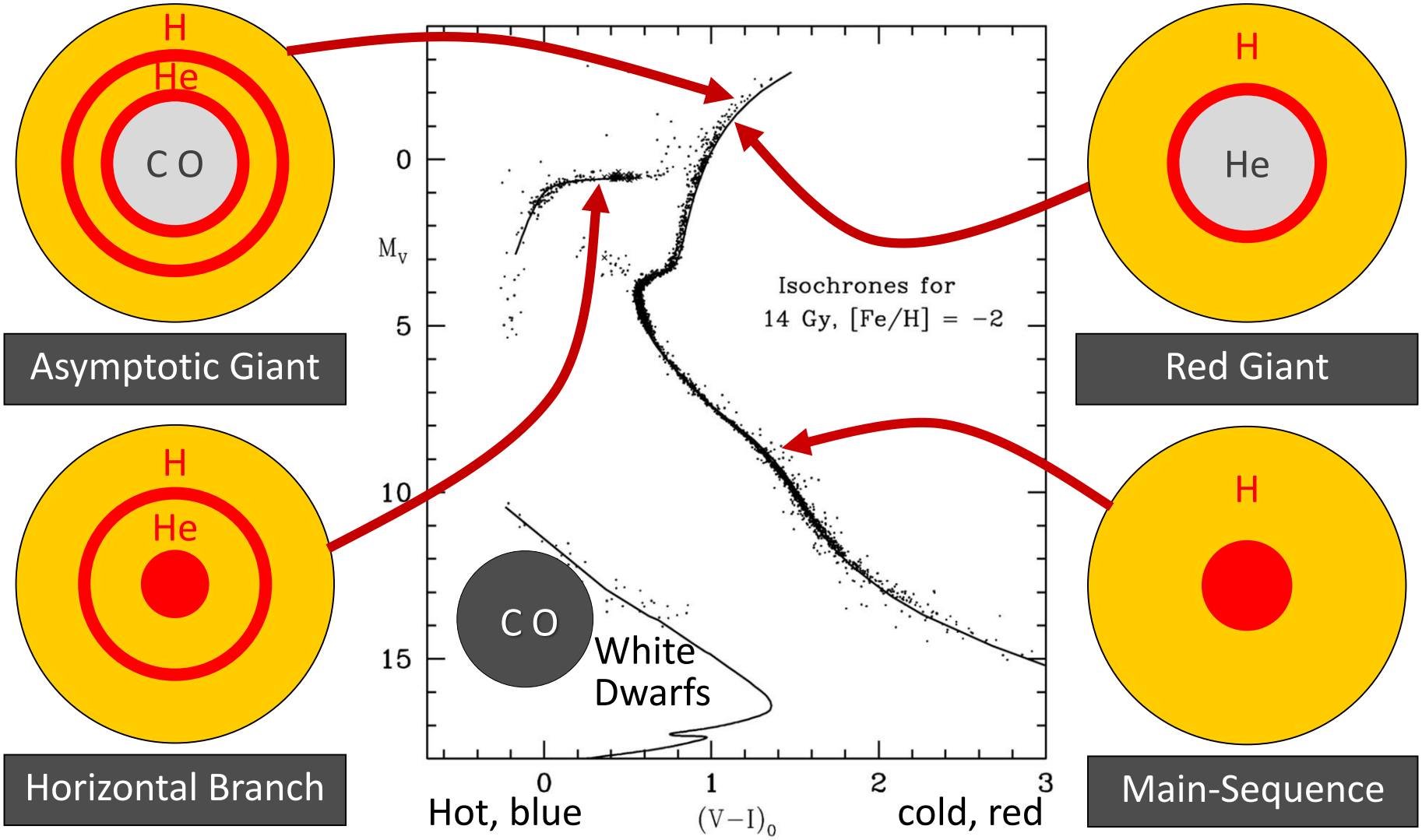

Color-magnitude diagram synthesized from several low-metallicity globular clusters and compared with theoretical isochrones (W.Harris, 2000)

Color-Magnitude Diagram for Globular Clusters

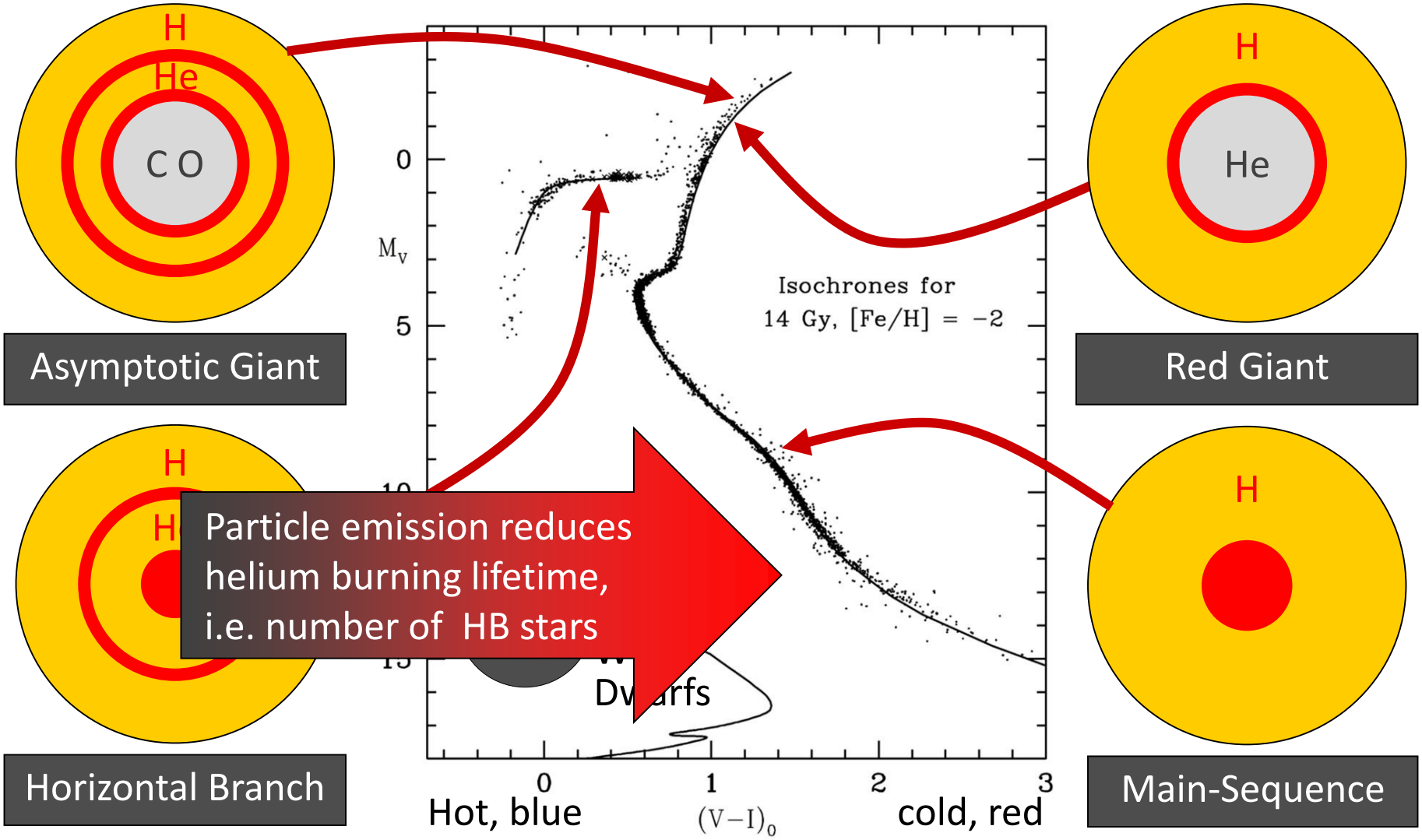

Color-magnitude diagram synthesized from several low-metallicity globular clusters and compared with theoretical isochrones (W.Harris, 2000)

Thermal Axions: Production Processes

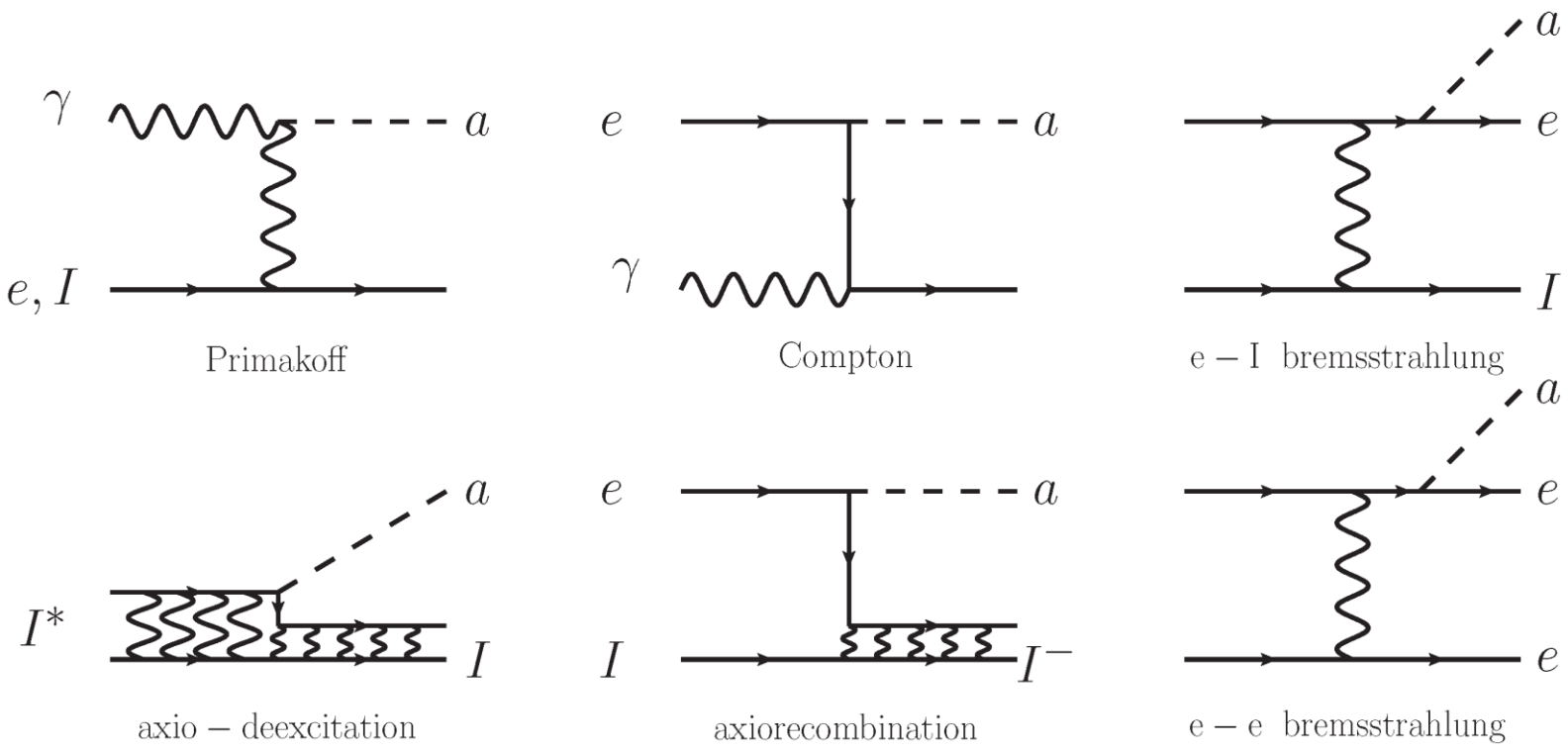

Figure 1. ABC reactions responsible for the solar axion flux in non-hadronic axion models.

Redondo, arXiv:1310.0823

Color-Magnitude Diagram for Globular Clusters

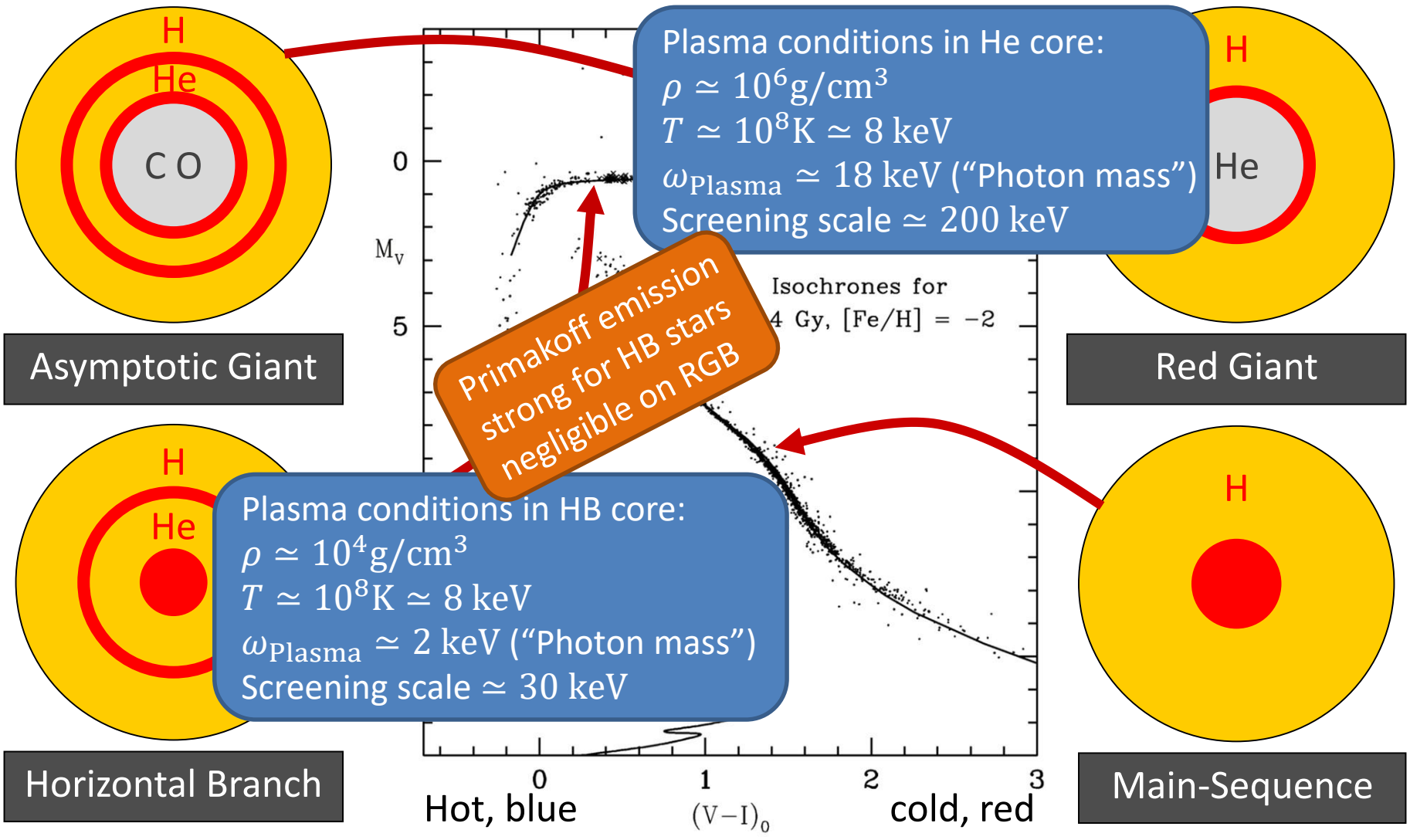

Color-magnitude diagram synthesized from several low-metallicity globular clusters and compared with theoretical isochrones (W.Harris, 2000)

Globular-Cluster Limit on Axion-Photon Coupling

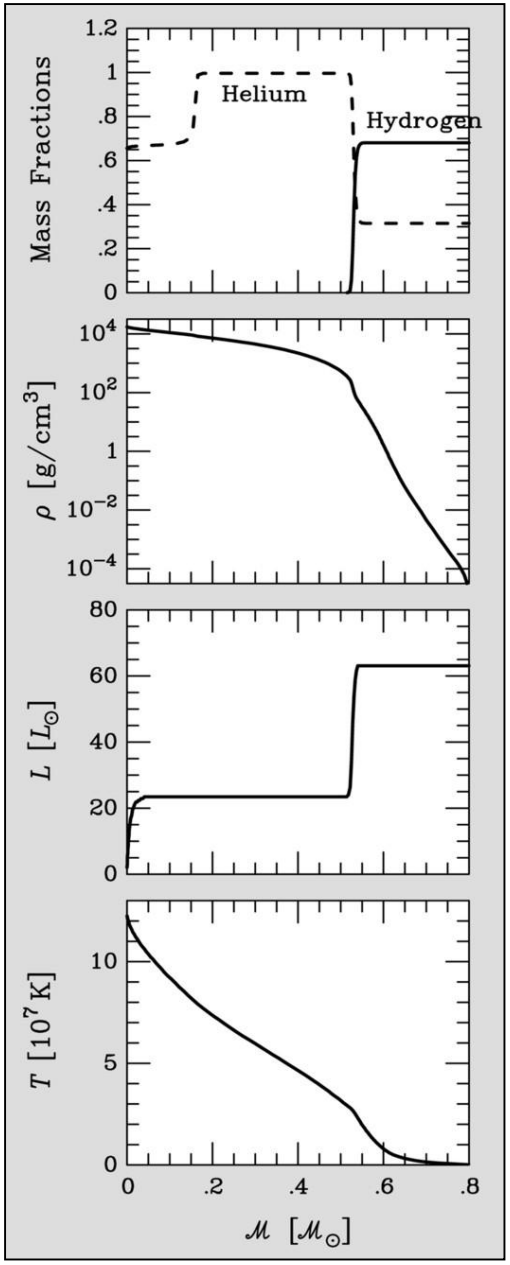

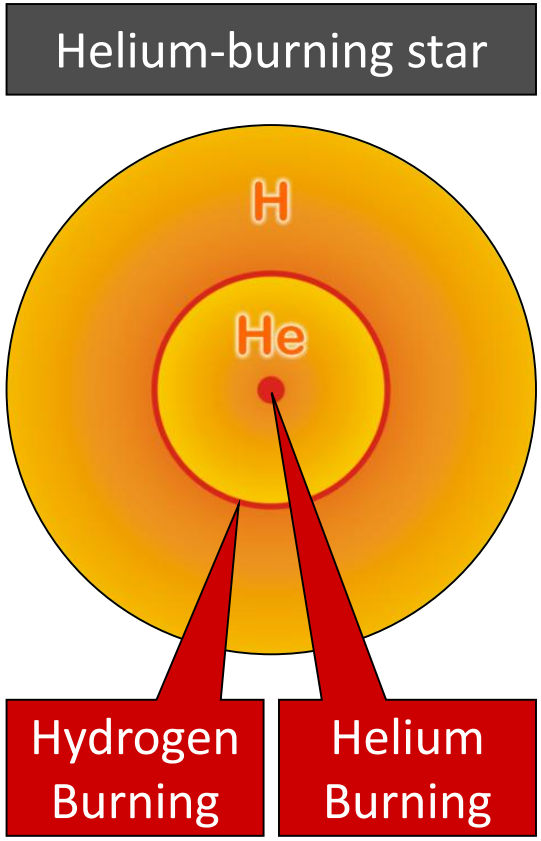

- Helium-burning luminosity

  $L_{3\alpha} \sim 20\ L_{\rm sun}$

  $T \sim 10\ {\rm keV}$

  $\rho \sim 10^4 {\rm g\ cm^{-3}}$

- Core-averaged nuclear energy generation rate

  $\epsilon_{3\alpha} \sim 80\ {\rm erg\ g^{-1}\ s^{-1}}$

- Core-averaged Primakoff emission rate

  $\epsilon_{\rm Primakoff} \sim g_{10}^2\ 30\ {\rm erg\ g^{-1}\ s^{-1}}$

- Reduction of helium-burning lifetime

  $$\frac{\tau}{\tau_0} \sim \frac{1}{1 + 0.4\ g_{10}^2}$$

- Adopt nominal limit $g_{10} < 1$

  (More restrictive limit if using 10% precision for helium burning lifetime)

Helium Burning Lifetime: R-Method

Number ratio ("R") of HB/RGB fixes He-burning lifetime
(if RGB not affected by new energy loss)

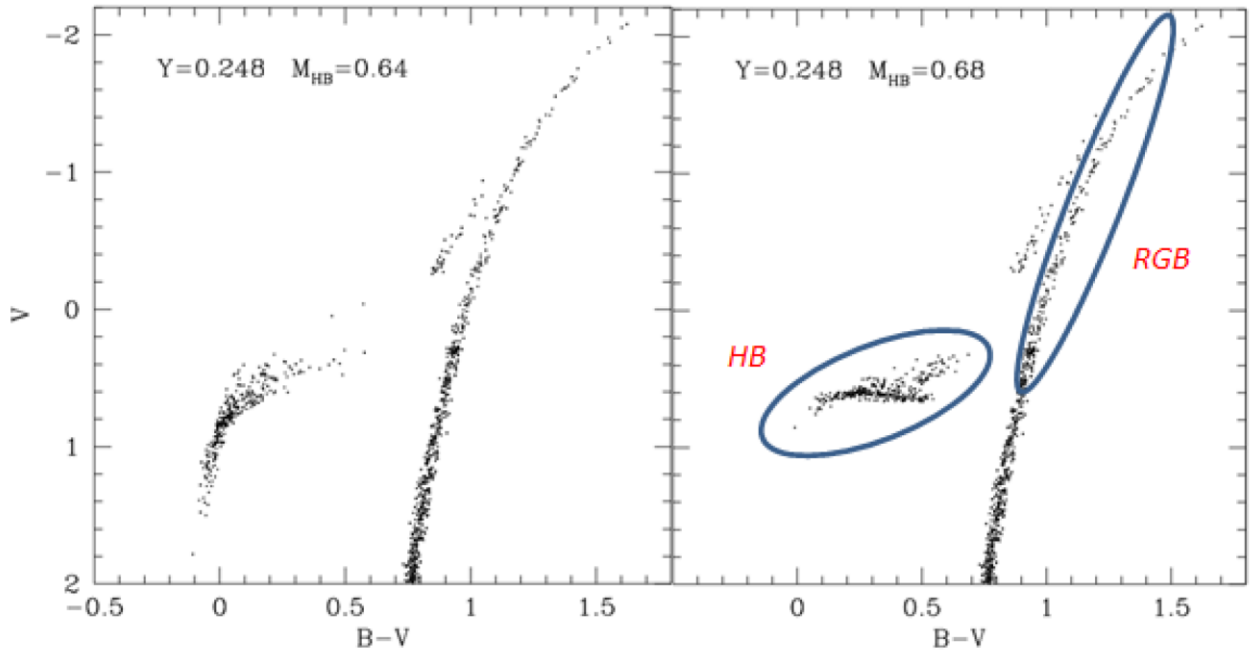

Figure 1: Example of synthetic CM diagrams. The diagram in the left panel has been obtained by assuming a stronger average mass loss rate during the RGB. As a result, the mean mass of HB stars (M_{HB}) is lower than that of the diagram in the right panel. The HB and the RGB portions used in the calculation of the R parameter are surrounded by ellipses.

Straniero, Ayala, Giannotti, Mirizzi & Domínguez,
doi:10.3204/DESY-PROC-2015-02/straniero_oscar

ALP Limits from Globular Clusters

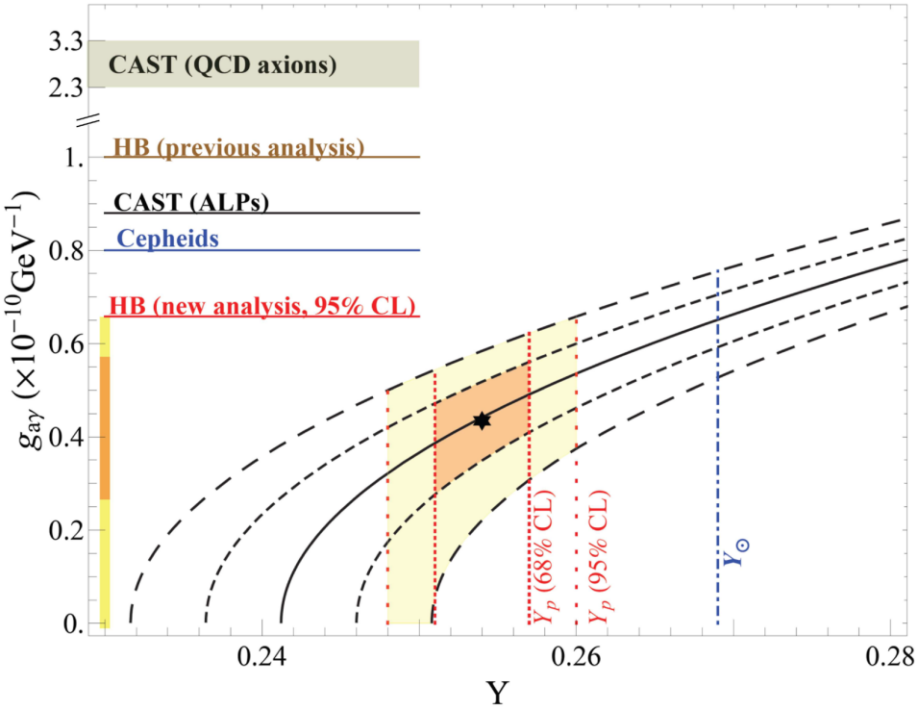

Helium abundance and energy loss rate from modern number counts HB/RGB in 39 globular clusters R = 1.39 ± 0.03

$$R_{\rm th} = 1.48 + 6.26(Y - 0.255) - 0.41 g_{10}^2$$

$$\boldsymbol{g_{a\gamma} < 0.66 \times 10^{-10}\,\mathrm{GeV}^{-1}\ \text{(95\% CL)}}$$

Same as CAST limit within 2 digits ☺

Parameter	error	Reference
$^{14}\mathrm{N}(p,\gamma)^{15}\mathrm{O}$	7%	[1]
$^{4}\mathrm{He}(2\alpha,\gamma)^{12}\mathrm{C}$	10%	[2]
$^{12}\mathrm{C}(\alpha,\gamma)^{16}\mathrm{O}$	20%	[6]
R	1.39 ± 0.03	[4]
Y	0.255 ± 0.002	[5],[3]

Small "cooling hint" almost certainly systematics (as usual in astrophysics) eg nuclear reaction rates
Need more systematic exploration of systematics!

Ayala, Dominguez, Giannotti, Mirizzi & Straniero, arXiv:1406.6053
doi:10.3204/DESY-PROC-2015-02/straniero_oscar

AGB/HB Counts in 48 Globular Clusters

				Piotto et al. (2002)			Sarajedini et al. (2007)			Sandquist (2000)		
NGC	[Fe/H]	$L1$	$L2$	n_{HB}	n_{AGB}	R_2	n_{HB}	n_{AGB}	R_2	n_{HB}	n_{AGB}	R_2
104	-0.72	0.078	0.068	358	53	0.148	591	82	0.139	368	38	0.103
362	-1.26	0.086	0.608	238	40	0.168	318	43	0.135	94	14	0.149
1261	-1.27	0.088	0.644	94	22	0.234	233	34	0.146	148	26	0.176
1851	-1.18	0.098	0.679	272	37	0.136	411	49	0.119	209	24	0.115
1904	-1.60	...	...	163	11	0.067	...	...	...	122	16	0.131
2419	-2.15	0.192	0.852	225	22	0.098	...	...	...	...	...	...
2808	-1.14	0.094	0.904	809	61	0.075	1200	104	0.087	247	22	0.089
4833	-1.85	0.287	0.538	94	10	0.106	...	...	...	...	...	...
5024	-2.10	0.158	0.602	224	18	0.080	360	44	0.122	302	39	0.129
5272	-1.50	0.150	0.613	...	...	...	323	40	0.124	562	65	0.116
5634	-1.88	...	...	130	15	0.115	...	...	...	...	...	...
5694	-1.98	...	...	222	26	0.117	...	...	...	56	14	0.250
5824	-1.91	...	...	463	63	0.136	...	...	...	...	...	...
5904	-1.29	0.150	0.681	162	21	0.130	280	52	0.186	555	94	0.169
5927	-0.49	0.043	0.062	201	12	0.060	...	...	...	134	20	0.149
6093	-1.75	0.464	0.447	162	31	0.191	341	51	0.150	170	39	0.229
6139	-1.65	...	...	282	35	0.124	...	...	...	114	24	0.211
6171	-1.02	0.100	0.513	...	...	...	56	10	0.179	117	29	0.248
6205	-1.53	0.527	0.441	192	20	0.104	390	48	0.123	90	12	0.133
6218	-1.47	0.561	0.299	...	...	...	82	11	0.134	91	12	0.132
6229	-1.18	...	...	278	34	0.122	...	...	...	92	19	0.207
6254	-1.26	0.588	0.260	...	...	...	157	18	0.115	69	13	0.188
6266	-1.18	...	...	446	40	0.090	...	...	...	114	18	0.158
6284	-1.26	...	...	127	16	0.126	...	...	...	...	...	...
6304	-0.45	0.062	0.060	99	8	0.081	...	...	...	...	...	...
6341	-2.31	0.261	0.542	...	...	...	245	33	0.135	140	20	0.143
6356	-0.40	...	...	362	25	0.069	...	...	...	...	...	...
6362	-0.59	0.122	0.621	38	6	0.158	...	...	...	...	...	...
6388	-0.55	0.057	0.836	1347	176	0.131	...	...	...	...	...	...
6402	-1.28	...	...	349	29	0.083	...	...	...	...	...	...
6441	-0.46	0.048	0.904	1380	154	0.112	...	...	...	...	...	...
6539	-0.63	...	...	114	15	0.132	...	...	...	...	...	...
6541	-1.81	0.563	0.347	...	...	...	248	41	0.165	...	...	...
6569	-0.76	...	...	166	30	0.181	...	...	...	...	...	...
6584	-1.50	0.102	0.558	55	8	0.145	...	...	...	...	...	...
6624	-0.44	0.077	0.085	121	9	0.074	188	20	0.106	126	30	0.238
6637	-0.64	0.078	0.065	135	25	0.185	244	43	0.176	127	21	0.165
6638	-0.95	...	...	101	28	0.277	...	...	...	...	...	...
6652	-0.81	0.073	0.080	61	5	0.082	83	9	0.108	75	20	0.267
6681	-1.62	0.558	0.334	100	9	0.090	...	...	...	82	8	0.098
6723	-1.10	0.127	0.704	102	11	0.108	194	22	0.113	101	15	0.149
6752	-1.54	0.378	0.578	...	...	...	173	20	0.116	225	13	0.058
6864	-1.29	...	...	363	69	0.190	...	...	...	55	12	0.218
6934	-1.47	0.097	0.678	149	18	0.121	99	17	0.172	...	...	...
6981	-1.42	0.142	0.570	61	7	0.115	188	36	0.191	45	10	0.222
7078	-2.37	0.174	0.713	376	48	0.128	537	57	0.106	153	23	0.150
7089	-1.65	0.150	0.790	167	18	0.108	702	100	0.142	...	...	...
7099	-2.27	0.462	0.261	89	6	0.067	...	...	...	202	11	0.054

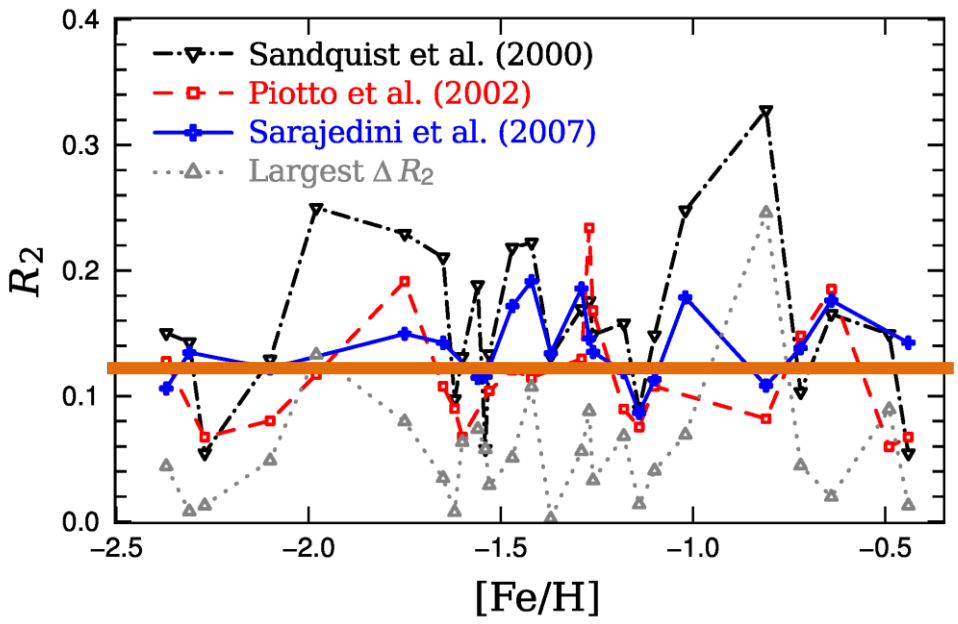

Figure 1. Comparison of R_2 for clusters shown in Table 1, limited to those with at least two different sources of photometry. The R_2 determined from the Sandquist (2000), Piotto et al. (2002), and Sarajedini et al. (2007) data are shown in black dash-dots, red dashes, and a blue solid line, respectively. The dotted grey line shows the maximum difference between R_2 determinations from different photometry.

$$R_2 = N_{AGB}/N_{HB} = 0.117 \pm 0.005$$

The treatment of mixing in core helium burning models II. Constraints from cluster star counts
Constantino, Campbell, Lattanzio & van Duijneveldt, arXiv:1512.04845

Predicting the Axion-Modified Ratios

M.J. Dolan, F.J. Hiskens & R.R. Volkas, arXiv:2207.03102

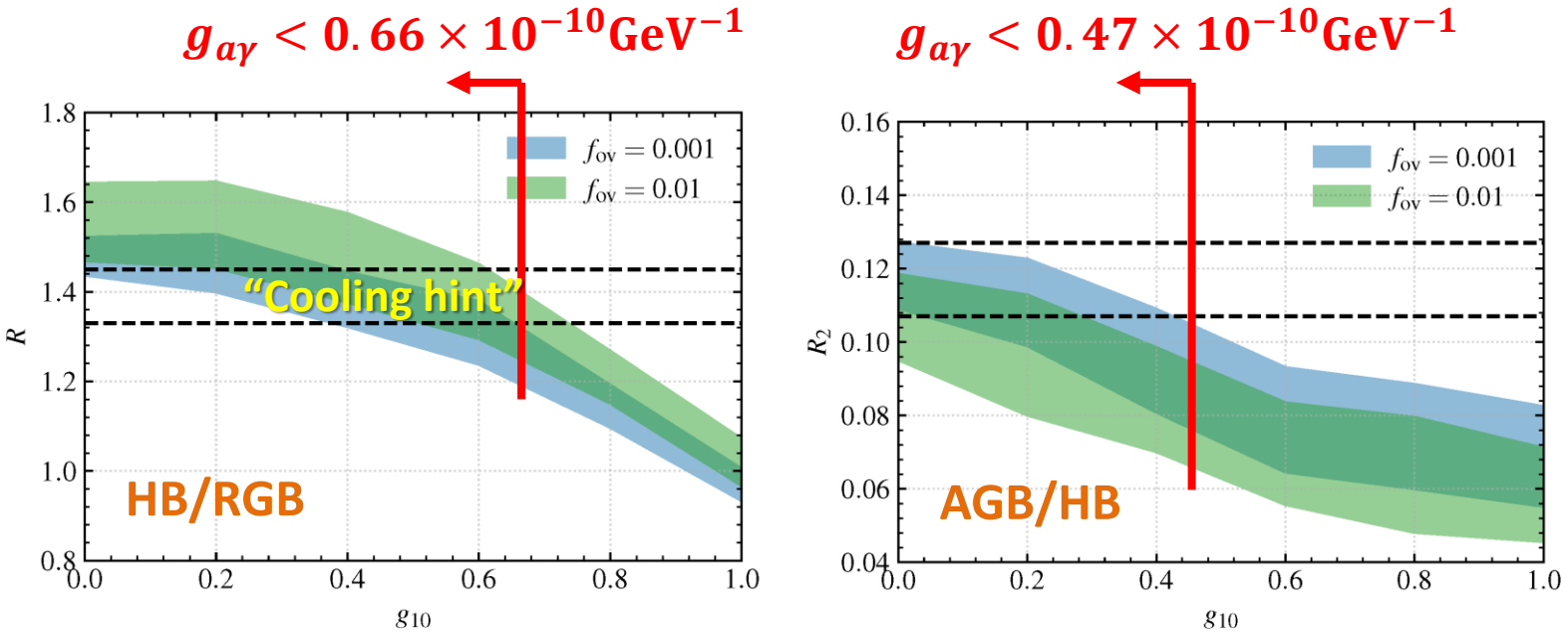

Figure 2. (Left panel): Predicted values of R as a function of g_{10} given standard convective core overshoot with $f_{\rm ov} = 0.001$ (blue) and $f_{\rm ov} = 0.01$ (green). The observed limit on R is indicated by the region between the dashed black lines (95% C.I.). (Right panel): The full range of R_2 values predicted as functions of g_{10} given standard overshoot with $f_{\rm ov} = 0.001$ (blue) and $f_{\rm ov} = 0.01$ (green). The observed limit is again shown by the dashed black lines.

Probably one should analyze GCs for all observables simultaneously using modern high-statistics (GAIA) data

ALP Scape: Helioscope Close-Up

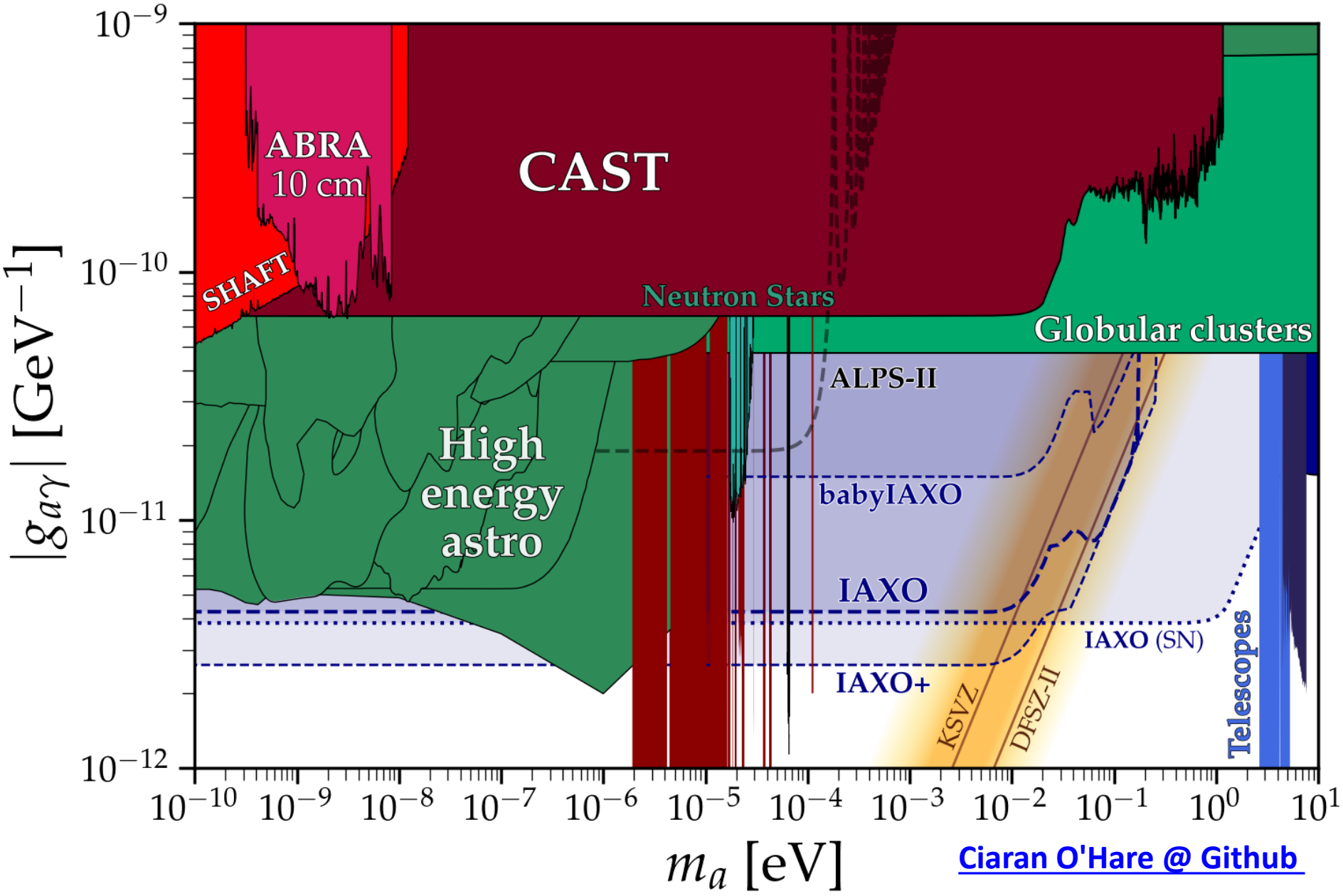

Ciaran O'Hare @ Github

Color-Magnitude Diagram for Globular Clusters

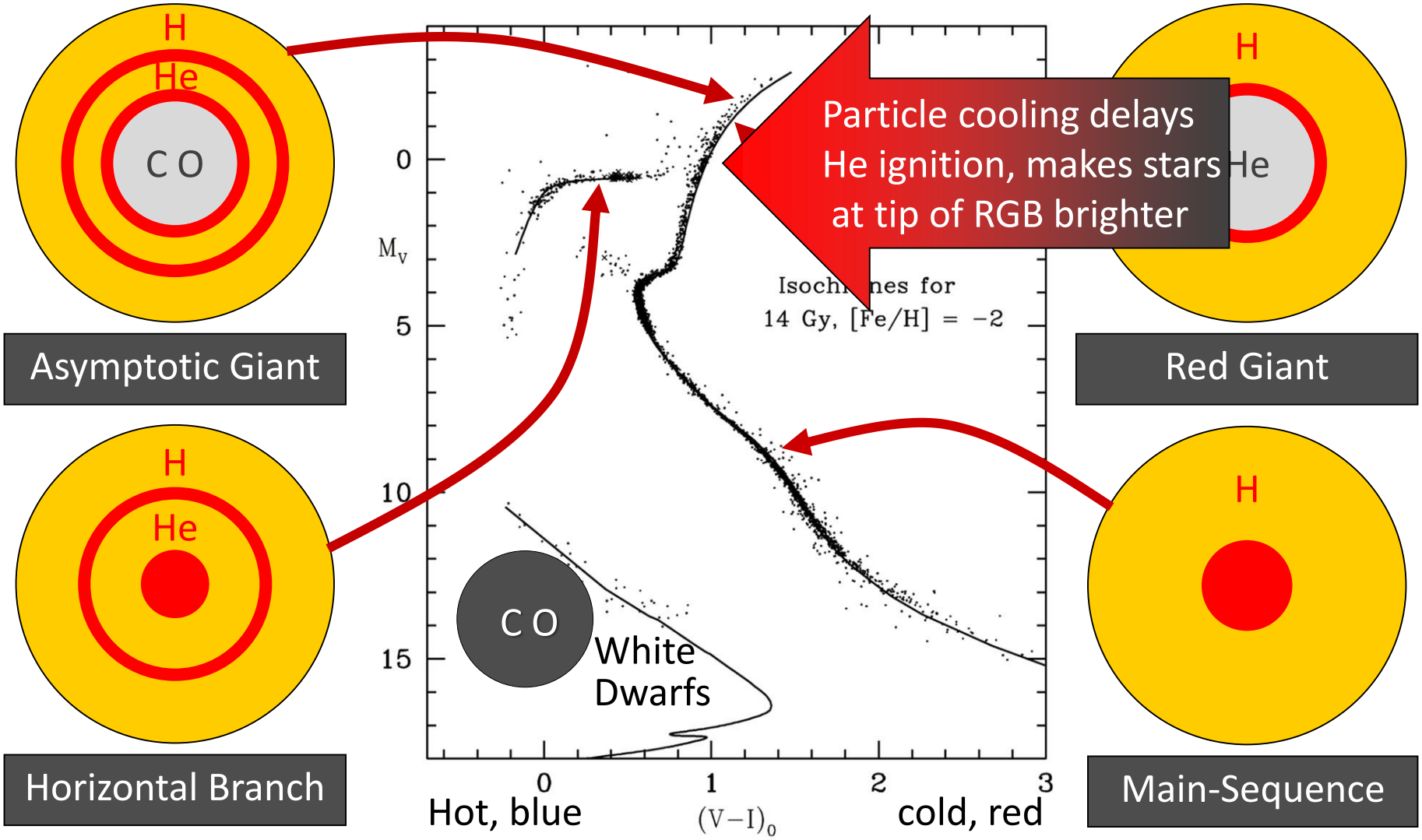

Color-magnitude diagram synthesized from several low-metallicity globular clusters and compared with theoretical isochrones (W.Harris, 2000)

Color-Magnitude Diagram for Globular Clusters

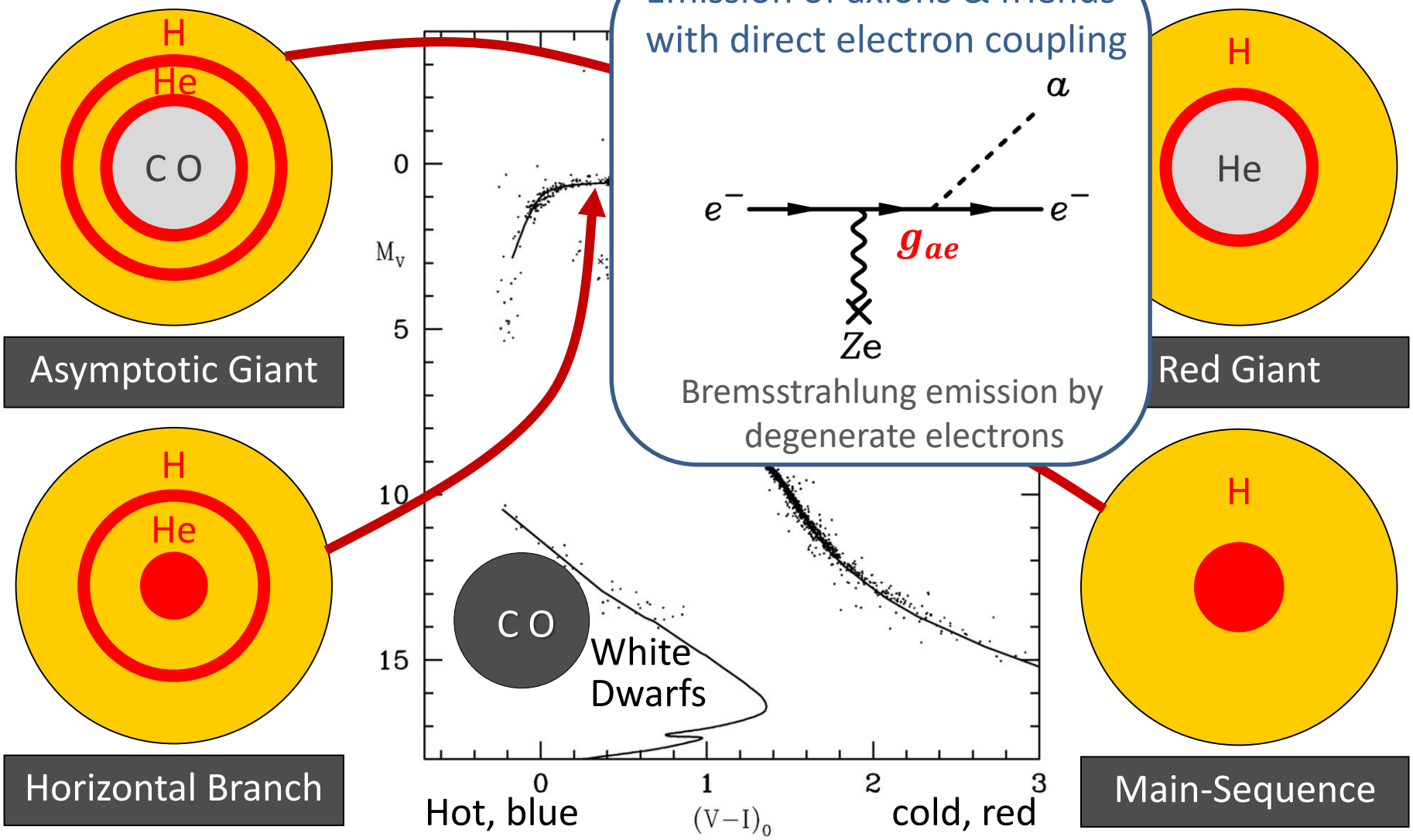

Color-magnitude diagram synthesized from several low-metallicity globular clusters and compared with theoretical isochrones (W.Harris, 2000)

TRGB in 46 Globular Clusters [Cerny+ 2012.09701]

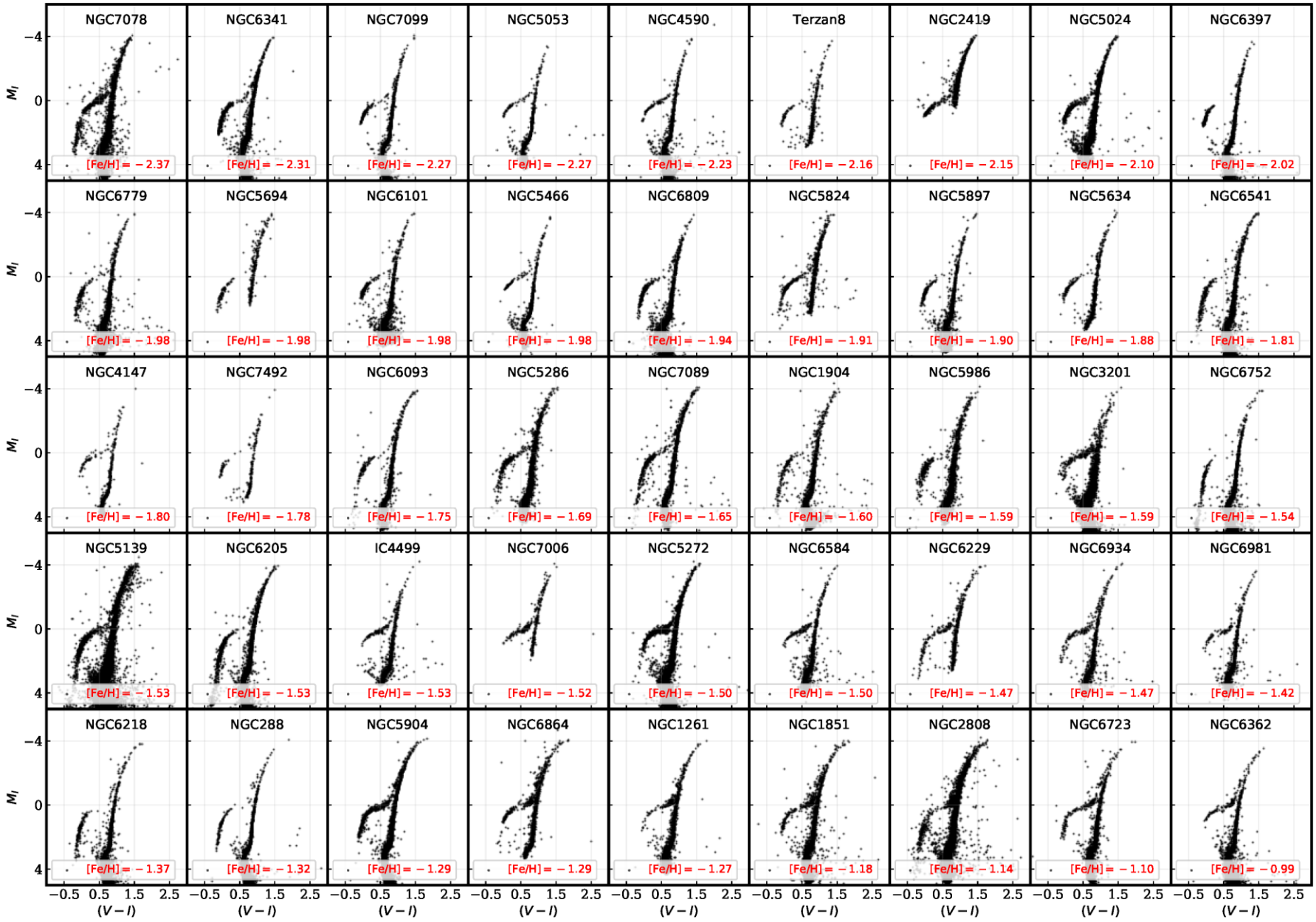

New TRGB Calibration from 22 Globular Clusters

Straniero+ arXiv:2010.03833

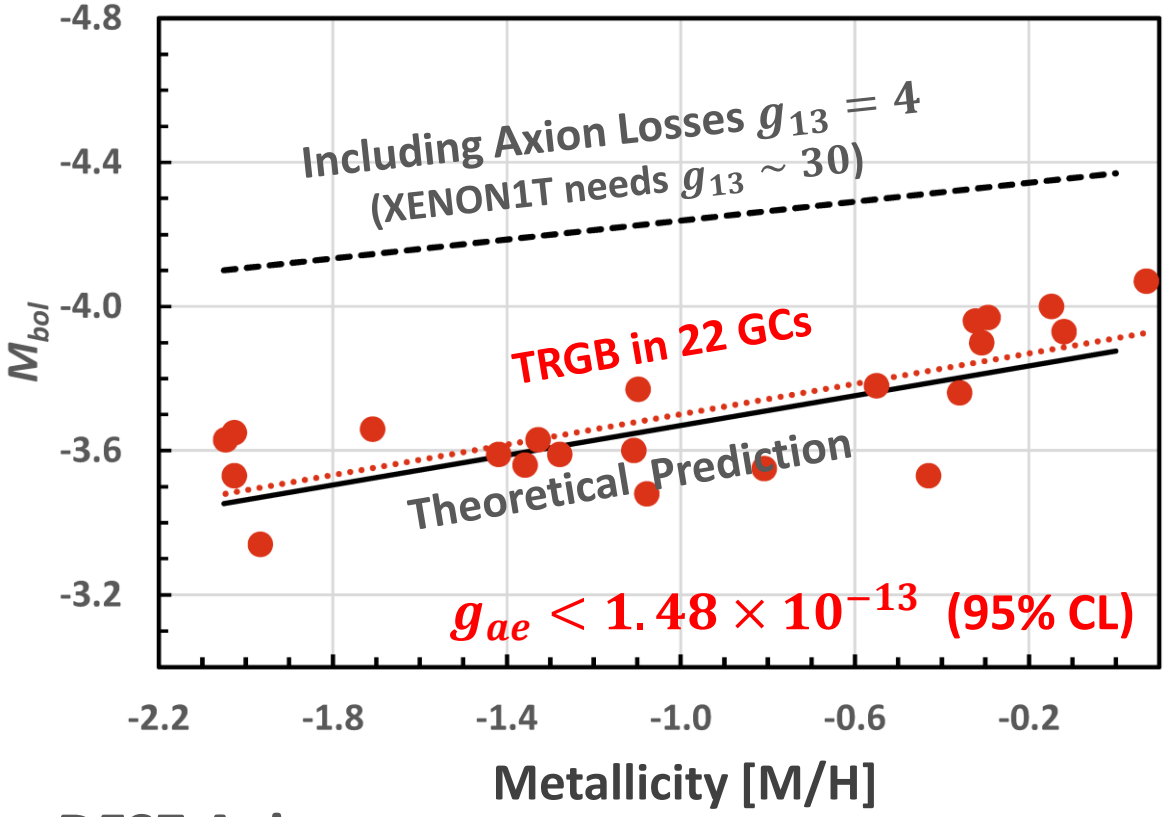

Emission of axions & friends with direct electron coupling

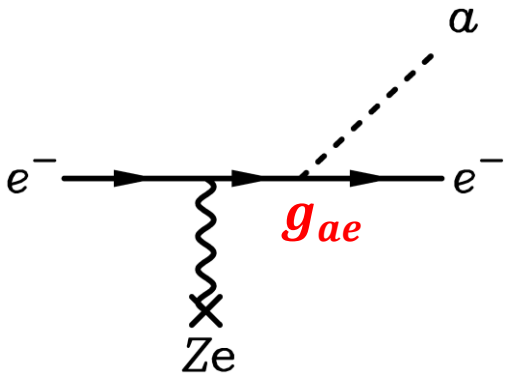

Bremsstrahlung emission by degenerate electrons

DFSZ Axions

$$m_a = 6\,\mathrm{meV}\frac{10^9\mathrm{GeV}}{f_a} \qquad g_{\mathrm{ae}} = \frac{m_e C_e}{f_a}$$

$$\mathcal{L}_{\mathrm{ae}} = \frac{C_e}{2f_a}\bar{e}\gamma^\mu\gamma_5 e\partial_\mu a \qquad C_e = \frac{\cos^2\beta}{3}$$

$$\frac{f_a}{\cos^2\beta} > 1.15 \times 10^9\ \mathrm{GeV}$$

Tip of the Red-Giant Branch in the Galaxy NGC 4258

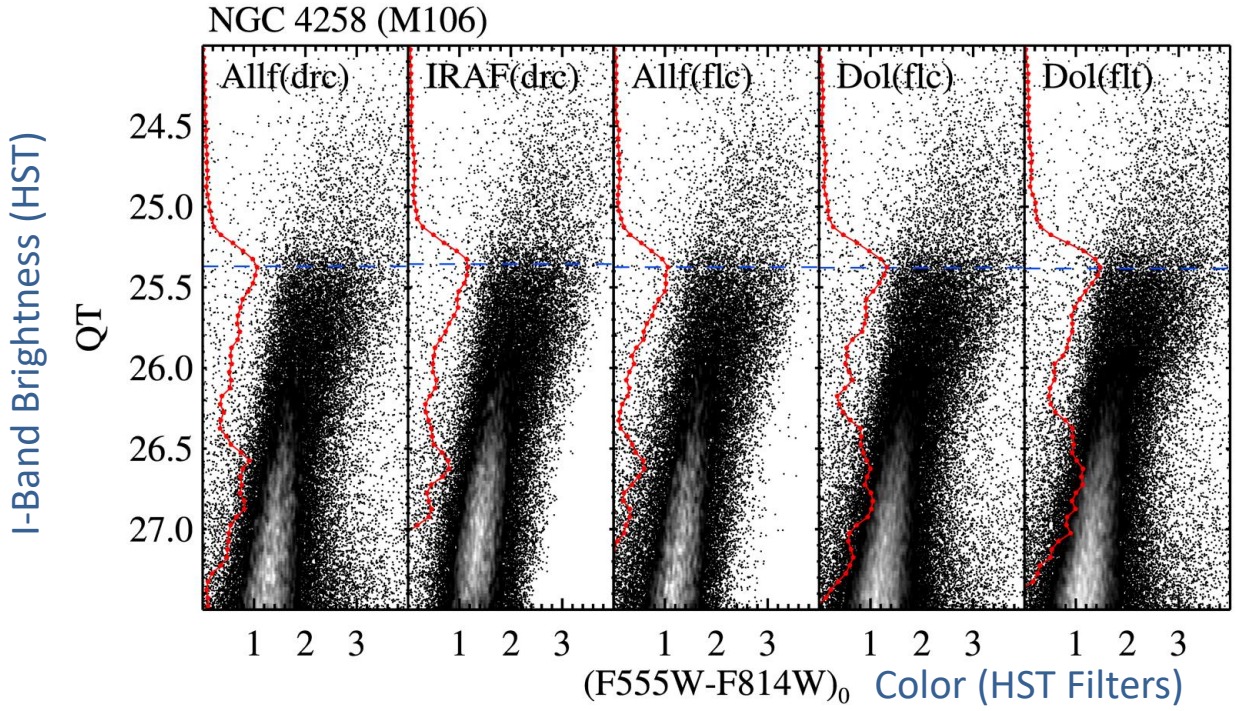

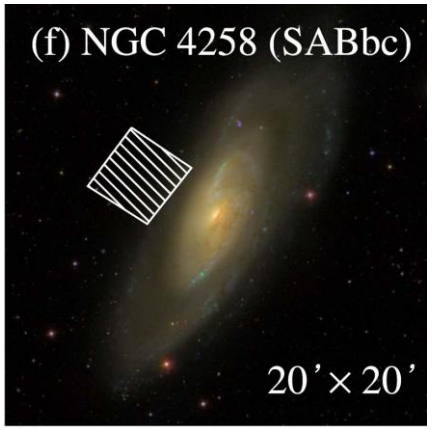

Figure 7. $QT - (F555W - F814W)_0$ CMDs of NGC 4258 from five different reduction methods : ALLFRAME on drc, IRAF/DAOPHOT on drc, ALLFRAME on flc, DOLPHOT on flc, and DOLPHOT on flt (from left to right). Edge detection responses are shown by the solid lines. Note that the estimated TRGB magnitudes (dashed lines) agree very well.

NGC 4258 hosts a water megamaser

→ Quasi-geometric distance determination

→ Among the best absolute TRGB calibrations

Hubble Tension

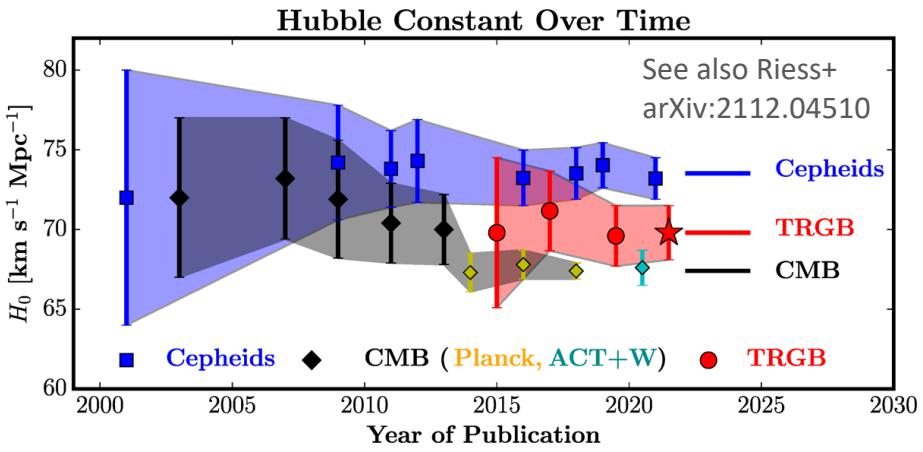

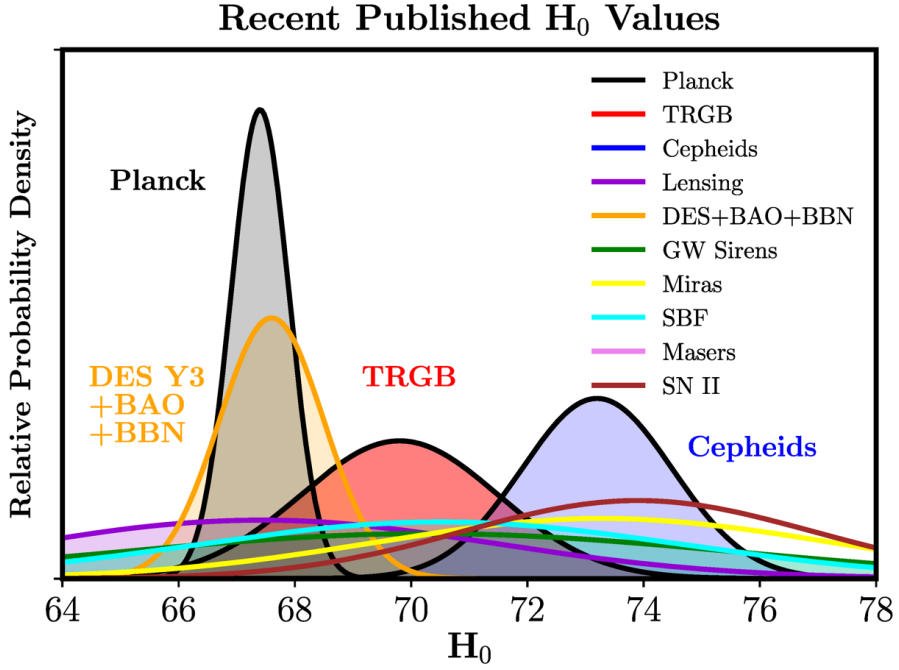

Freedman ApJ 919 (2021) 16 [2106.15656]

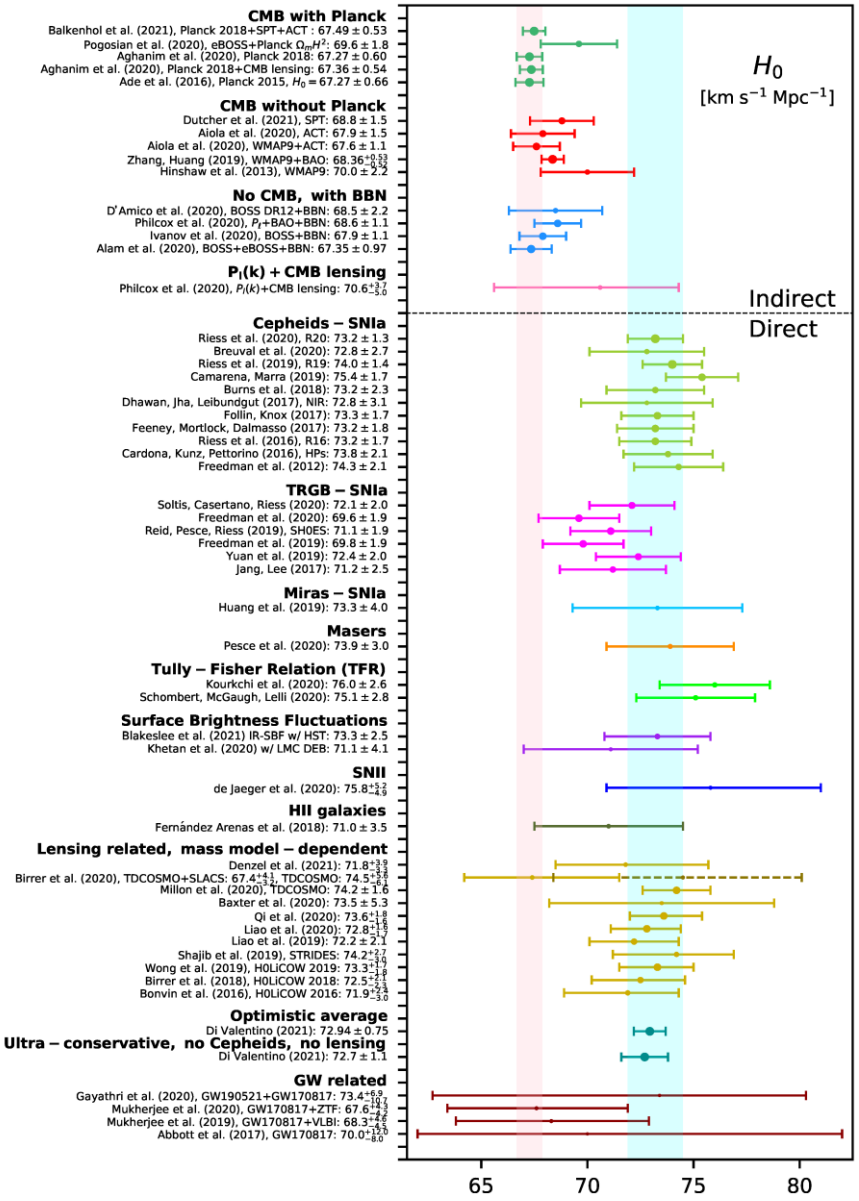

Di Valentino+ arXiv:2103.01183

Axion Bounds from TRGB Calibrations

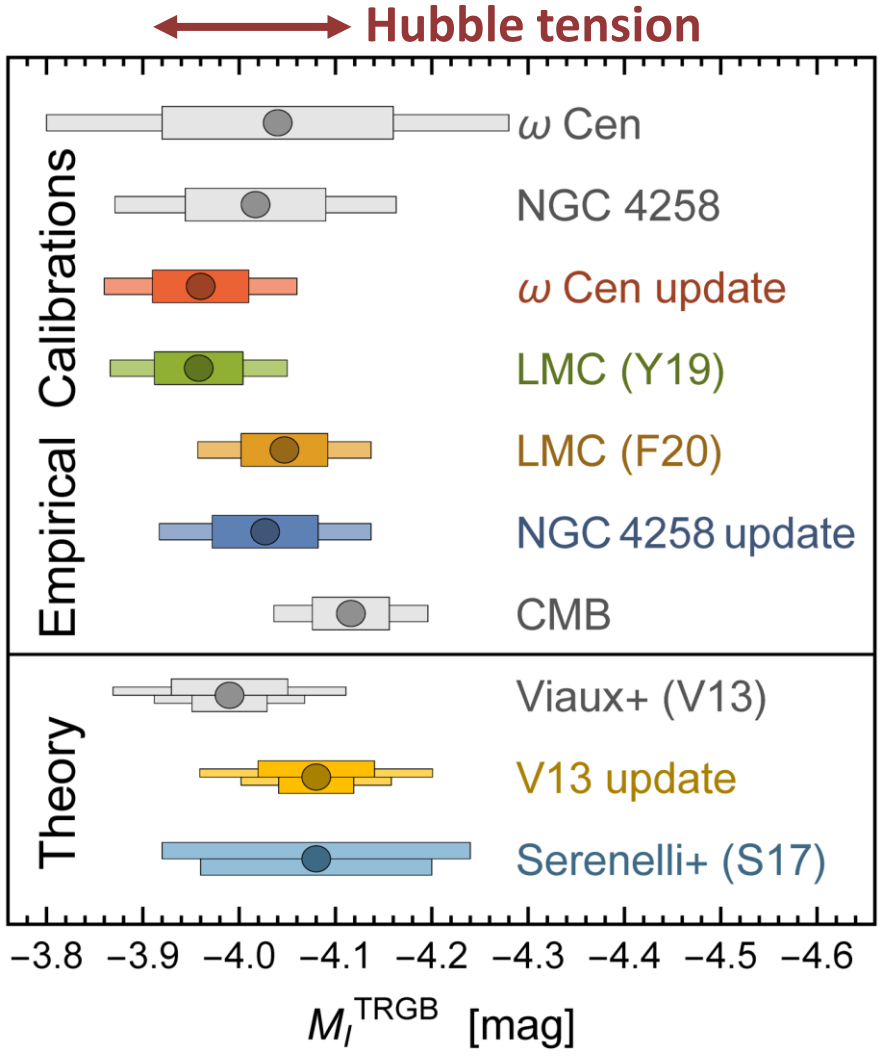

Updated TRGB Calibrations
Capozzi & Raffelt, arXiv:2007.03694

Bounds from "water megamaser" galaxy NGC 4258, compared with stellar evolution theory (95% CL)

$$g_{ae} < 1.6 \times 10^{-13}$$

DFSZ-axions

$$\frac{f_a}{\cos^2\beta} > 1.1 \times 10^9 \text{ GeV}$$

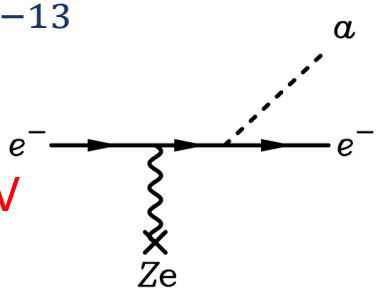

Neutrino Dipole Moments

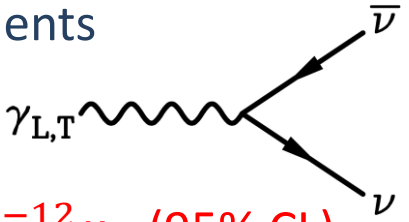

$$\sqrt{\sum_i |\mu_i|^2} < 1.5 \times 10^{-12} \mu_{\mathrm{B}} \text{ (95\% CL)}$$

Neutrino-electron scattering (Borexino)

$$\mu_\nu^{\mathrm{eff}} < 28 \times 10^{-12} \mu_{\mathrm{B}} \text{ (90\% CL)}$$

Hertzsprung Russel Diagram

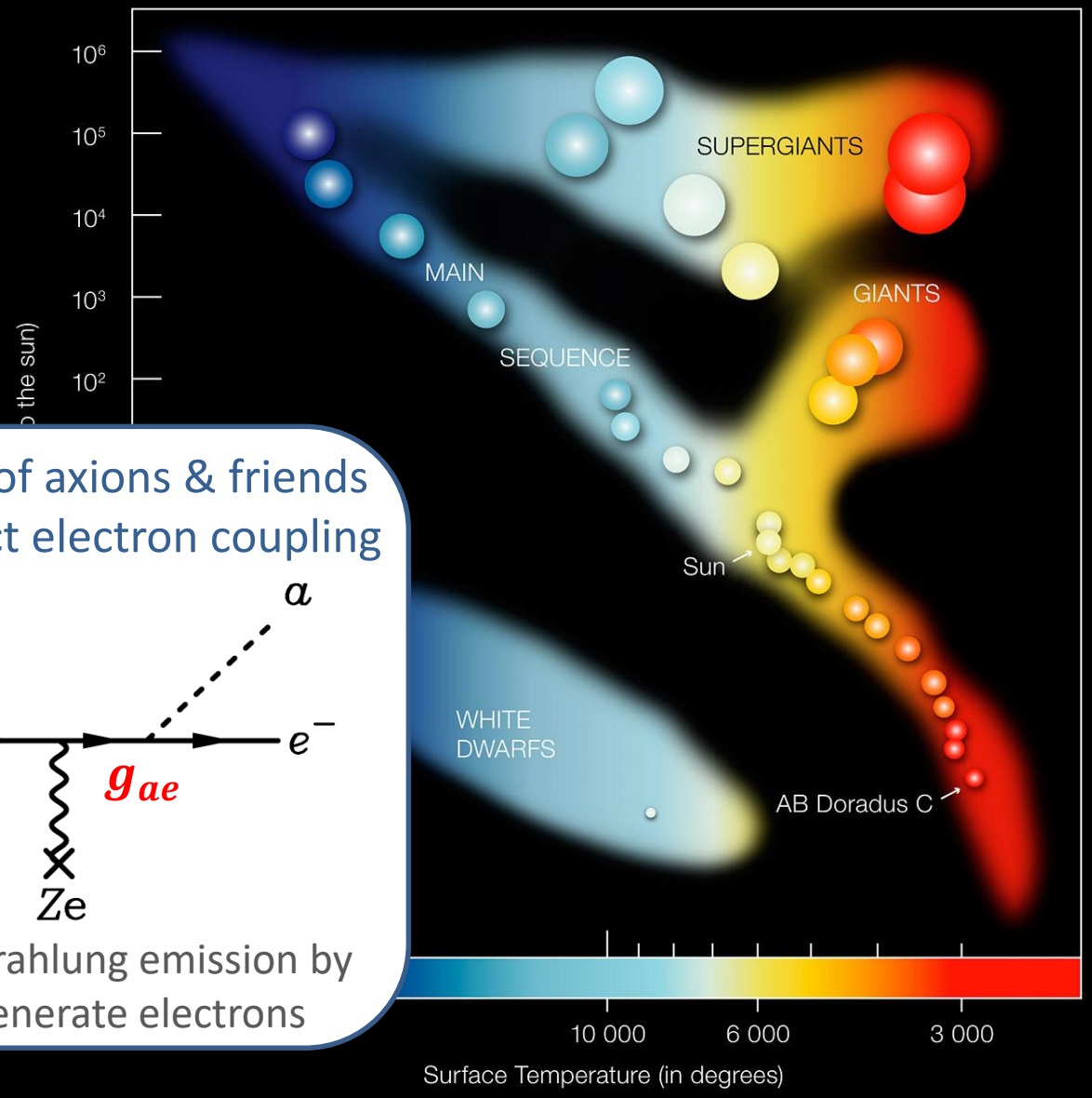

Emission of axions & friends with direct electron coupling

Bremsstrahlung emission by degenerate electrons

https://www.eso.org/public/images/eso0728c/

White Dwarfs

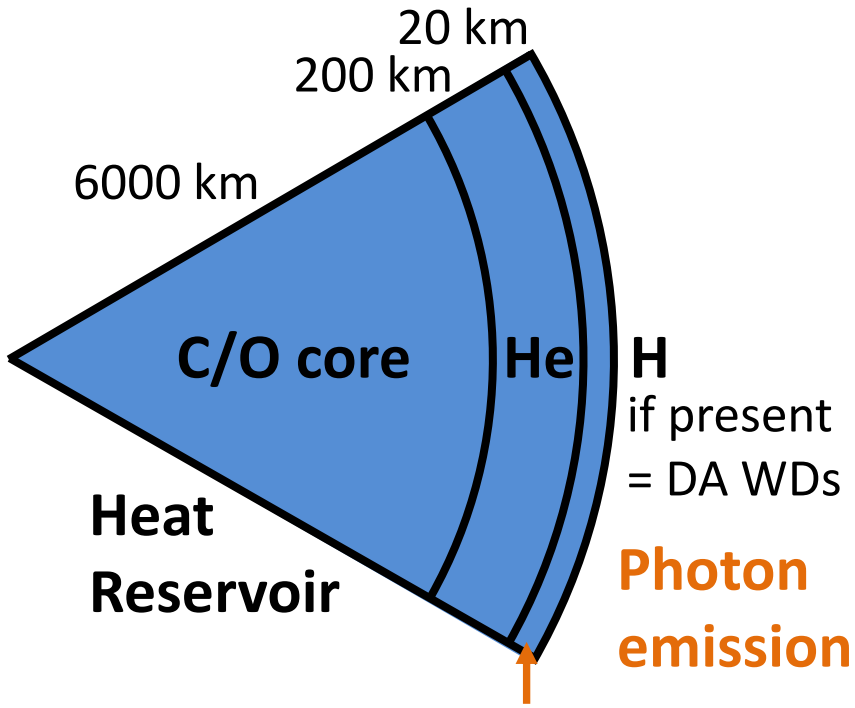

$R \simeq 6000$ km (Size of the Earth)
$T_{\rm eff} \simeq 10{,}000$–$30{,}000$K (Sun 6000 K)
$L \simeq 10^{-4}$–$10^{-1} L_\odot$
$M \simeq 0.5$–$0.8 M_\odot$
$\rho \simeq 10^6 {\rm g/cm^3}$ (very degenerate)

White Dwarf Luminosity Function (WDLF)

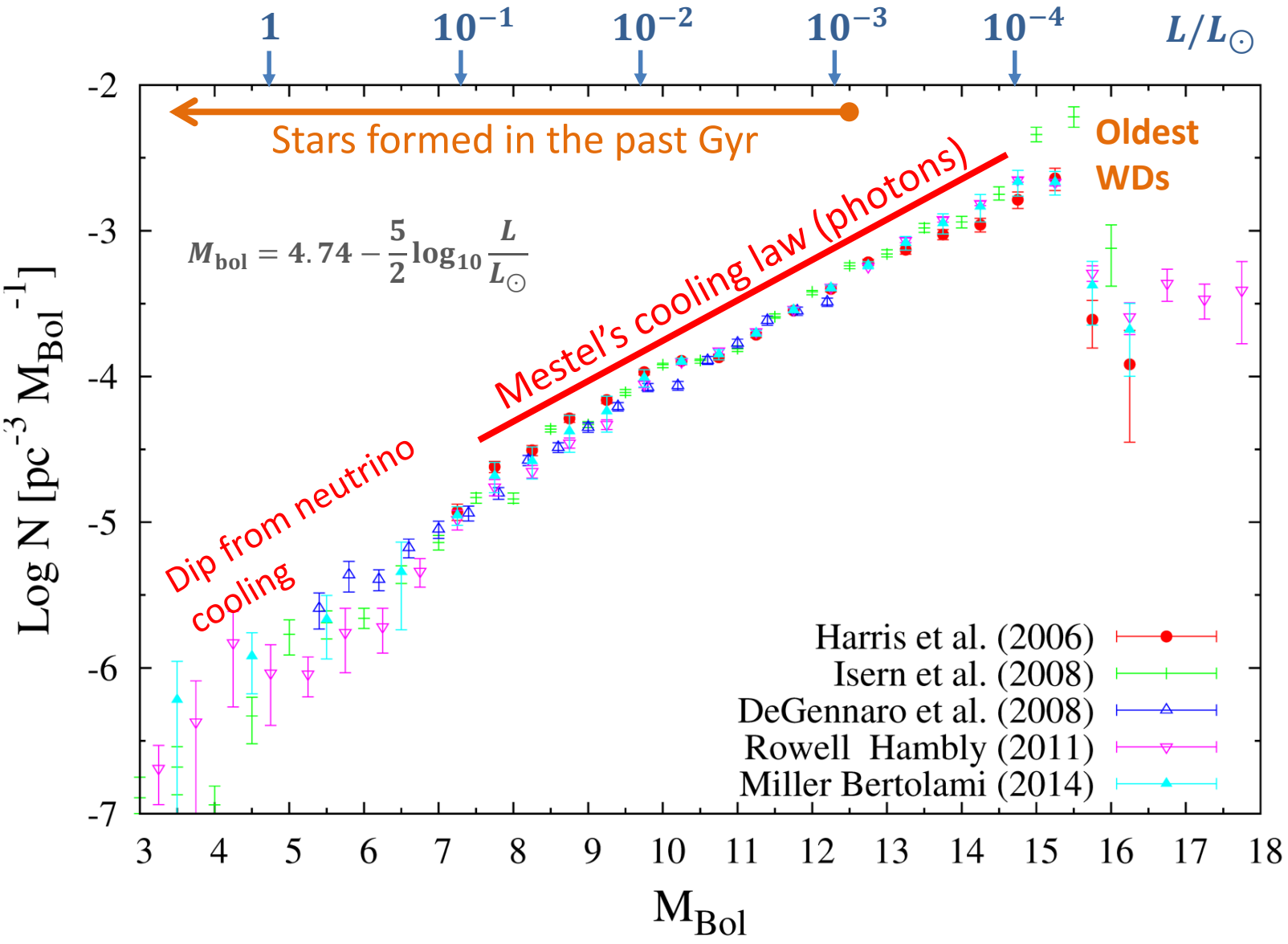

Miller Bertolami, Melendez, Althaus & Isern, arXiv:1406.7712

Axion Bounds from WD Luminosity Function

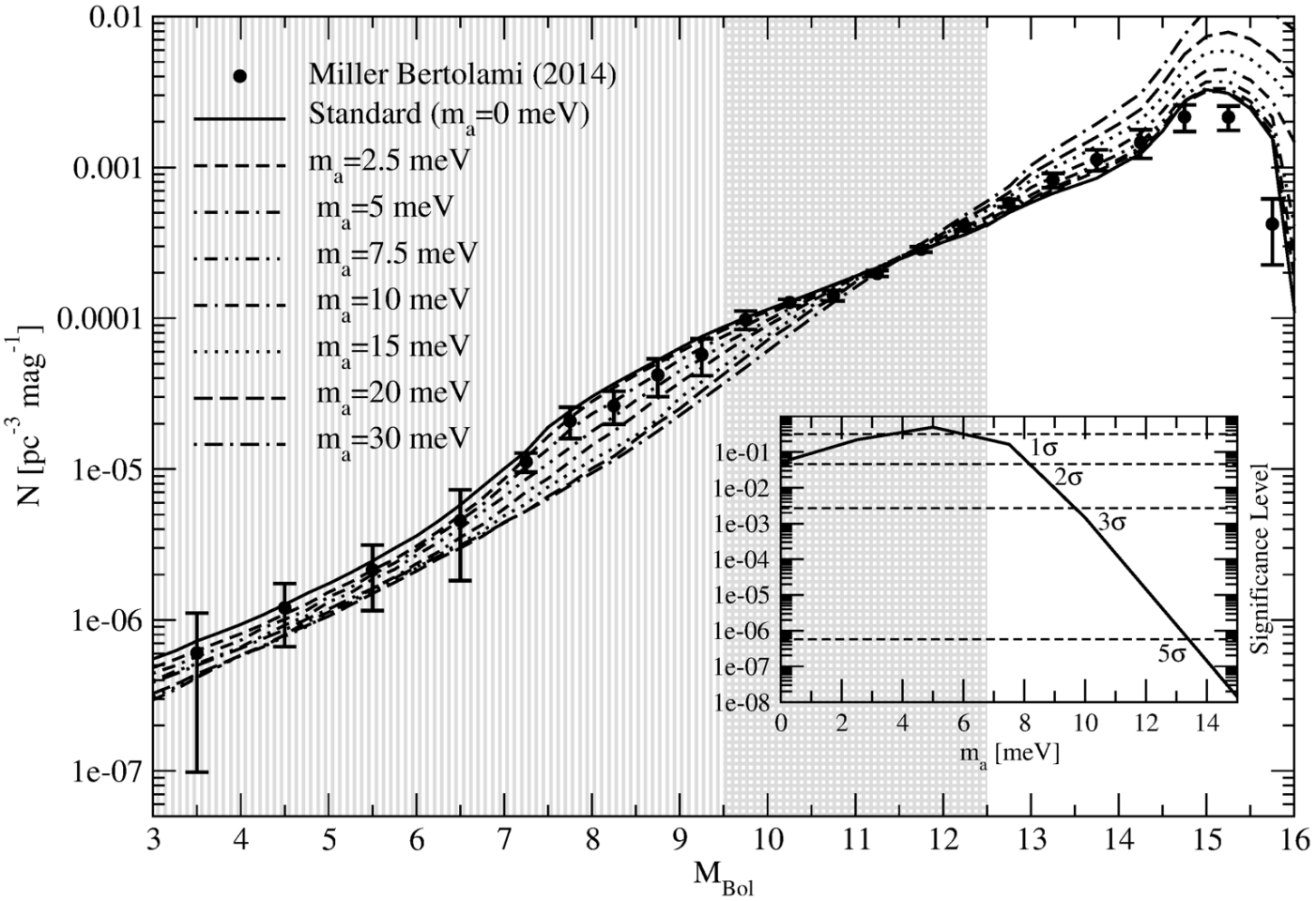

Limits on axion-electron coupling and mass limit in DFSZ model:

$g_{ae} \lesssim 3 \times 10^{-13}$ $\qquad$ $m_a \cos^2 \beta \lesssim 10$ meV

Miller Bertolami, Melendez, Althaus & Isern, arXiv:1406.7712, 1410.1677

For extensions and review see: Isern, arXiv:2002.08069

Pulsating Stars

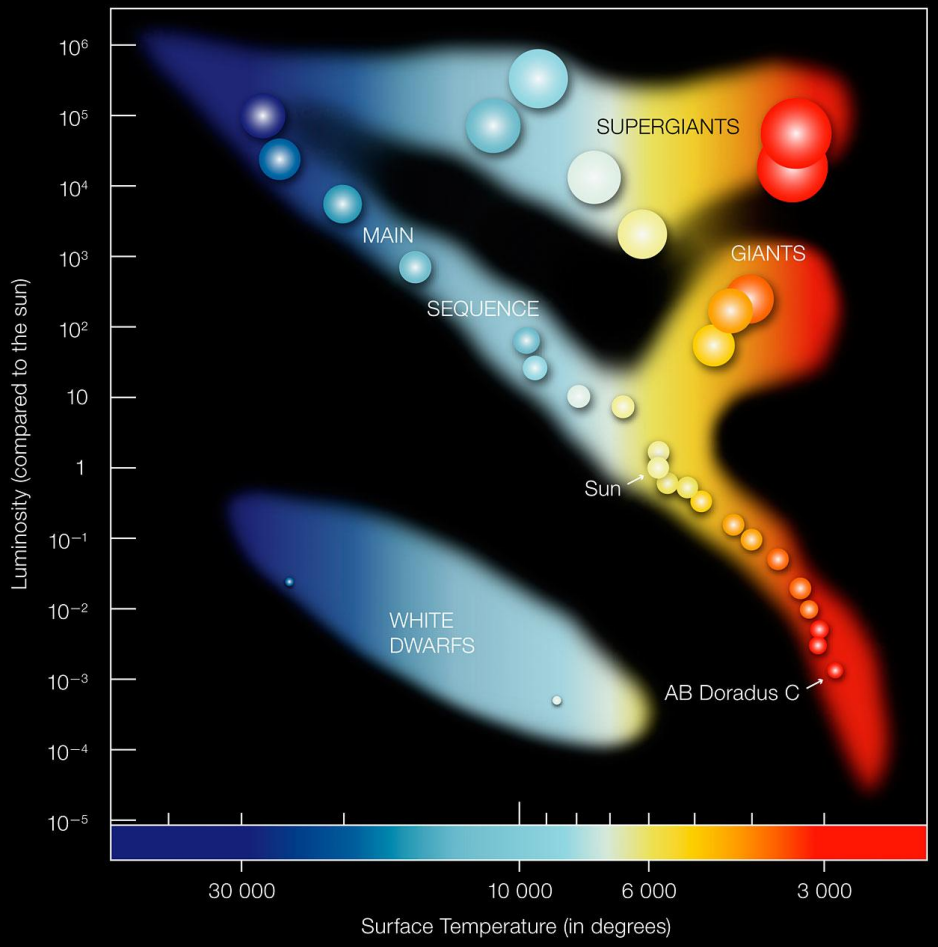

https://www.eso.org/public/images/eso0728c/

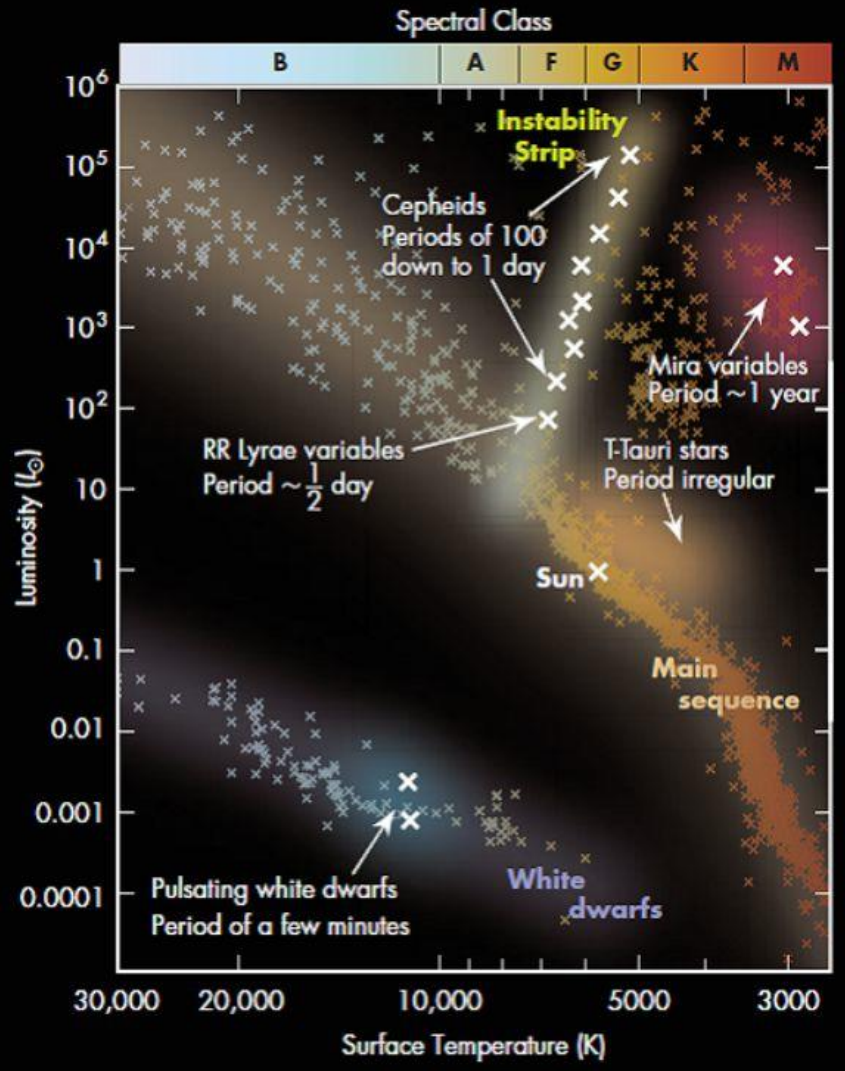

https://scienceatyourdoorstep.com/2021/01/04/what-are-variable-stars/

Non-Radial g-Modes

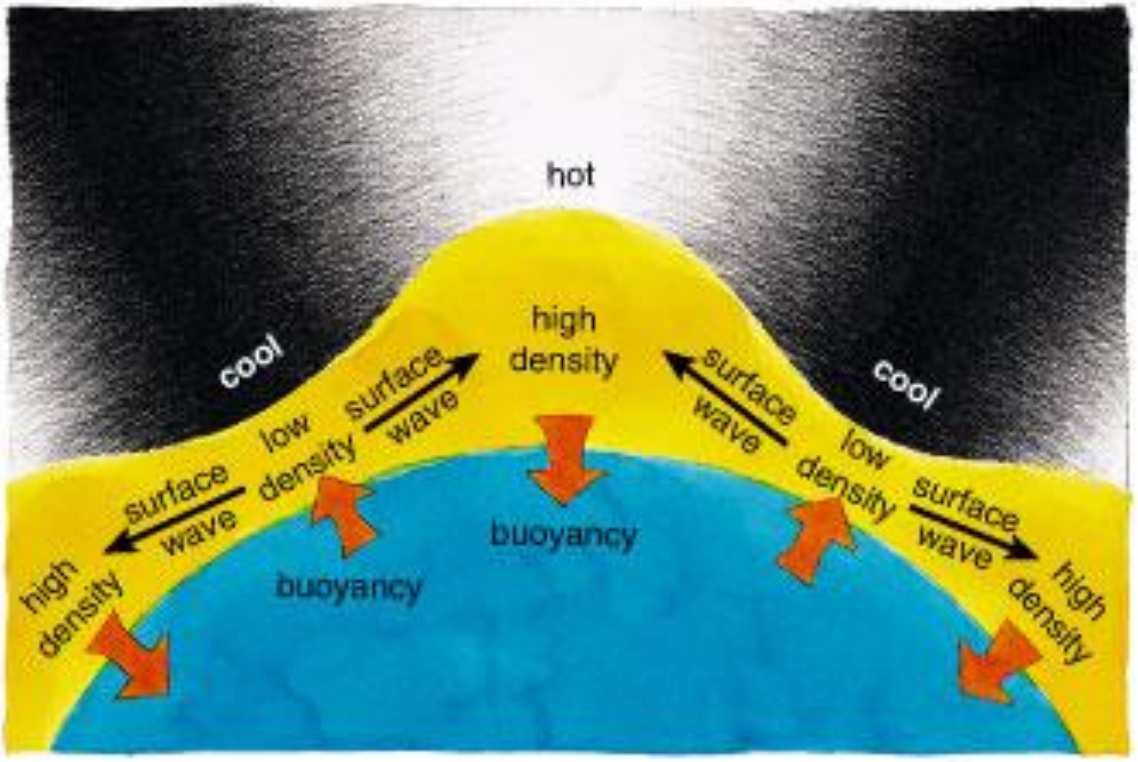

From a talk by J. Isern

- Long period waves (100 – 1000 s)
- Gravity is the restoring force

$$\frac{d \log \Pi}{dt} \propto -\frac{d \log T}{dt}$$

- Period decreases as the star cools
- Characteristic rate 10^{-15} s/s
- Measures cooling speed of a single star

Pulsating White Dwarf G117–B15A

Kepler+ ApJ 254 (1982) 676

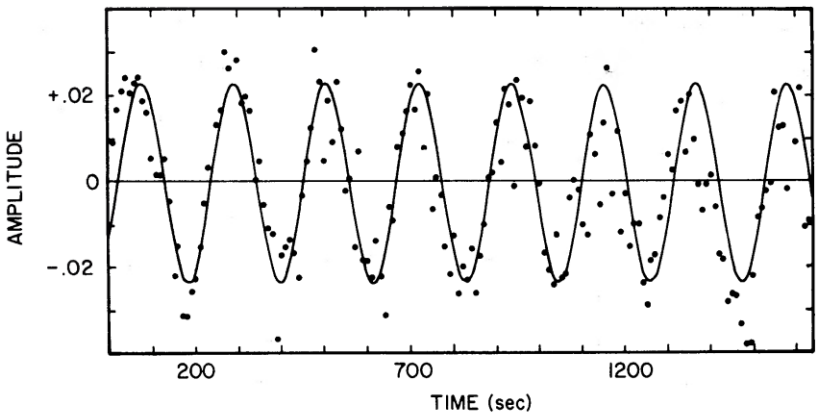

FIG. 1.—A portion of the light curve of G117−B15A in unfiltered light during run 2075. The light curve has been normalized so that the time-averaged brightness of G117−B15A is equal to 1.00, and then 1.00 has been subtracted from the light curve. The solid line is a sine curve with a period of 215.19 s and a semiamplitude of 0.022 mag.

$D = 57.5 \pm 0.1$ pc

$T = 12{,}400$ K

$M = 0.69\ M_\odot$

Period 215.2 s

Kepler+ ApJ 906 (2021) 7

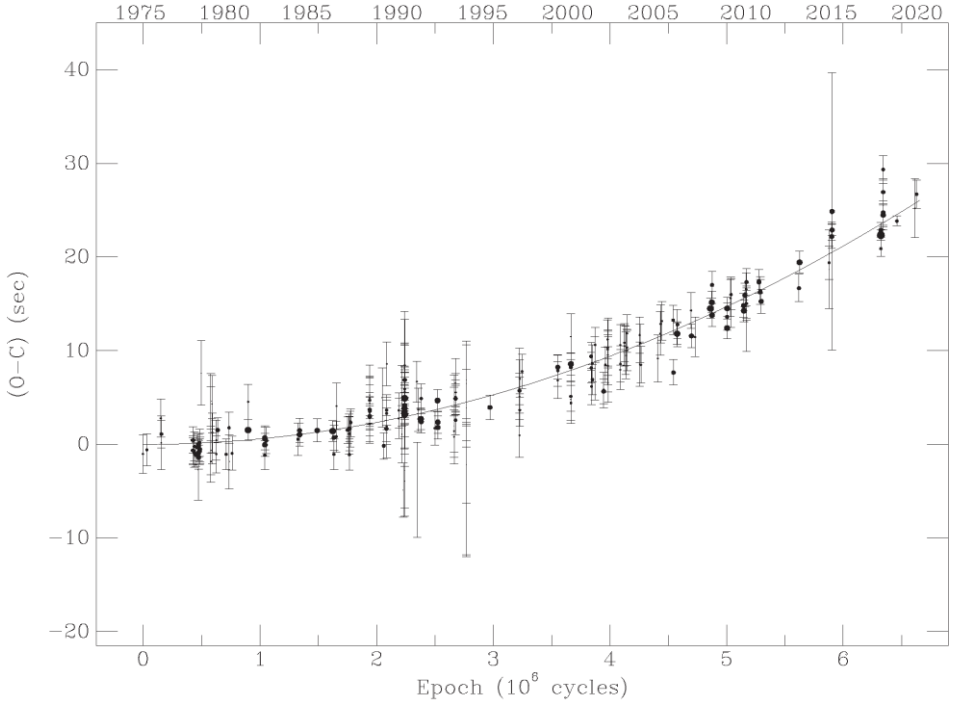

Figure 1. $(O - C)$: observed minus calculated times of maxima for the 215 s pulsation of G 117-B15A. The size of each point is proportional to its weight, i.e., inversely proportional to the uncertainty in the time of maxima squared. We show $\pm 1\sigma$ error bars for each point, and the line shows our best-fit parabola to the data. The fact that the line does not overlap these error bars is a demonstration that they are underestimated. Note that as the period of pulsation is 215.1973882 s, the observed total change in phase is only 50 deg.

"Most stable optical clock", slipped by 26 s (of 215.2 s period) in 45 years

$$\dot{P}/P = (5.12 \pm 0.82) \times 10^{-15}\ \mathrm{s/s}$$

G117–B15A Period Decrease: Hint for Axion Cooling?

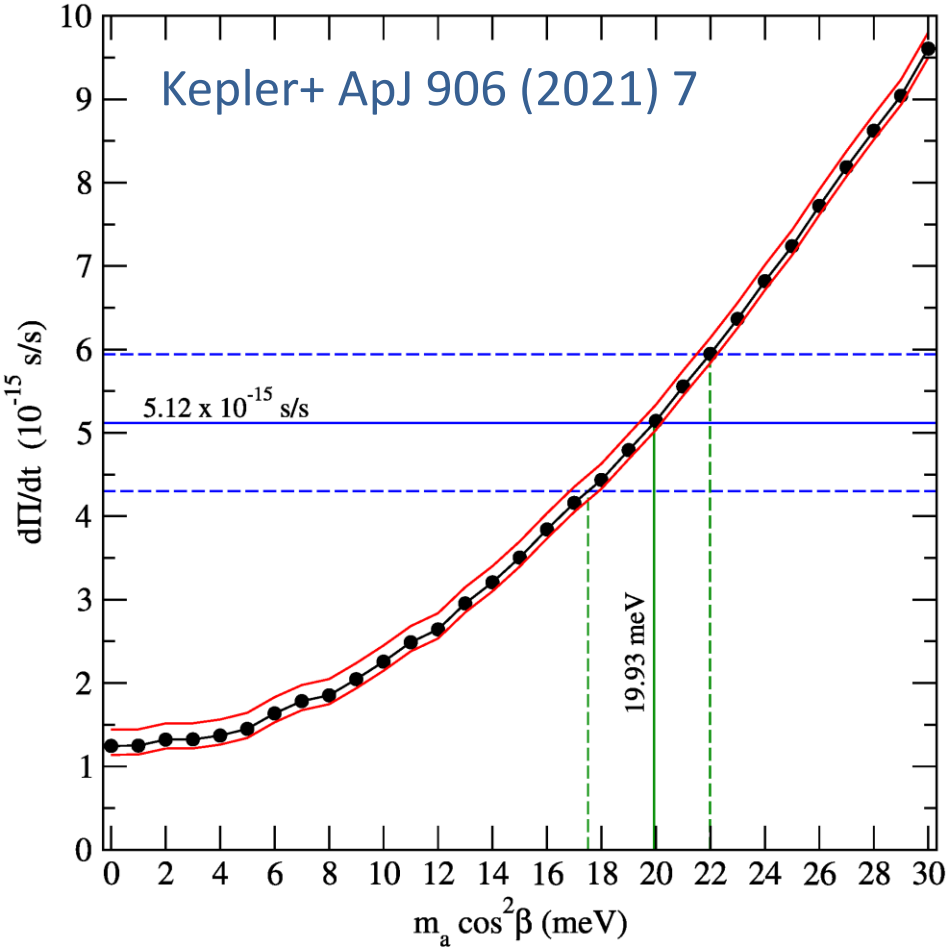

Figure 2. The rate of period change for the mode with $\ell = 1$ and $k = 2$, corresponding to a period of ~215 s in terms of the axion mass (black circles). Dashed lines represent the uncertainties in the value in the observed $\dot{P}$ and the axion mass, while the red curves represent the internal uncertainties in $\dot{P}$ due to modeling.

$$\dot{P}/P = (5.12 \pm 0.82) \times 10^{-15}\ \mathrm{s/s}$$

Emission of axions & friends with direct electron coupling

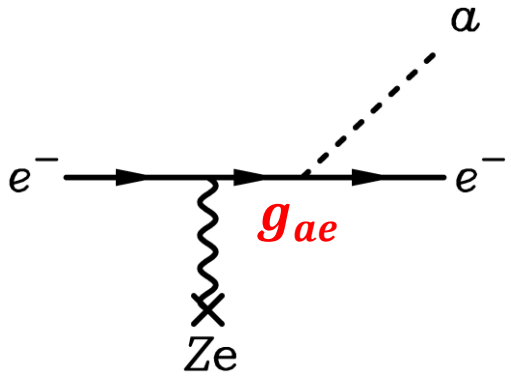

Bremsstrahlung emission by degenerate electrons

Case of DFSZ Axion

$$g_{ae} = 0.28 \times 10^{-13}\ \frac{m_a \cos^2\beta}{\mathrm{meV}}$$

Nominal cooling signal

$$g_{ae} = (5.7 \pm 0.6) \times 10^{-13}$$

White-Dwarf Bounds on Axion-Electron Coupling

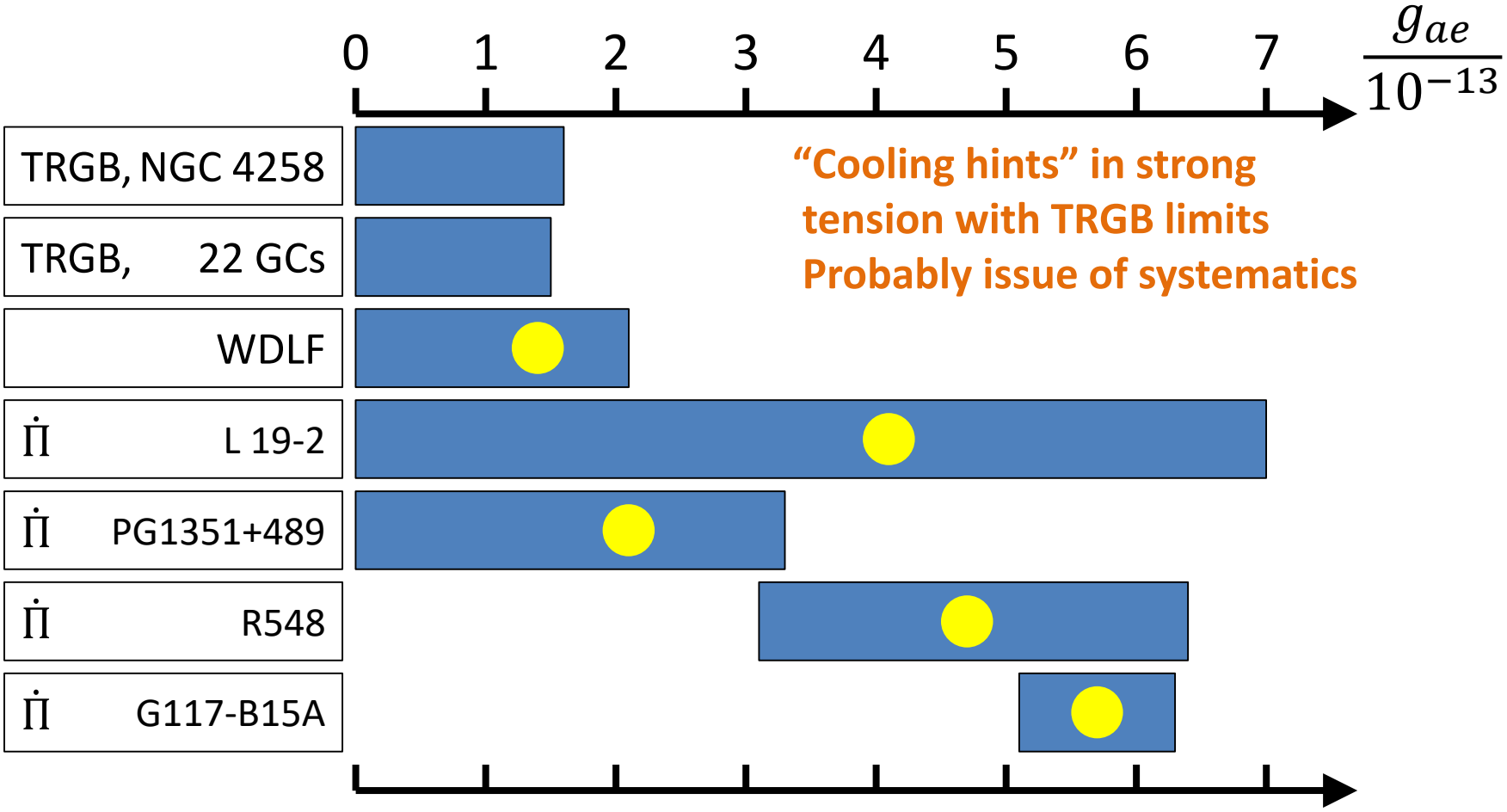

White Dwarfs as Physics Laboratories: Lights and Shadows, arXiv:2202.02052
J. Isern, S. Torres & A. Rebassa-Mansergas
Stellar Evolution Confronts Axion Models, arXiv:2109.10368
L. Di Luzio, M. Fedele, M. Giannotti, F. Mescia & E. Nardi

Global Fit for Axion-Photon vs. Axion-Electron

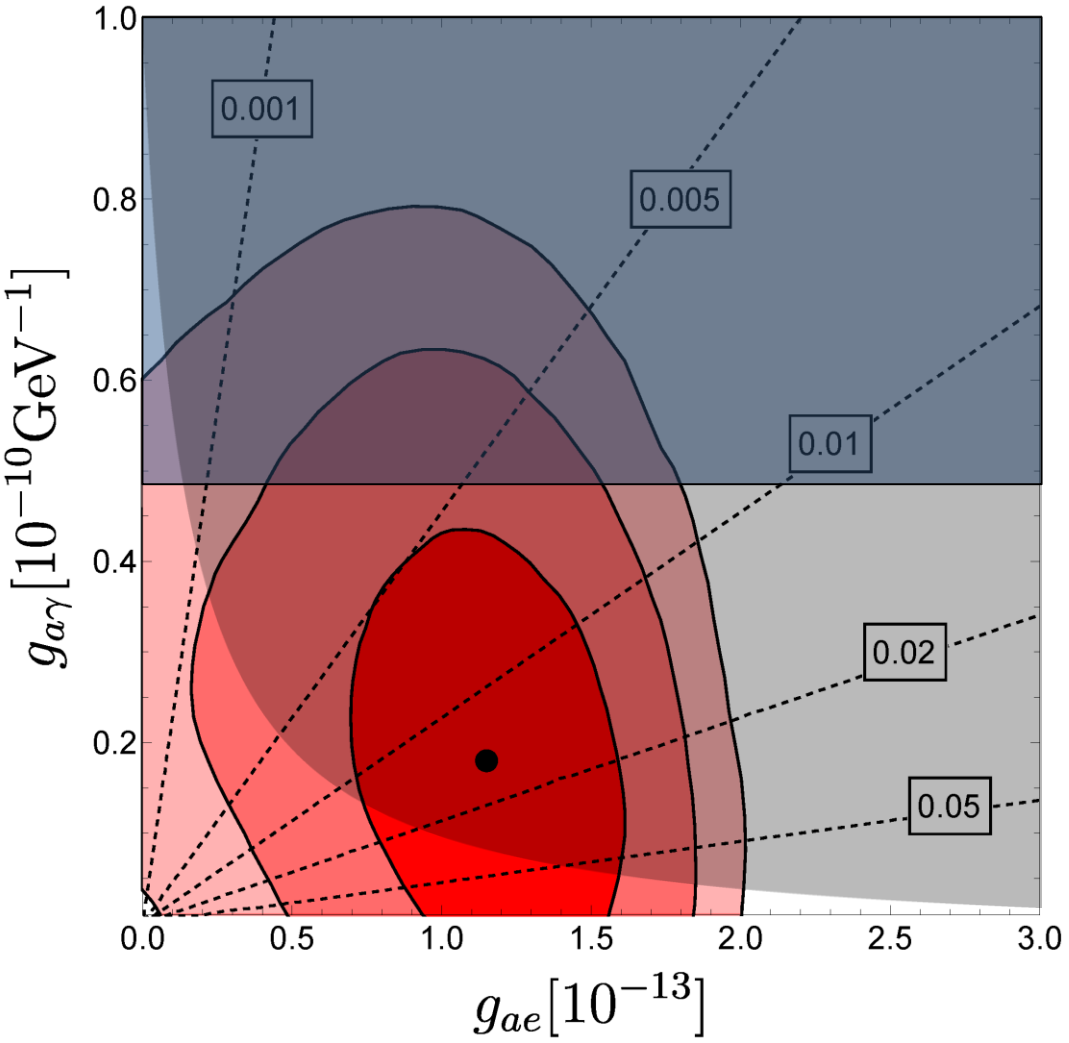

R2-parameter in globular clusters (AGB/HB)

Magnetic white dwarf ($m_a < 10^{-5}\mathrm{eV}$)

Stellar Evolution Confronts Axion Models, arXiv:2109.10368

L. Di Luzio, M. Fedele, M. Giannotti, F. Mescia & E. Nardi

Axion-Electron Coupling

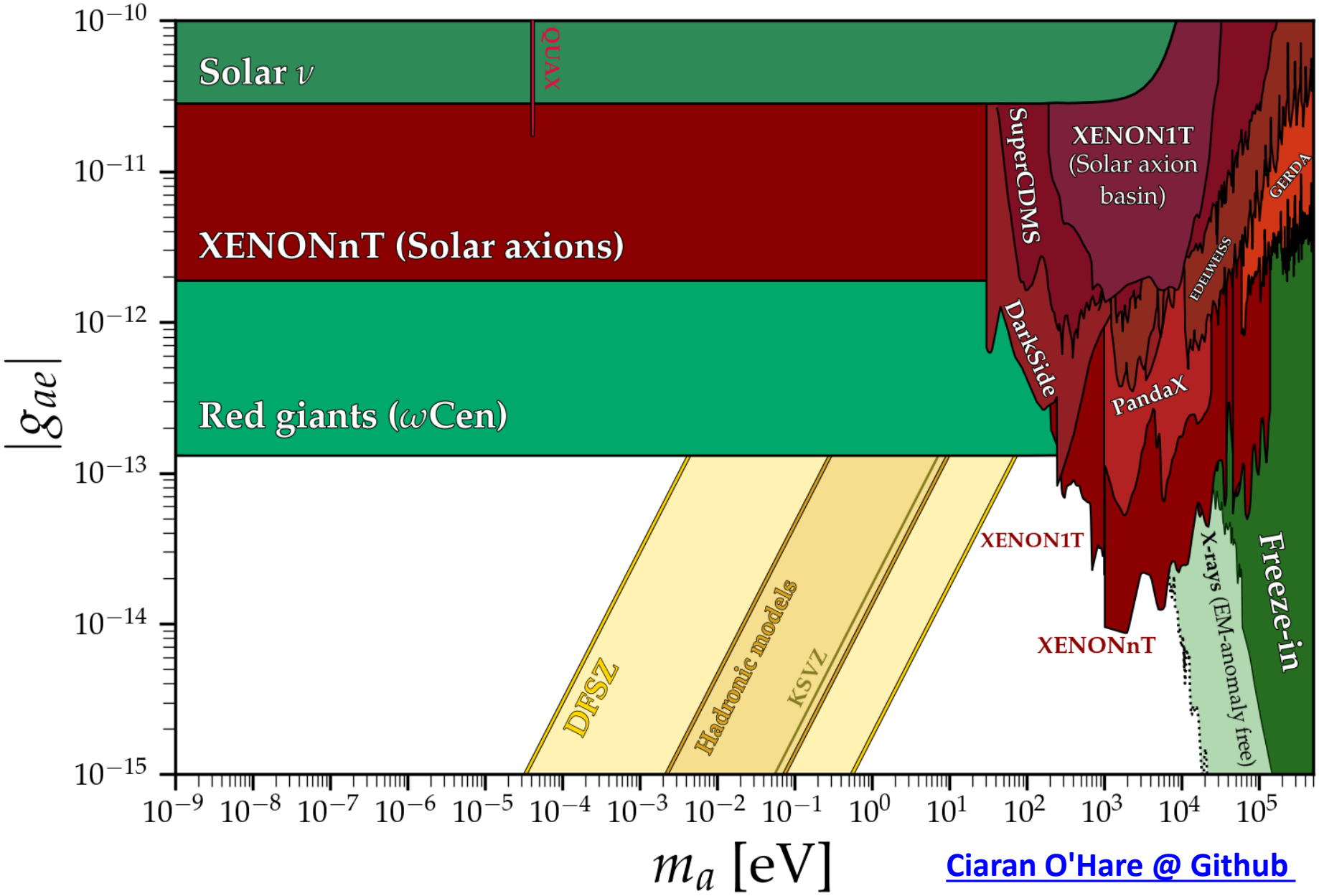

Ciaran O'Hare @ Github

Axion-Photon Conversion in the Sky

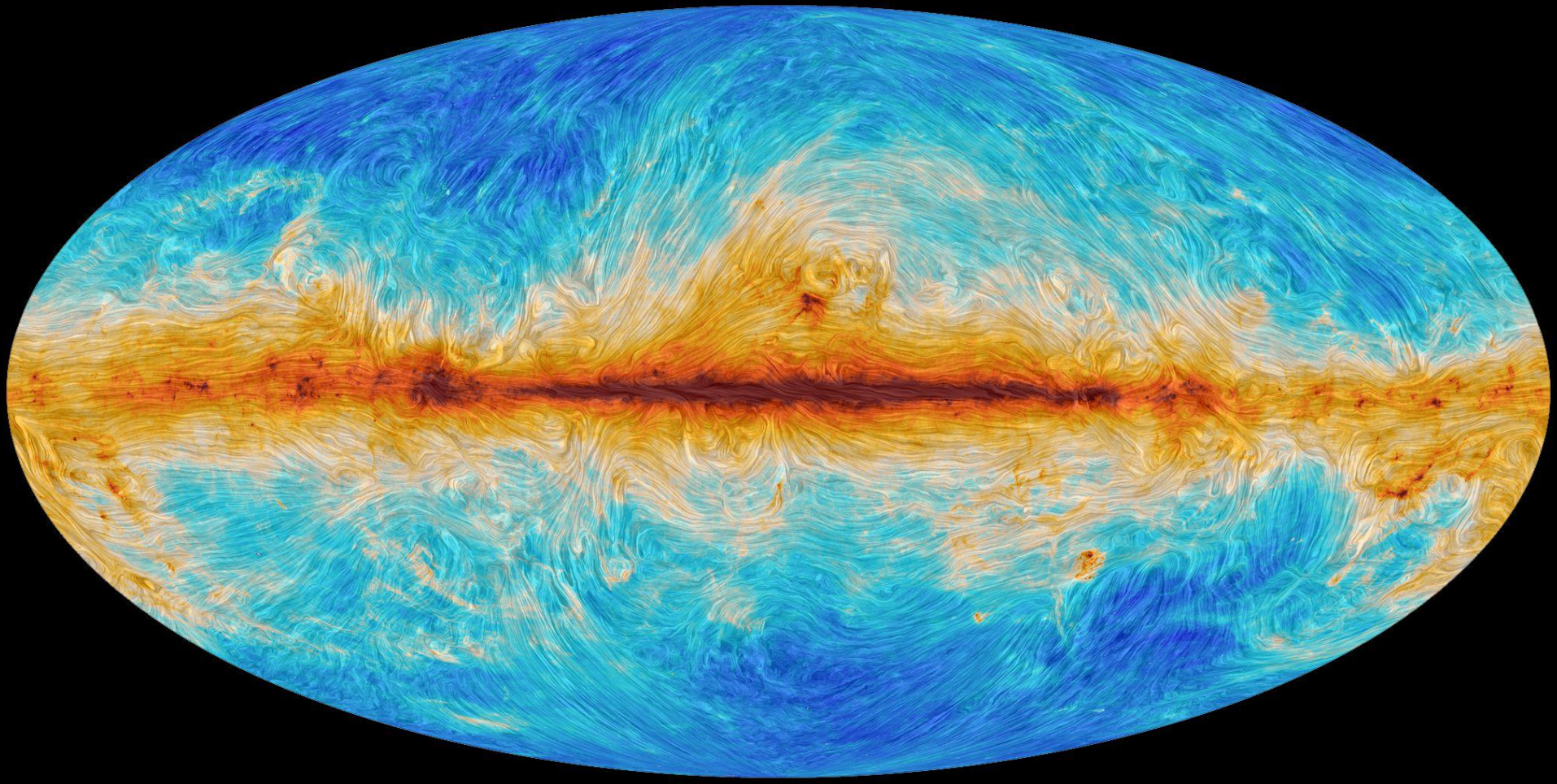

Planck: Galactic magnetic field lines traced by synchrotron radiation at 30 GHz
https://www.cosmos.esa.int/web/planck/picture-gallery

CAST in the Sky

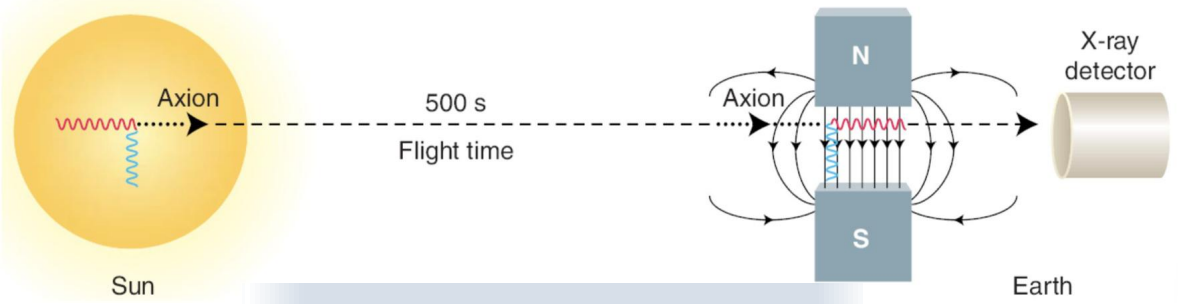

B-field region

Axion Source	$a \cdots\cdots \gamma$	Photon Detector	Photon Appearance
Photon Source	$\gamma \cdots\cdots a$	Photon Detector	Dimming
Photon Source	$\gamma \cdots\cdots a$	Photon Detector	Polarization (Dimming of 1 Pol.)
Photon Source	$\gamma \cdots\cdots a \cdots\cdots \gamma$	Photon Detector	Brightening

Hillas Plot

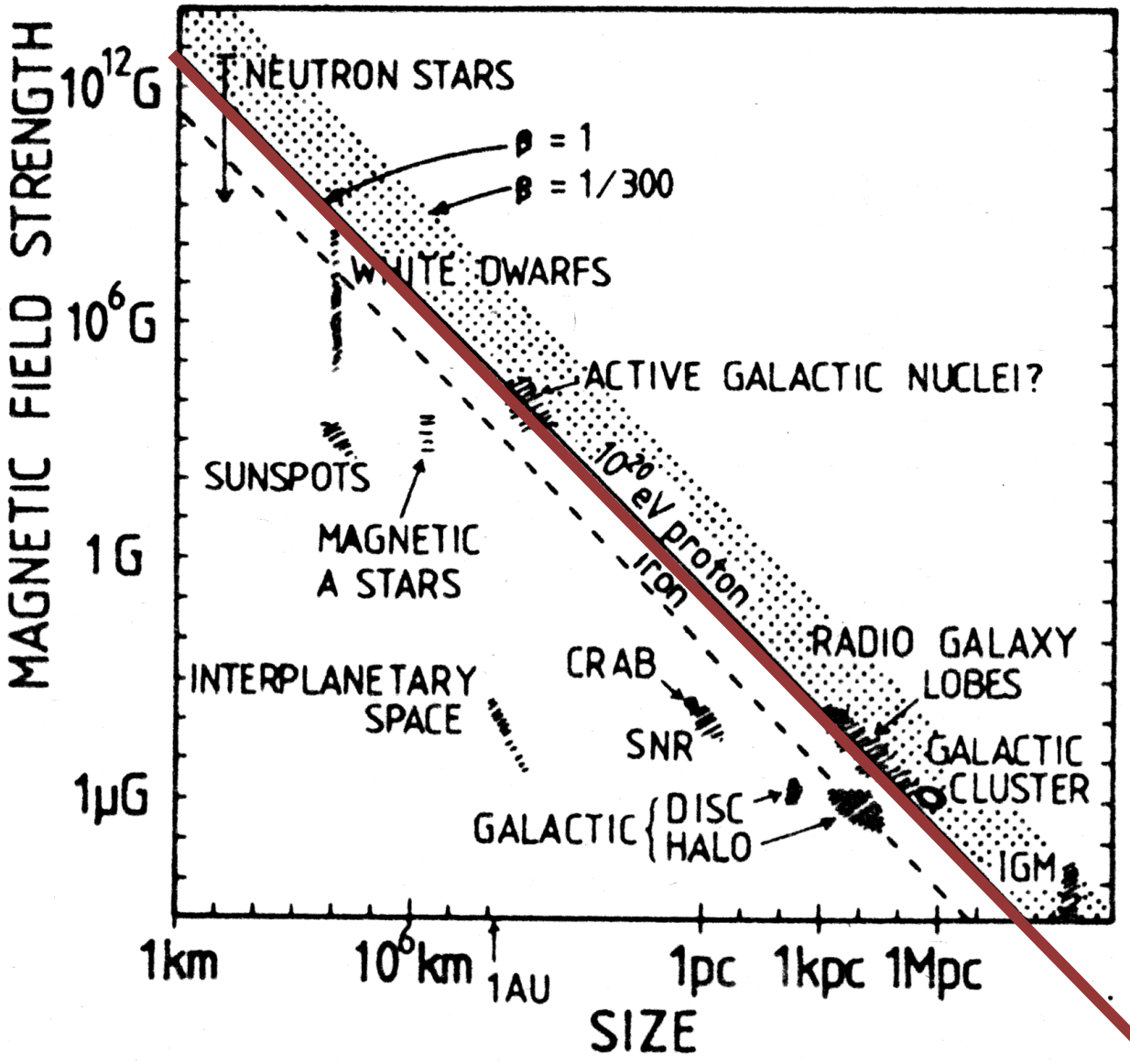

A. M. Hillas
Ann. Rev. Astron. Astrophys. 22, 425 (1984)

Size and B field strength of possible sites for particle acceleration. Objects below the line cannot accelerate protons to 10^{20} eV

ALP-γ conversion

$$\frac{g_{a\gamma}}{10^{12}\,\mathrm{GeV}} BL \sim 1$$

ALP Scape – High-Energy Closeup

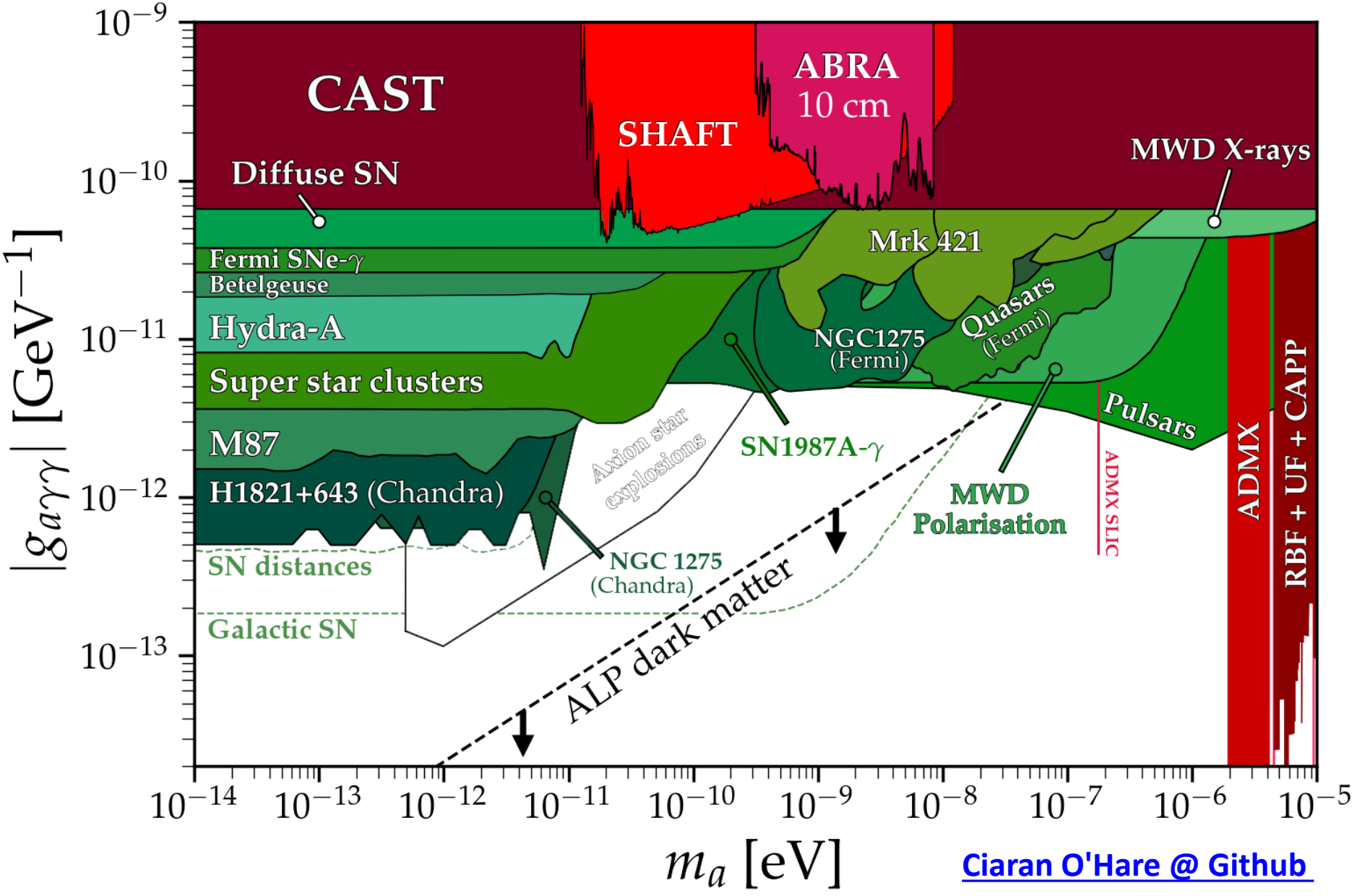

Ciaran O'Hare @ Github

ALP Constraints from Cosmic Distance Measurements

Manuel A. Buen-Abad, JiJi Fan, Chen Sun, arXiv:2011.05993

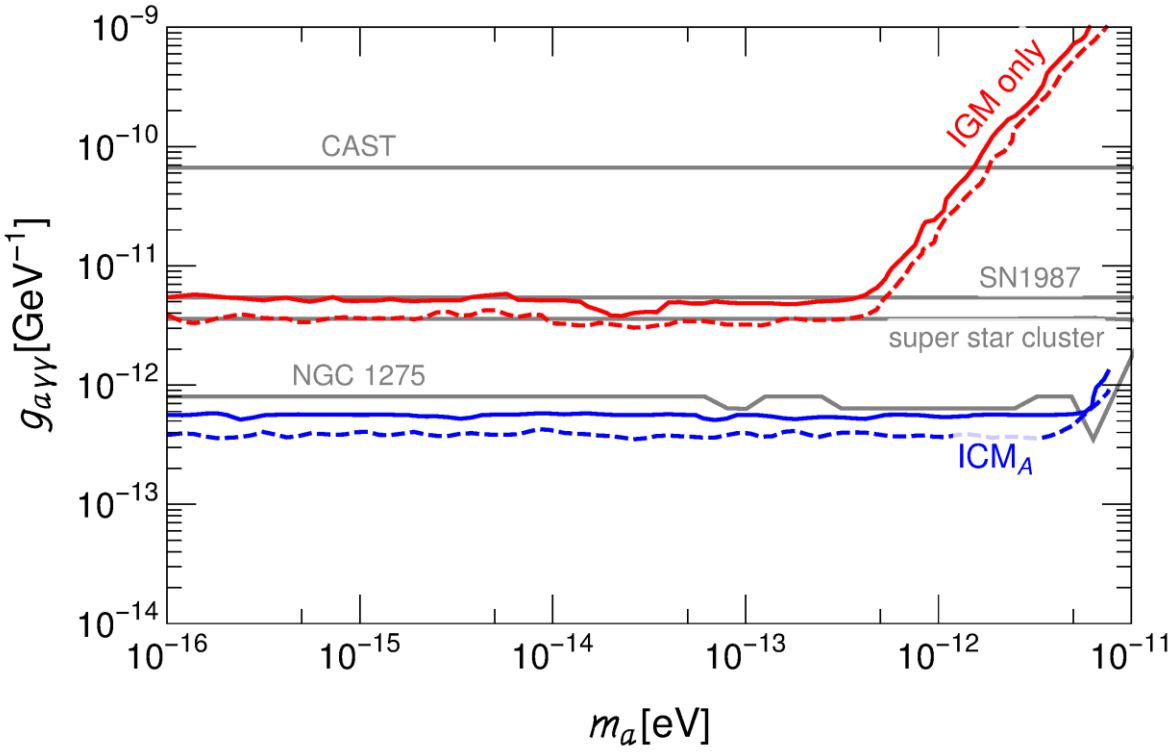

Avoid excessive dimming of distant sources by photon-ALP conversion

Figure 5. 95% C.L. upper limits on $g_{a\gamma\gamma}$ as a function of m_a. The solid curves are from $\mathcal{L}_{\rm late}$ while the dashed curves are from $\mathcal{L}_{\rm early}$, assuming $B_{\rm IGM} = 1$ nG and $s_{\rm IGM} = 1$ Mpc. To avoid clumsiness, we only show the upper limits from either assuming no ICM conversion effects on the galaxy cluster data (top red curves) or assuming model A in Eq. (2.10) for the effect (lower blue curves). The upper limits for model B and C in Eqs. (2.11) and (2.12) are in between them. We also show several existing bounds (grey lines) for comparison: CAST [72]; SN1987a [63]; X-ray searches from super star cluster [74] and X-ray spectroscopy from AGN NGC 1275 [57].

Hubble Tension

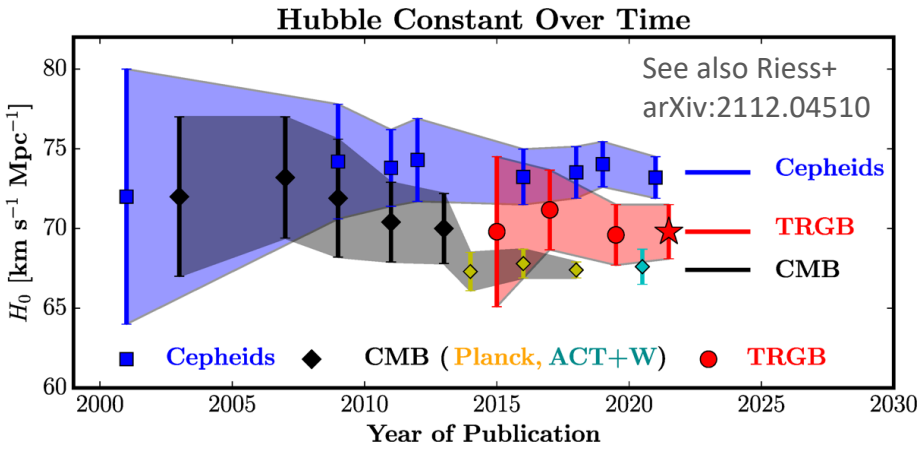

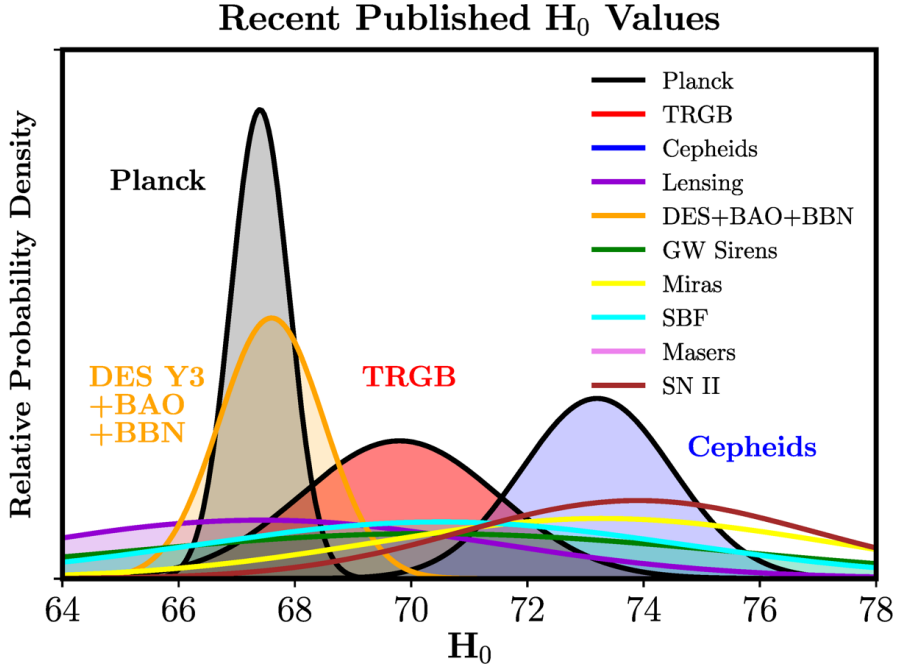

Freedman ApJ 919 (2021) 16 [2106.15656]

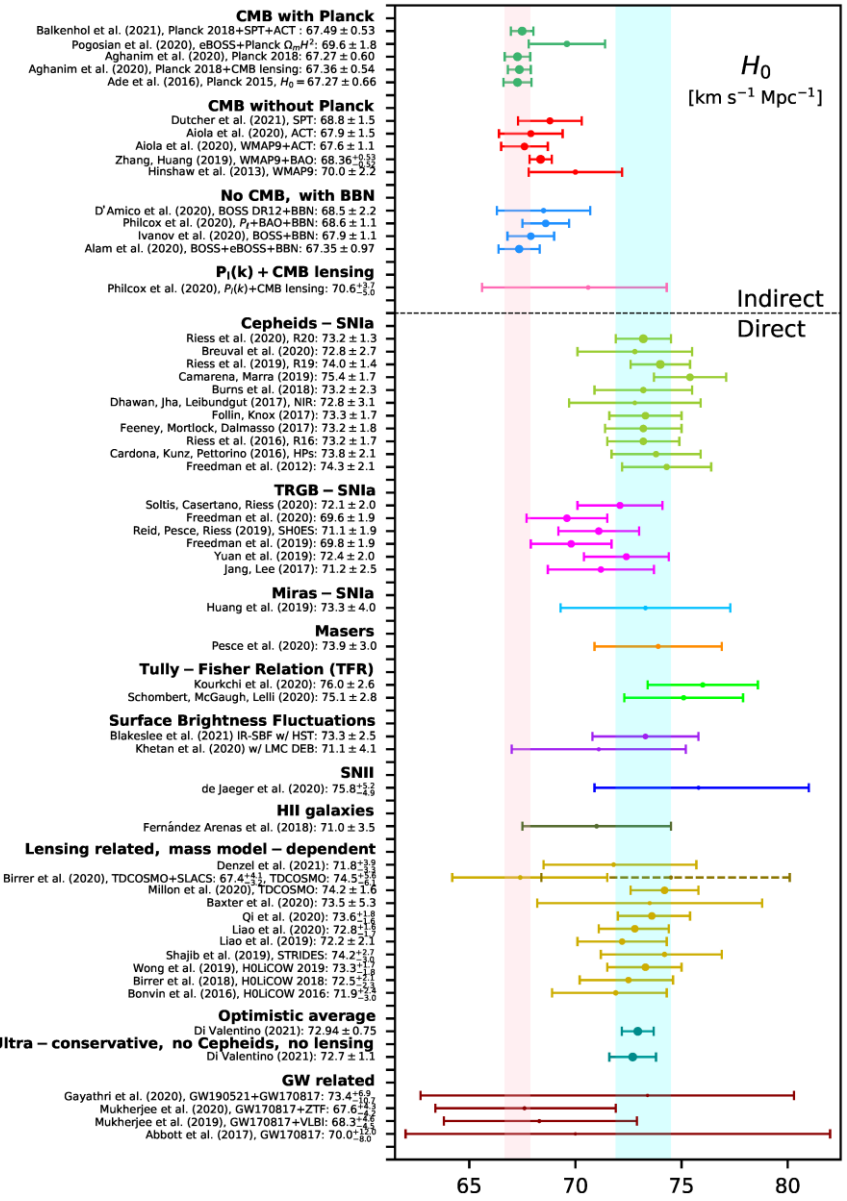

Di Valentino+ arXiv:2103.01183

Solving Hubble Tension with ALPs?

- Twenty years ago:
  Dimming of distant SNe Ia by ALP-photon conversion
  to avoid cosmic acceleration
  Csáki, Kaloper & Terning (2001), arXiv:hep-ph/0111311
  (but difficult to make consistent)

- Today:
  Brightening of distant SNe Ia by ALP-photon conversion
  to avoid Hubble tension

  - Impossible with simple models
  - Need to emit as many ALPs as photons from source

> In summary, to have axions brighten SNIa, we need resonant conversions inside or near SN in order to generate an initial axion flux as large as the initial photon flux. We also need more axions converting into photons in the IGM rather than the other way around. Yet as we show above by considering some simple necessary conditions for the scenario to work, the two requirements mentioned point towards very different axion mass ranges.

Manuel A. Buen-Abad, JiJi Fan, Chen Sun, Appendix of arXiv:2011.05993

Axion-Photon-Conversion from SN 1987A

Axion-photon conversion
in transverse galactic B-field

Primakoff
production
in SN core

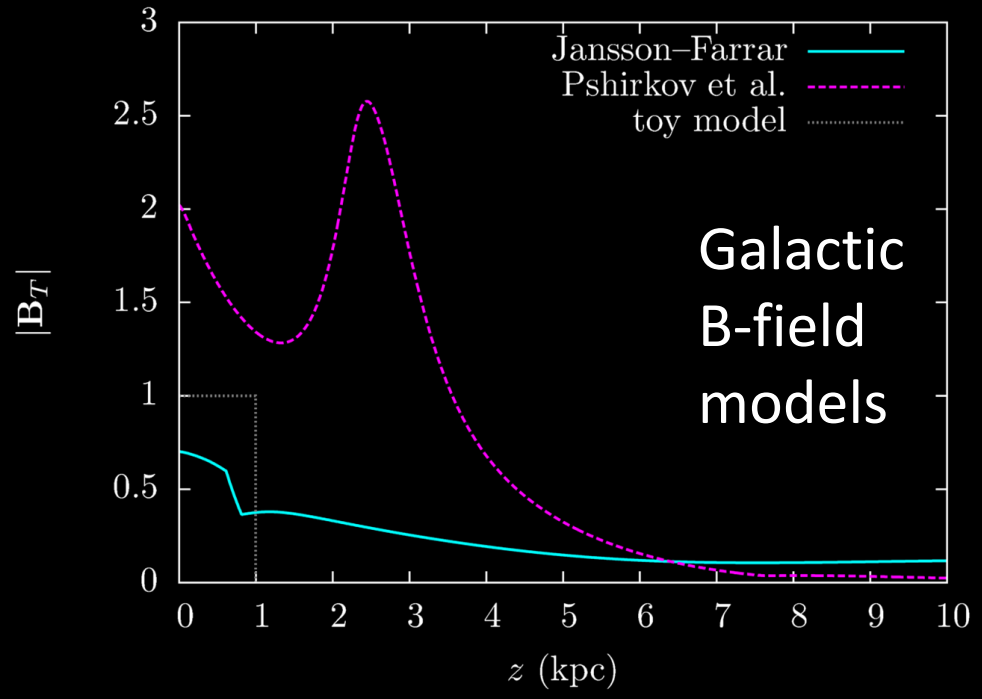

No excess γ rays
in coincidence
with SN 1987A

Payez, Evoli, Fischer, Giannotti, Mirizzi & Ringwald, arXiv:1410.3747

Gamma-Ray Observations of SMM Satellite

Counts in the GRS instrument on the Solar Maximum Mission Satellite

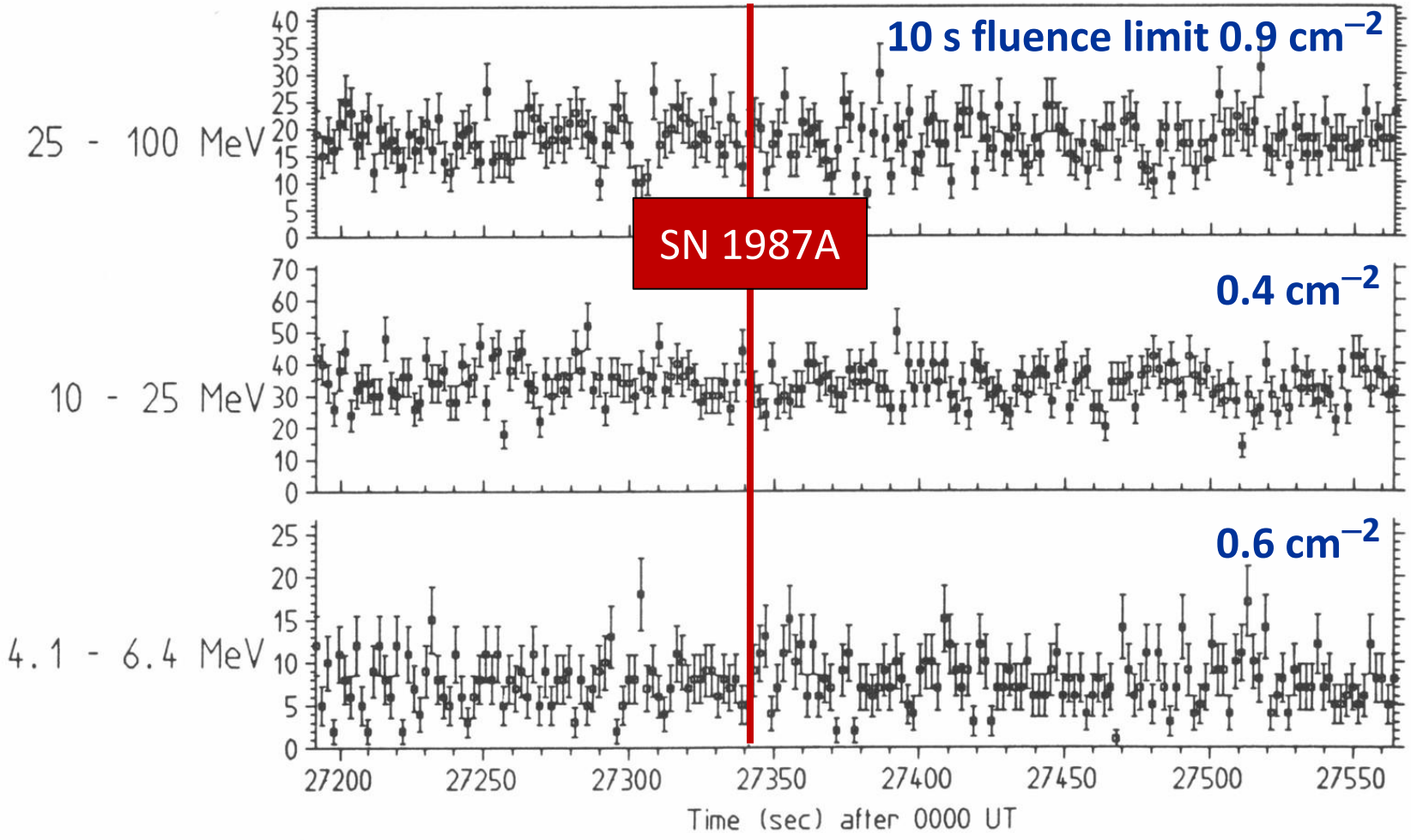

SN 1987A neutrino fluence $\sim 10^{10}\mathrm{cm}^{-2}$

$< 10^{-10}$ of neutrinos have decayed to photons on their way to Earth

SN 1987A Limits from Axion-Photon Conversion

- Primakoff production in SN core, several numerical models (fairly insensitive)
- Propagation in galactic B-field (main uncertainty)
- Non-detection of excess gamma rays in SMM satellite coincident with SN 1987A

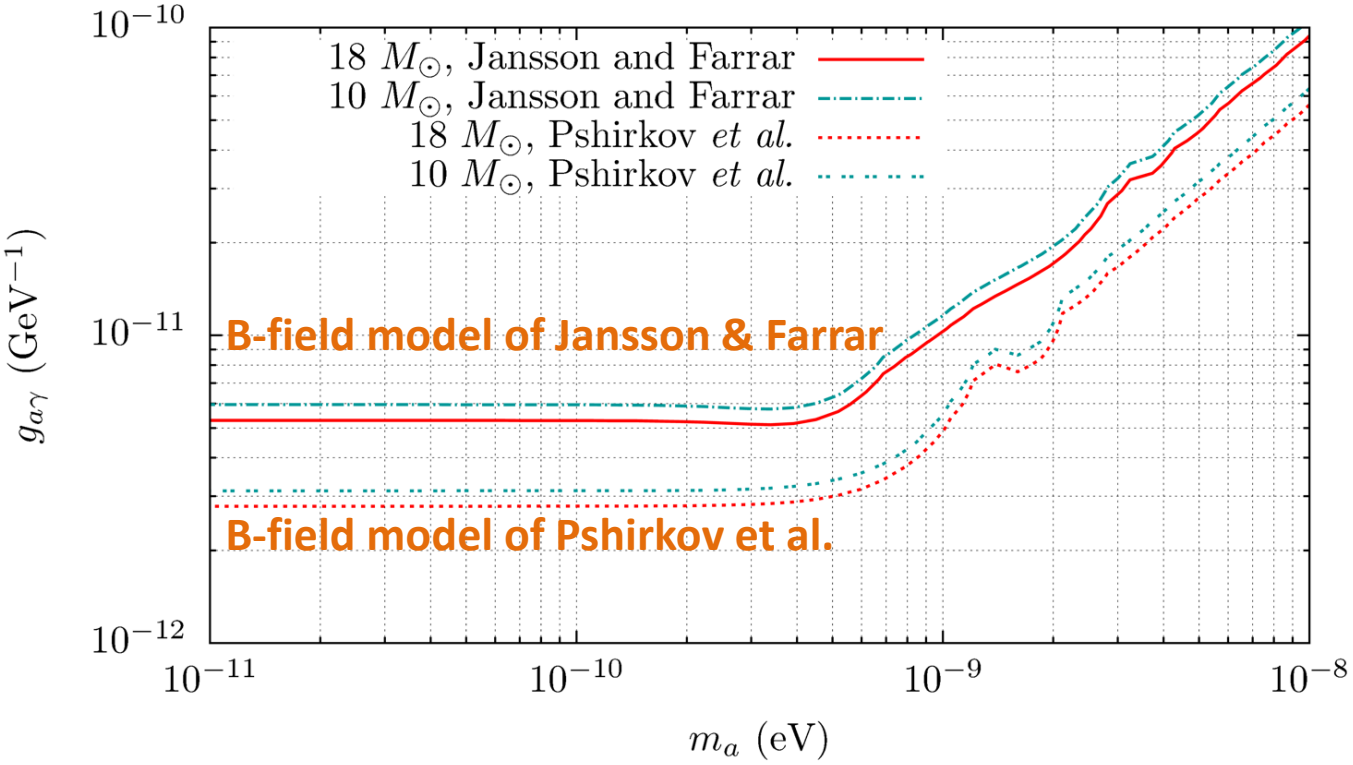

Payez, Evoli, Fischer, Giannotti, Mirizzi & Ringwald: arXiv:1410.3747

More recent analysis: Hoof & Schulz arXiv:2212.09764

Upper limit on the axion-photon coupling from magnetic white dwarf polarization

Christopher Dessert,[1, 2, 3] David Dunsky,[1, 2] and Benjamin R. Safdi[1, 2] arXiv:2203.04319

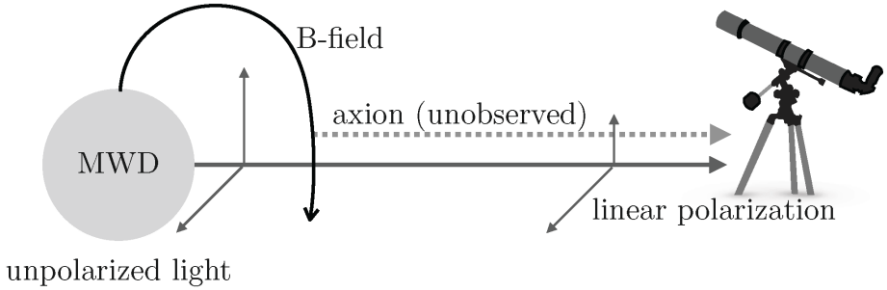

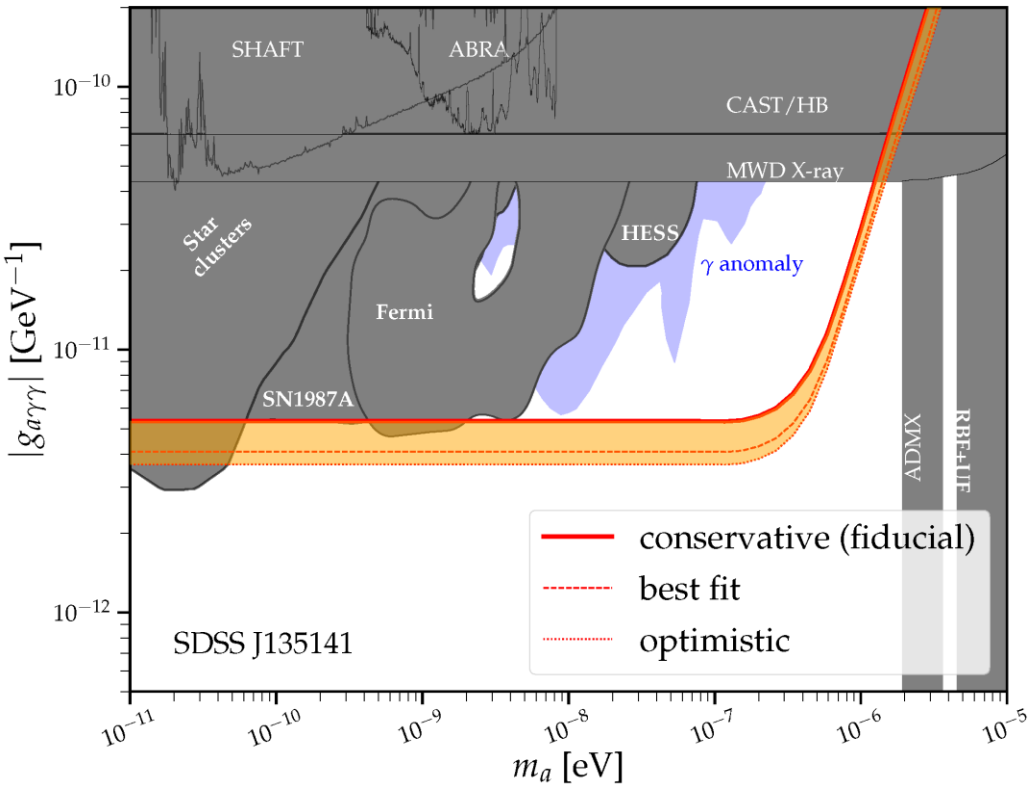

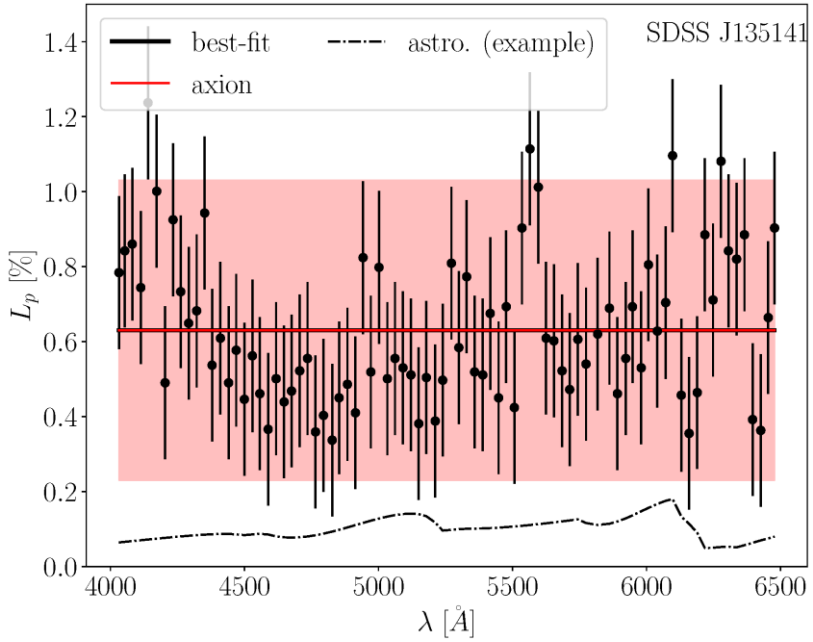

Measured polarization of MWD SDSS J135141

Axion Bounds from Magnetic WDs and NSs

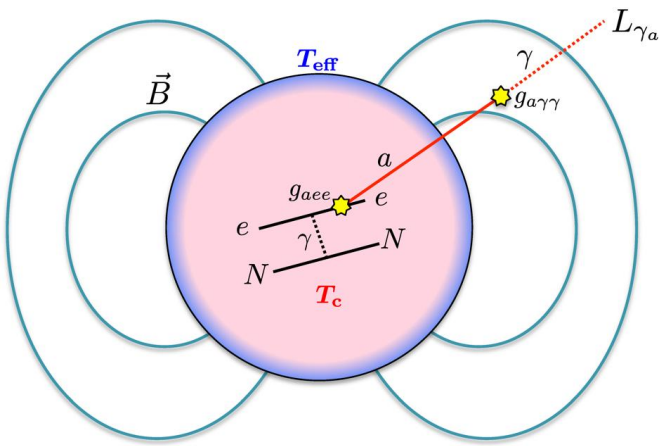

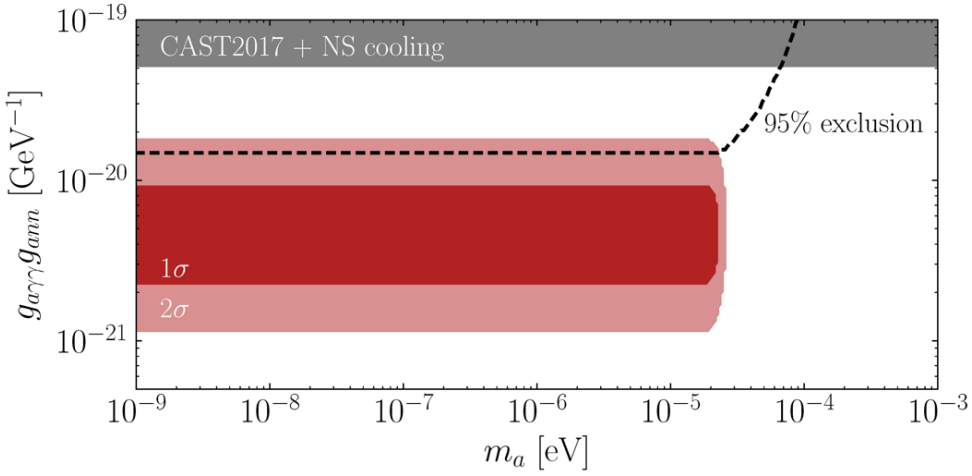

Magnetic White Dwarf

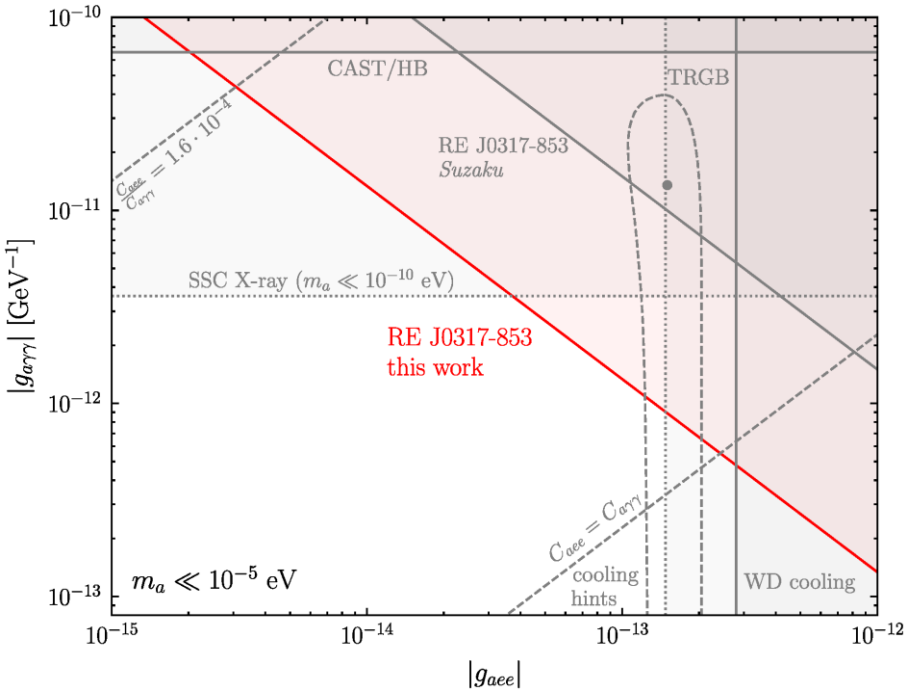

Magnificent Seven Neutron Stars X-Ray limits and excess

- Axion Emission Can Explain a New Hard X-ray Excess from Nearby Isolated Neutron Stars, Buschmann, Co, Dessert & Safdi, arXiv:1910.04164
- No Evidence for Axions from Chandra Observation of the Magnetic White Dwarf RE J0317-853 Dessert, Long & Safdi, arXiv:2104.12772

Bounds on axionlike particles from the diffuse supernova flux

Francesca Calore,[1,*] Pierluca Carenza,[2,3,†] Maurizio Giannotti,[4,‡] Joerg Jaeckel,[5,§] and Alessandro Mirizzi[2,3,‖]

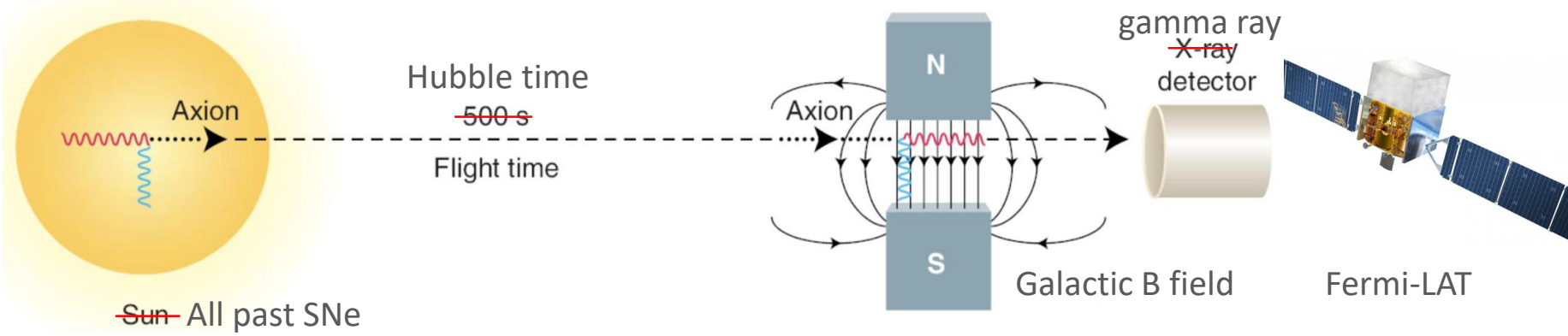

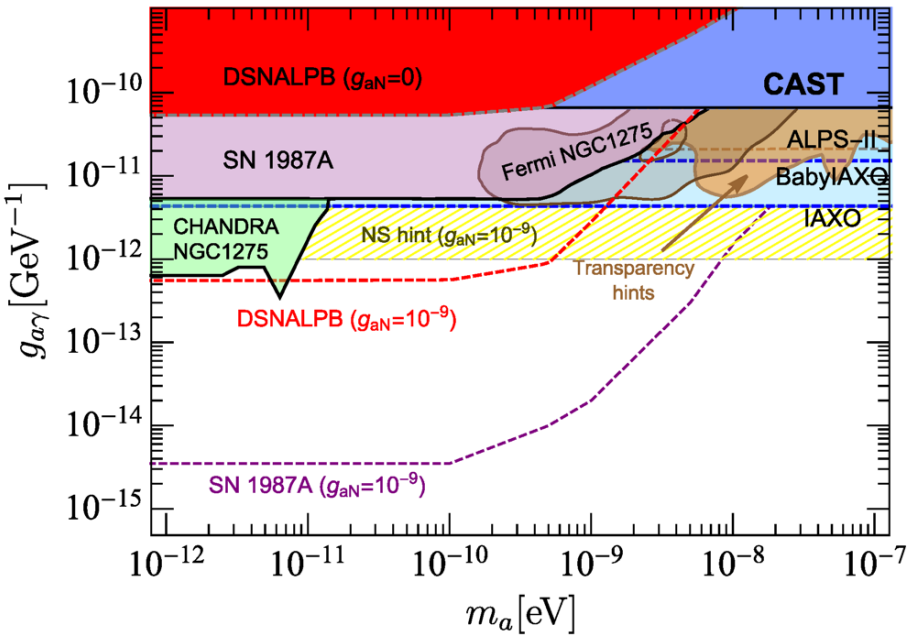

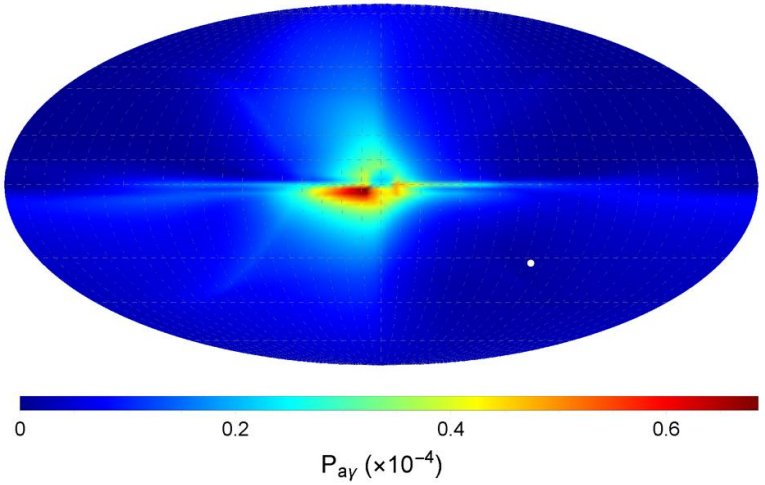

FIG. 3. Sky map in Galactic coordinates of the $a \to \gamma$ conversion probability, starting from a pure ALPs beam at the outside boundary of the Galaxy, for the Jansson and Farrar magnetic field model derived in [36]. We have taken the energy to be $E = 50$ MeV, the coupling $g_{a\gamma} = 3 \times 10^{-13}\text{GeV}^{-1}$

Shining TeV Gamma Rays through the Universe

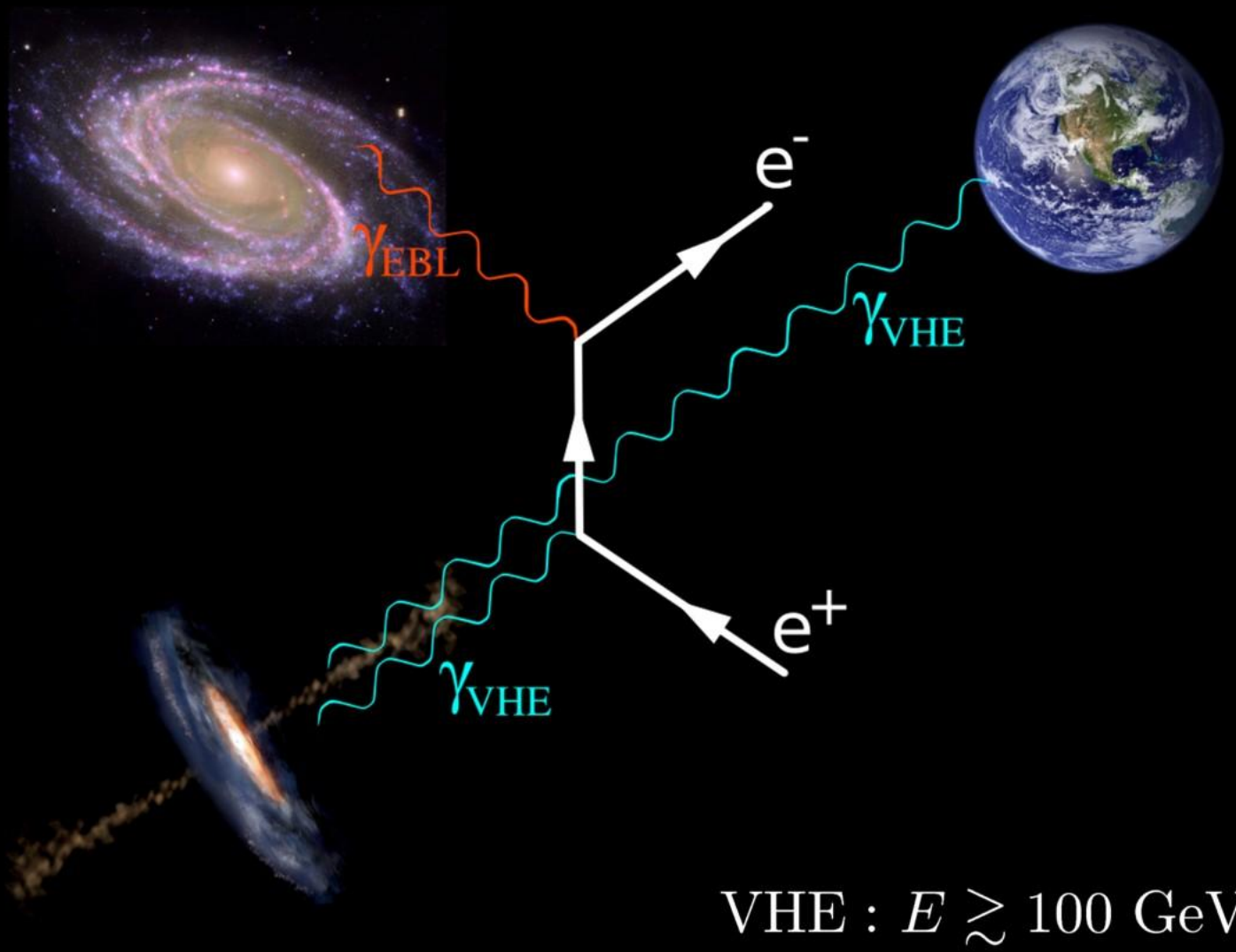

Figure from a talk by Manuel Meyer (Univ. Hamburg)

Shining TeV Gamma Rays through the Universe

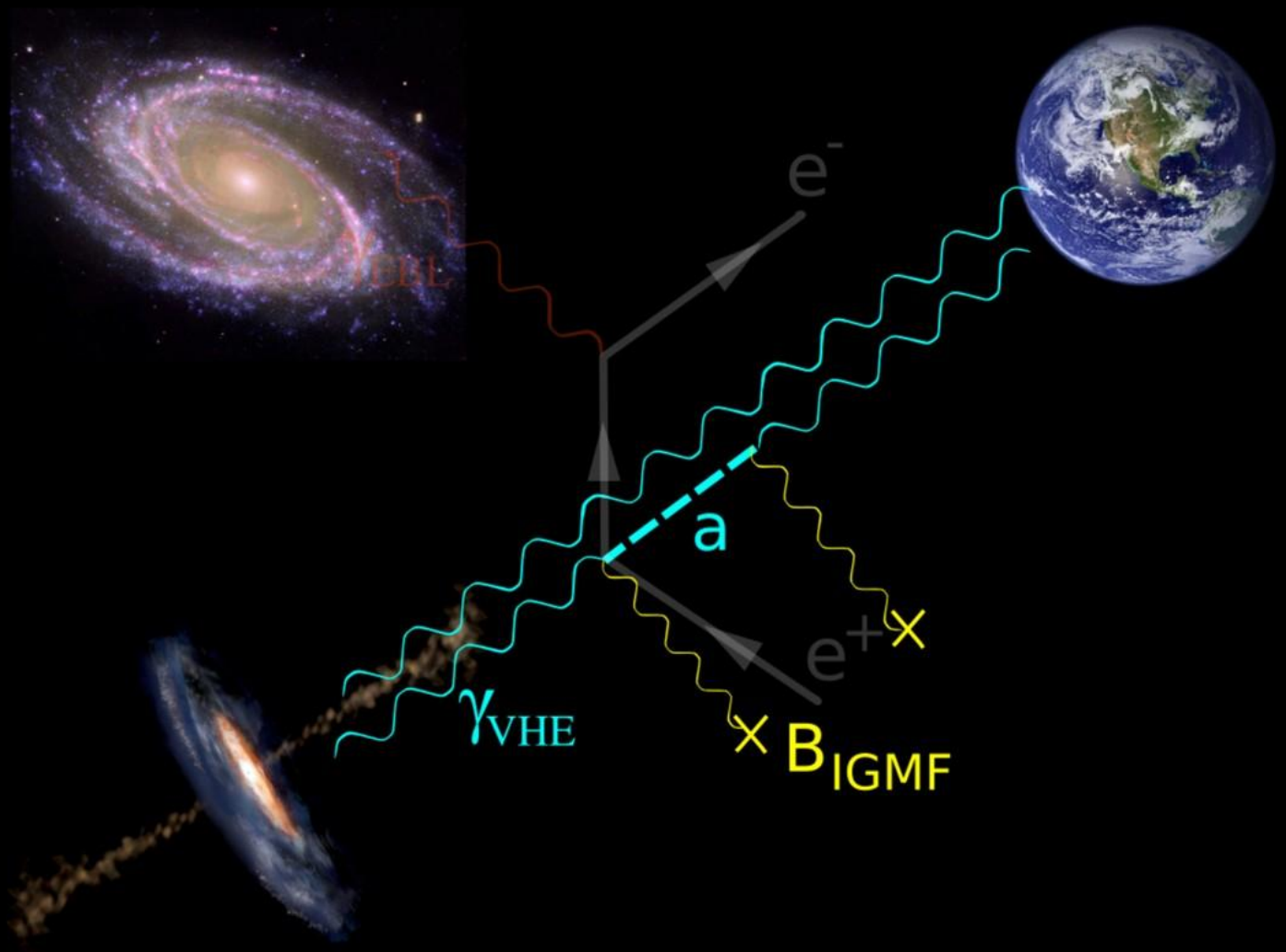

Figure from a talk by Manuel Meyer (Univ. Hamburg)

Gamma-ALP Conversion in Astrophysical B-Fields

Credit: SLAC National Accelerator Laboratory/Chris Smith
https://www.nasa.gov/sites/default/files/thumbnails/image/alp_2_sequences.gif

GRB 221009A (BOAT – Brightest Of All Times)

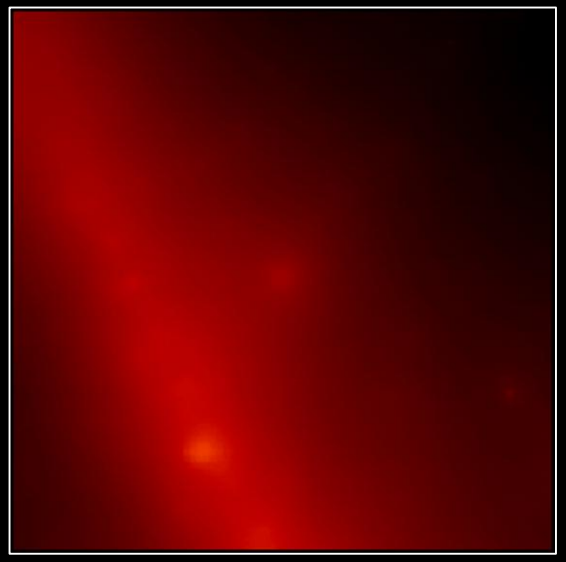

Ten-hour timelapse of Fermi Gamma-Ray Space Telescope

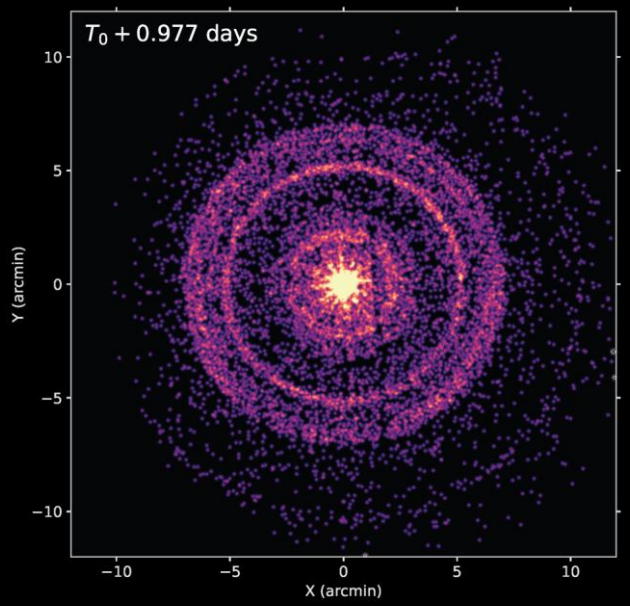

X-ray afterglow (Swift) arXiv:2302.03642

LHAASO
Large High-Altitude Air-Shower Observatory
5000 photons in 2000 sec
0.5 < E < 18 TeV
1 event at 18 TeV (±40%)

Paper submitted
Not yet publicly available

Redshift z = 0.151
Optical depth for 18 TeV photon
9.4–27.1
depending on EBL modeling

ALP-photon interpretation

Galanti+	arXiv:2210.05659
Baktash+	arXiv:2210.07172
Troitsky	arXiv:2210.09250
Nakagawa+	arXiv:2210.10022
Zhang+	arXiv:2210.13120
Carenza+	arXiv:2211.02010

GRB 221009A – ALP-Boosting 18 TeV Photon

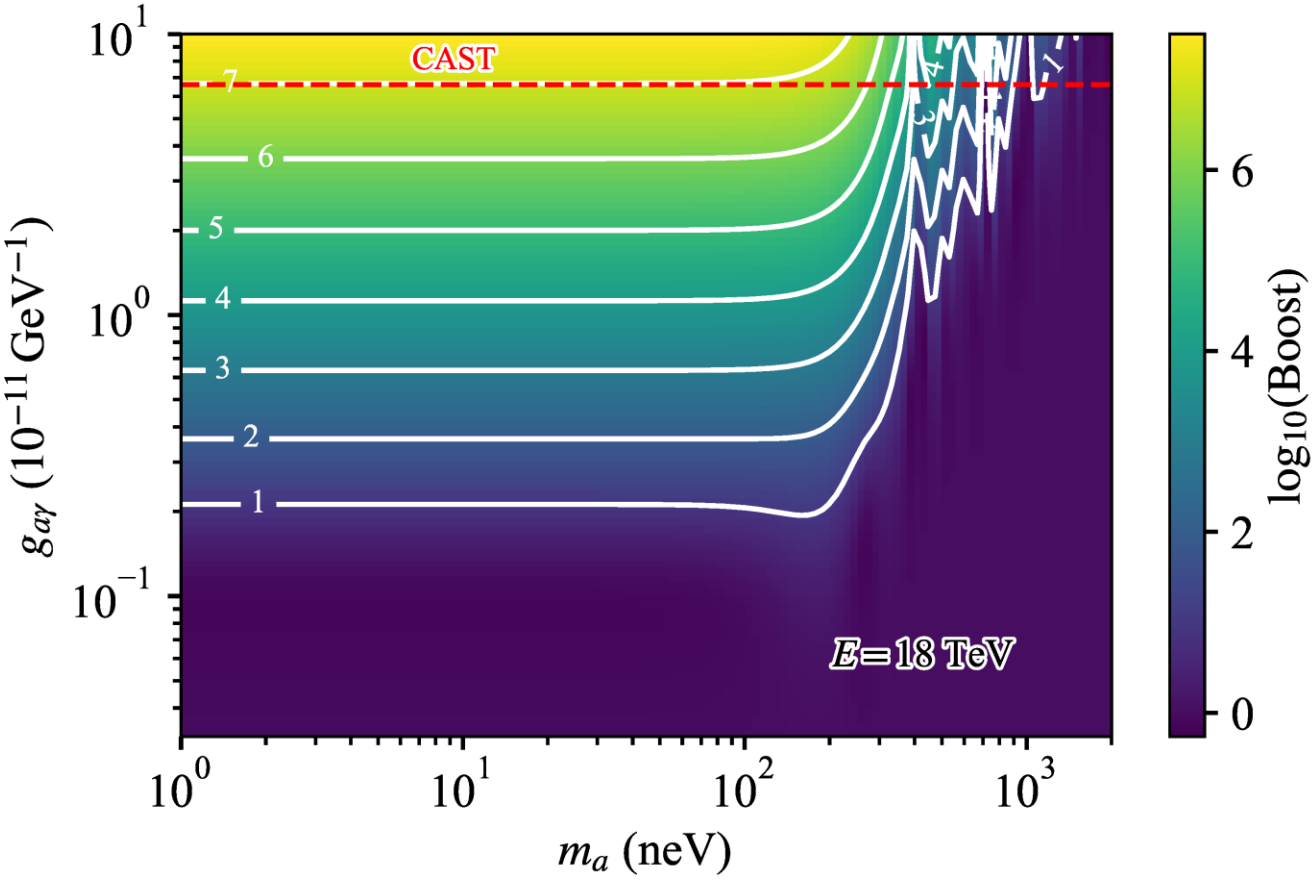

Figure 3. The logarithm of the boost factor of the photon flux over a grid of ALP parameters at $E_\gamma = 18$ TeV. The Do2011 EBL model is assumed. Parameters above the red dashed line are excluded by CAST.

Baktash, Horns & Meyer, Interpretation of multi-TeV photons from GRB221009A, arXiv:2210.07172

ALP Scape – High-Energy Closeup

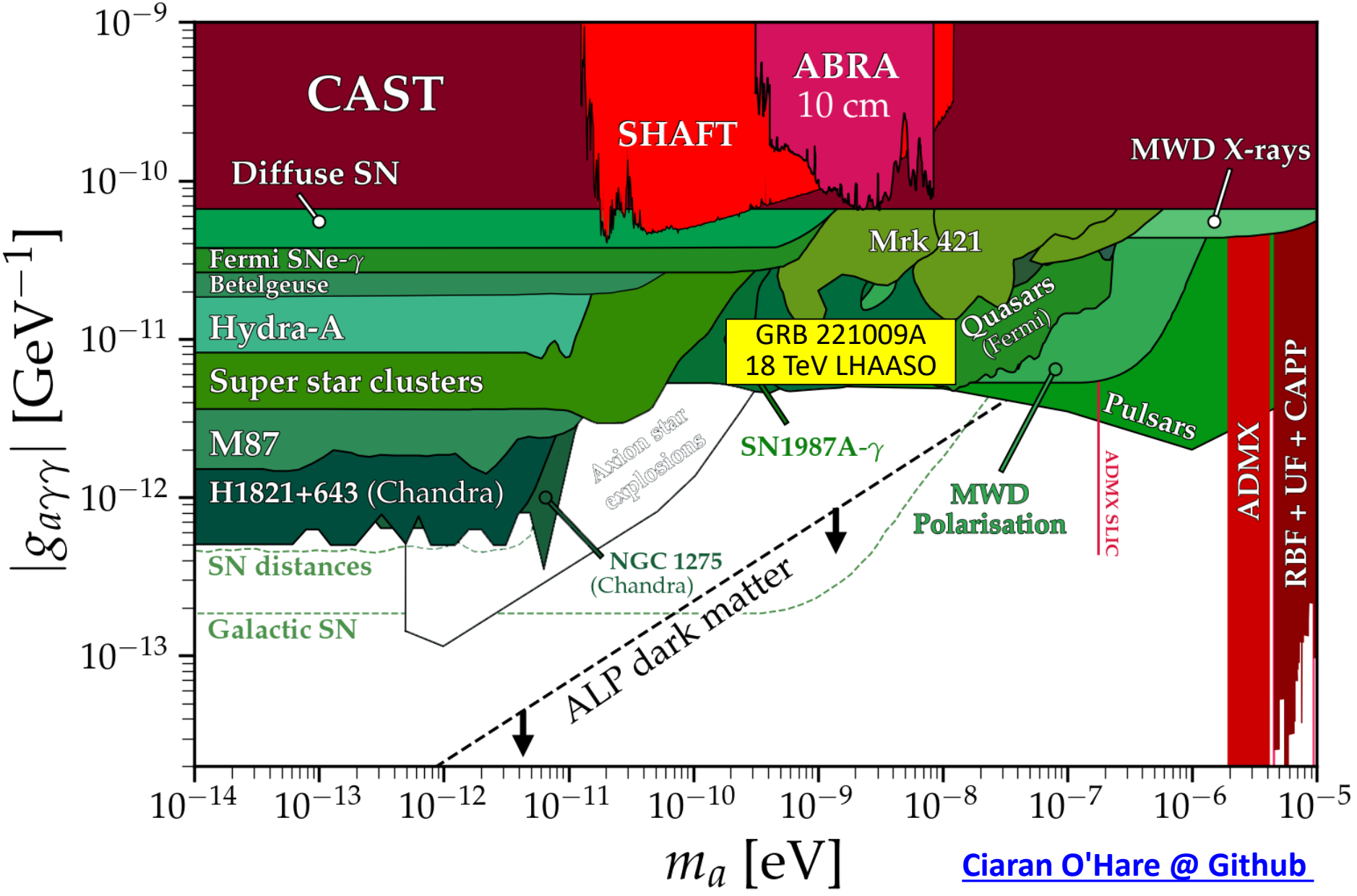

Ciaran O'Hare @ Github

The Mystery of the Yellow Ribbon

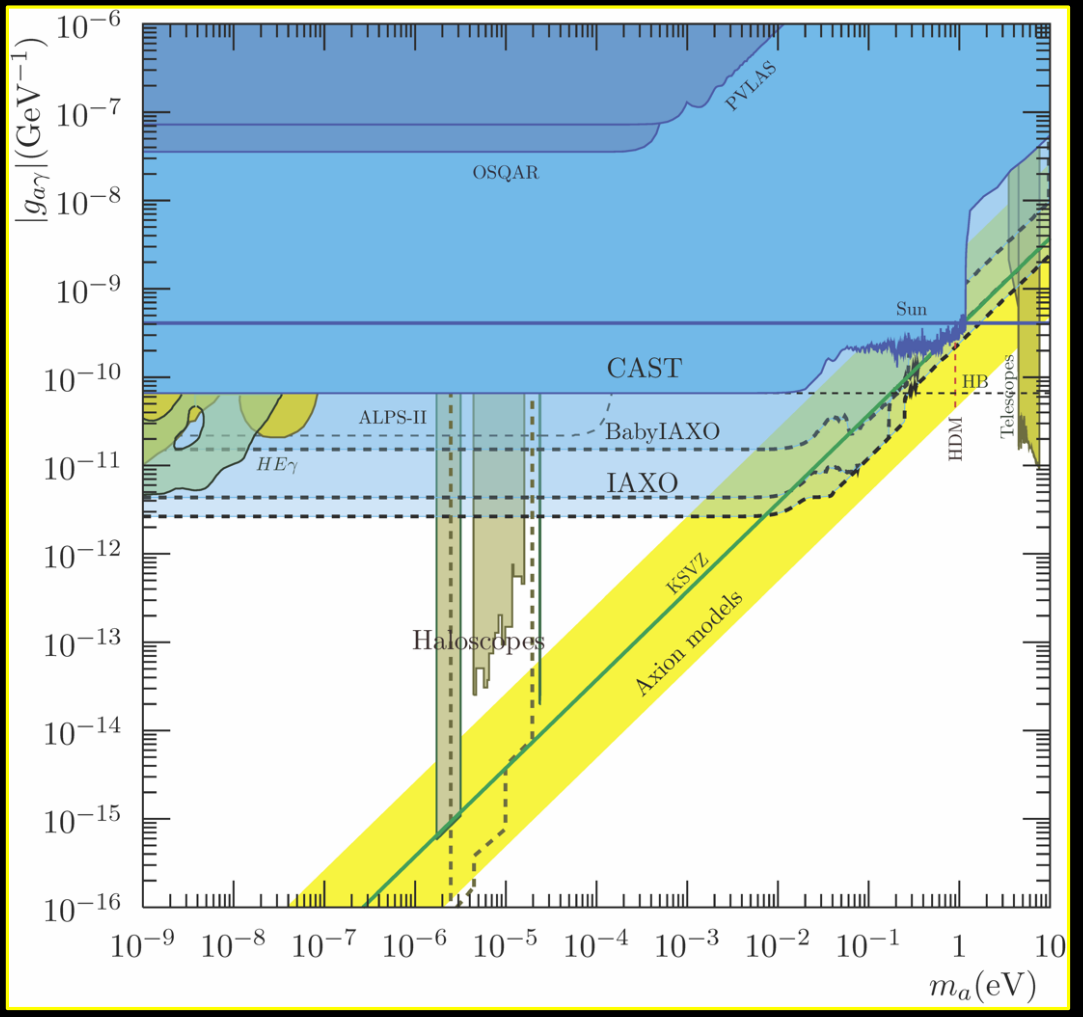

Axion-Photon Coupling

Gluon coupling (generic), defines normalization of axion scale f_a

$$\mathcal{L}_{aG} = \frac{\alpha_s}{8\pi}\frac{a}{f_a} G\tilde{G}$$

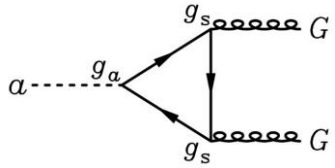

Mass (generic) depends on up/down quark masses

$$m_a = \frac{\sqrt{m_u m_d}}{m_u + m_d}\frac{m_\pi f_\pi}{f_a} = \frac{5.70\ \mu\text{eV}}{f_a/10^{12}\ \text{GeV}}$$

Axion-photon coupling (model dependent)

Generic from a-π-η mixing

$$\mathcal{L}_{a\gamma} = -\frac{g_{a\gamma}}{4} F\tilde{F}a = g_{a\gamma}\,\mathbf{E}\cdot\mathbf{B}\,a = \frac{\alpha}{2\pi}\left(\frac{E}{N} - 1.92\right)\frac{a}{f_a}\mathbf{E}\cdot\mathbf{B}$$

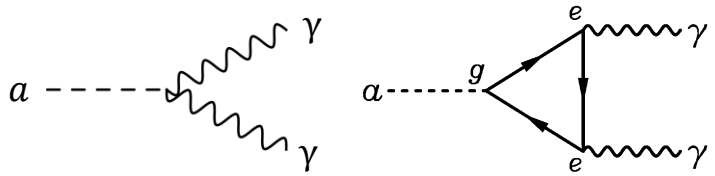

Model-dependent,
E/N = 0 (KSVZ), 8/3 (DFSZ), many others

$$g_{a\gamma} = \left(\frac{E}{N} - 1.92\right)\frac{0.203\ m_a}{\text{GeV}^2} = \left(\frac{E}{N} - 1.92\right) 2.03\times 10^{-16}\ \text{GeV}^{-1}\,\frac{m_a}{1\mu\text{eV}}$$

The QCD axion, precisely, Grilli di Cortona+, 1511.02867

What exactly is this region?

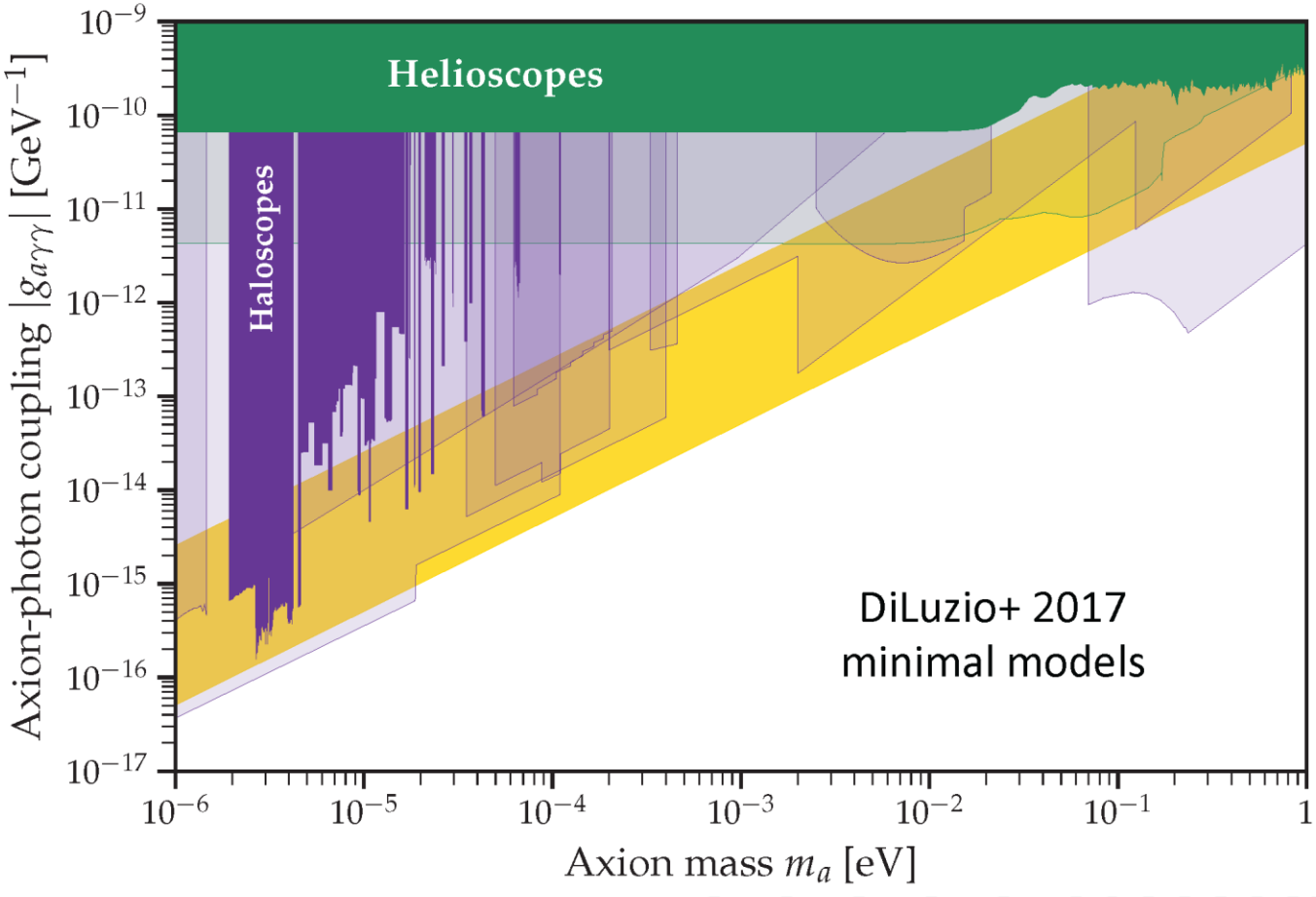

Diehl & Koutsangelas
arXiv:2302.04667

J. Diehl, Talk in Dresden

What exactly is this region?

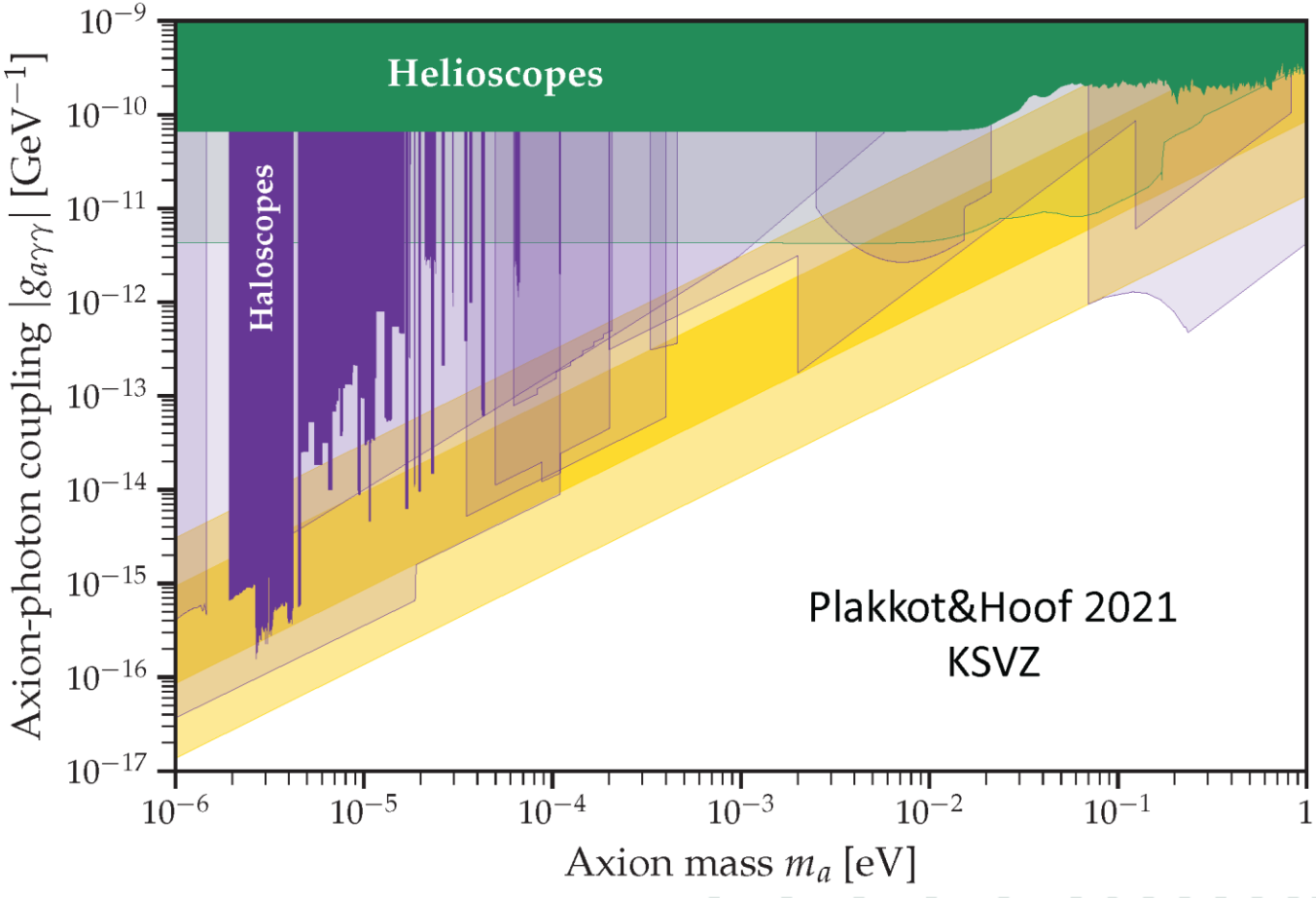

Diehl & Koutsangelas
arXiv:2302.04667

J. Diehl, Talk in Dresden

What exactly is this region?

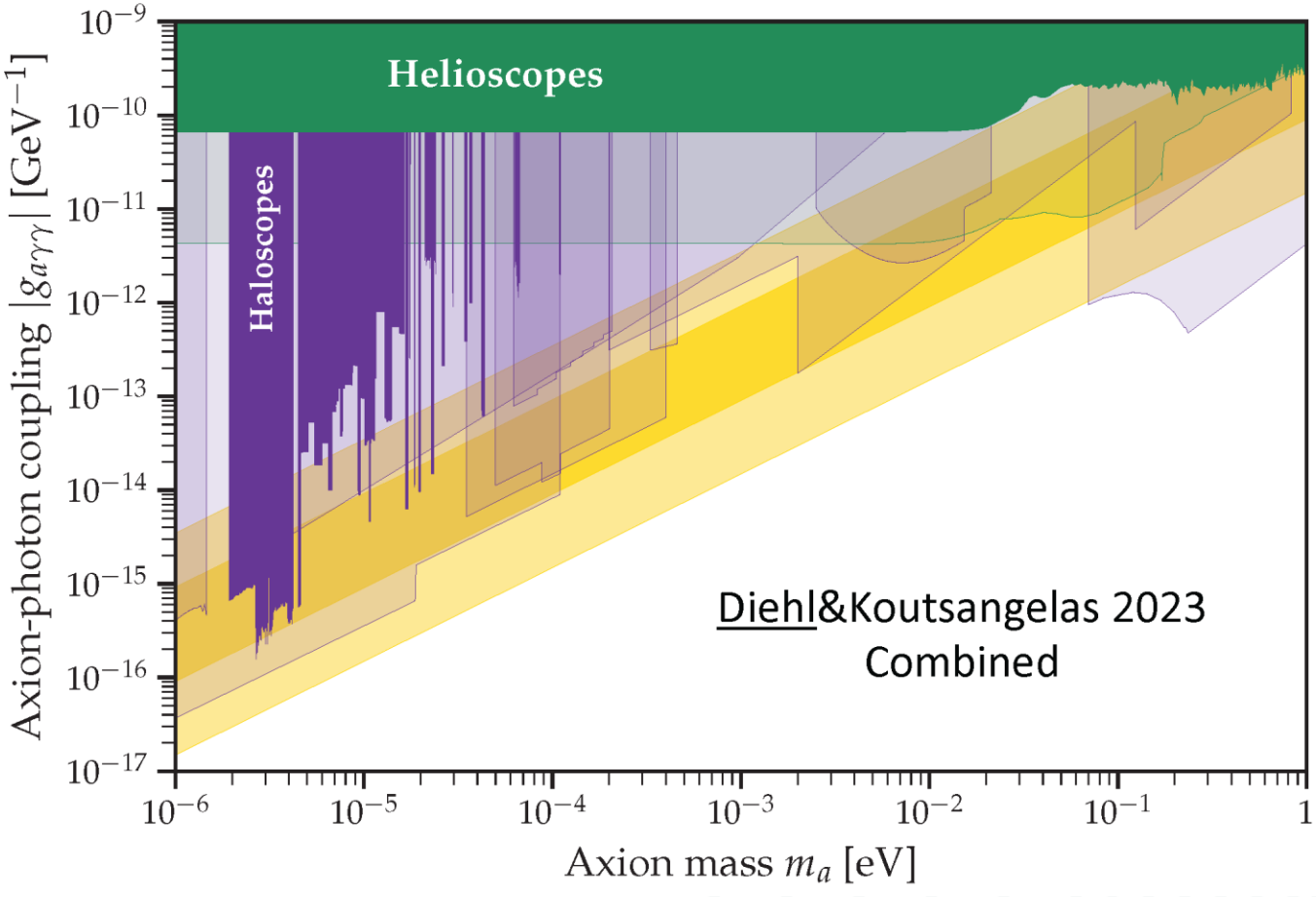

Diehl & Koutsangelas
arXiv:2302.04667

J. Diehl, Talk in Dresden

Axion sensitivity requirement

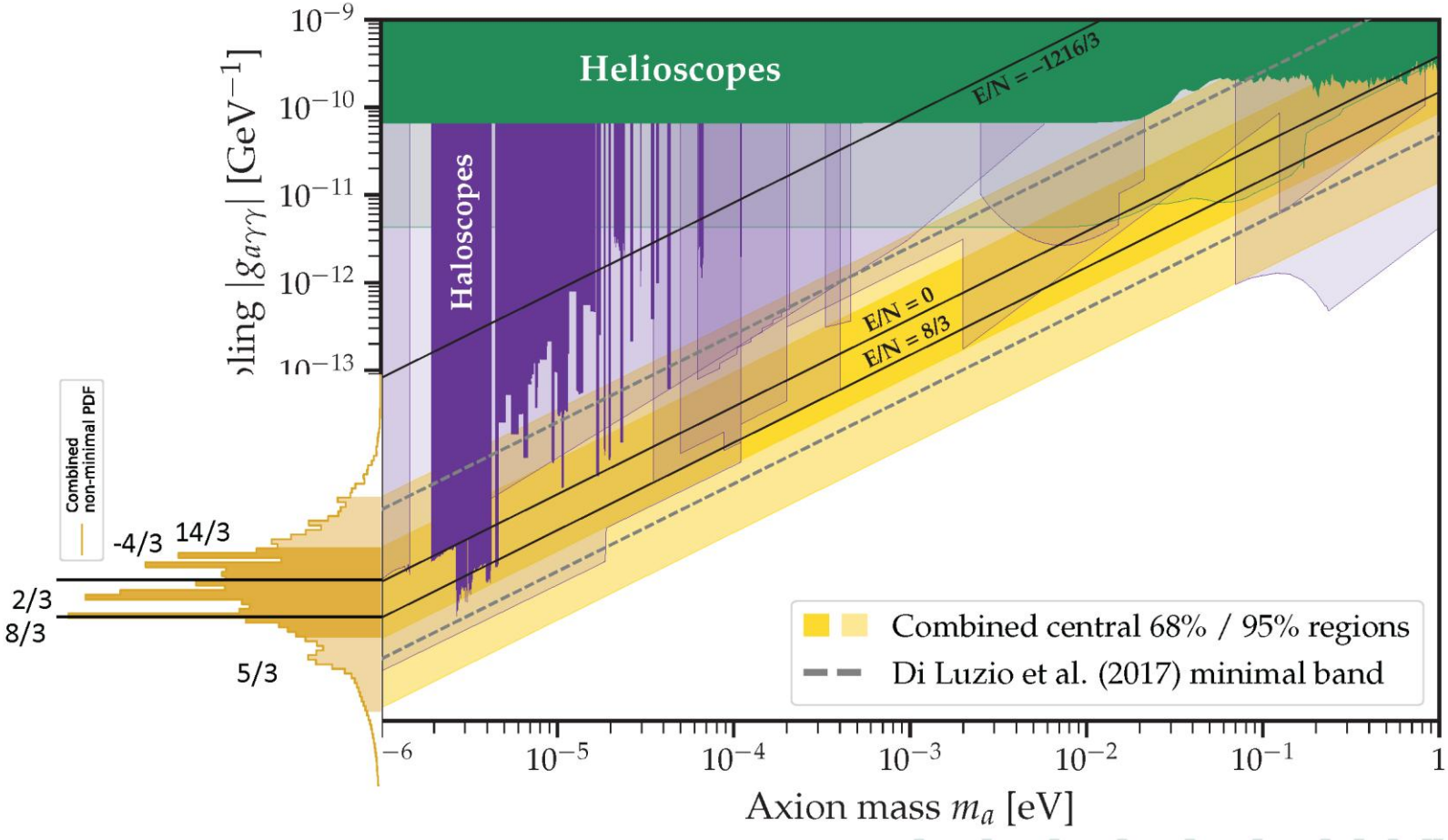

Diehl & Koutsangelas
arXiv:2302.04667

J. Diehl, Talk in Dresden

Which models are that?!

- KSVZ:
  - Minimal model: One $Q \sim (3,1,0) \rightarrow \frac{E}{N} = 0$ $(q_{em} = 0)$ (SU(3) SU(2) U(1))
  - Extending up to 28 Q is phenomenologically allowed (Plakkot, Hoof ,21)
- DFSZ:
  - Minimal model: two Higgs doublets, couple to right-handed fermions $\rightarrow E/N = 8/3$ or $E/N = 2/3$
  - What about $2 < n_D \leq 9$ doublets?
  - E/N depends only on charges of H:

u c t	d s b	e μ τ
H_1	H_2	H_1
or		
H_1	H_2	H_2

$$\frac{E}{N} = \frac{2}{3} + 2\frac{\sum \chi_u + \sum \chi_l}{\sum \chi_u + \sum \chi_d}$$

Diehl & Koutsangelas
arXiv:2302.04667

J. Diehl, Talk in Dresden

Comparison to KSVZ

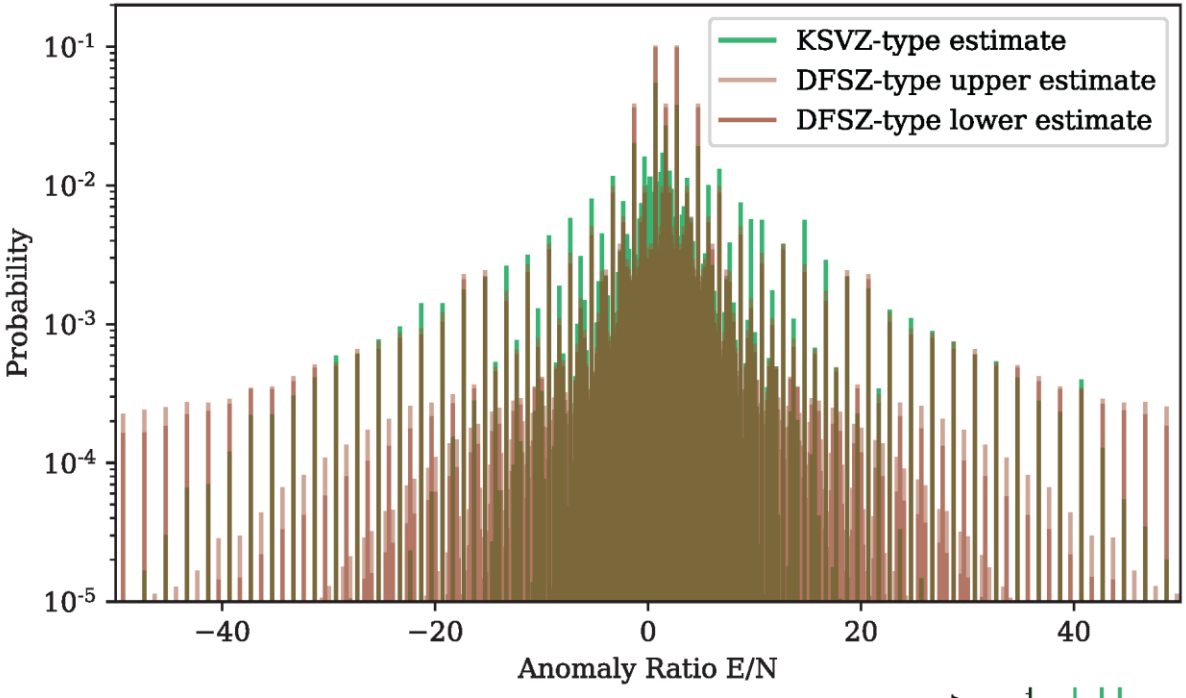

- Peaks at $\frac{E}{N} = \frac{5}{3} + k$, $k \in \mathbb{Z}$
- KSVZ models also peaked

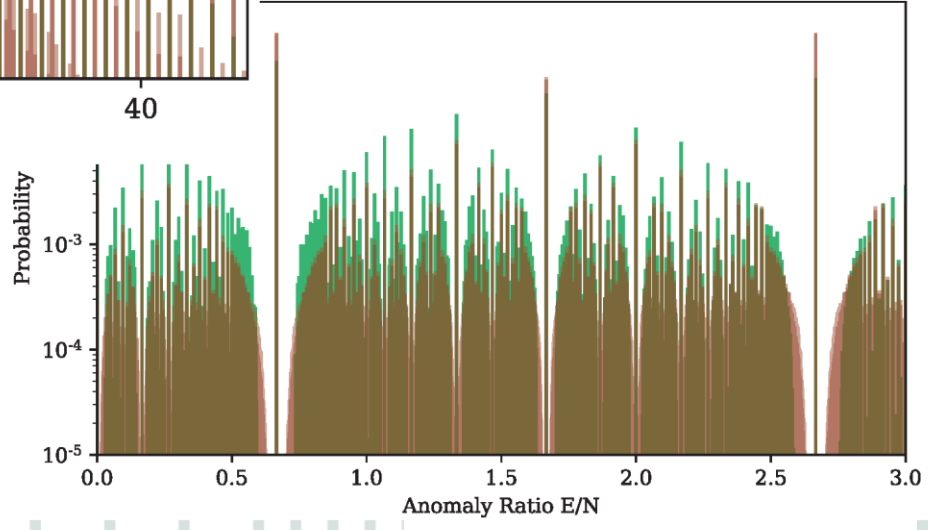

- $DFSZ_2$ remains important
- DFSZ and KSVZ look similar

Diehl & Koutsangelas
arXiv:2302.04667

J. Diehl, Talk in Dresden

Mystery Solved

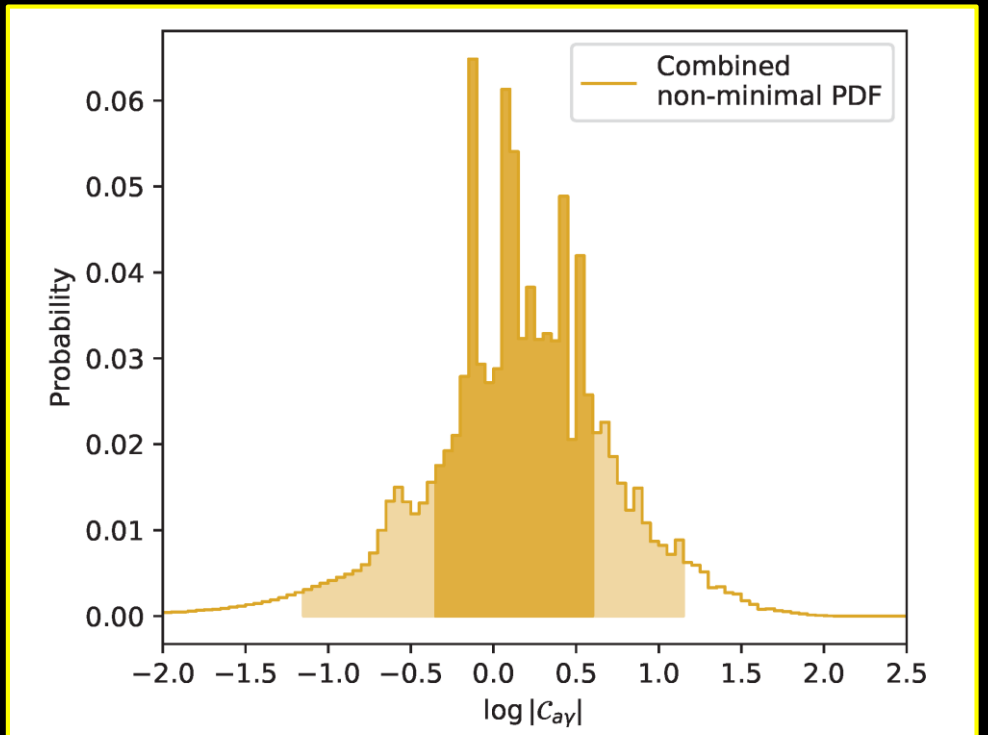

FIG. 7. Probability density in log $|\mathcal{C}_{a\gamma}|$-space of the combined DFSZ-type and KSVZ-type "all N_{DW}"-case. Central 68% and 95% regions used for Fig. 8 are indicated in different shades of yellow. Note that the underlying distribution is discrete and any illustration will in part depend on the binning chosen.

Diehl & Koutsangelas, 2302.04667